Technical Report HL-95-14
November 1995

US Army Corps of Engineers
Waterways Experiment Station

Montgomery Point Lock and Dam Gate Study

Report 1
Hydraulic Forces and Characteristics Acting on Spillway Gates

by Bobby P. Fletcher, Luis A. de Bejar

Prepared for U.S. Army Engineer District, Little Rock

The contents of this report are not to be used for advertising, publication, or promotional purposes. Citation of trade names does not constitute an official endorsement or approval of the use of such commercial products.

PRINTED ON RECYCLED PAPER

DISCLAIMER NOTICE

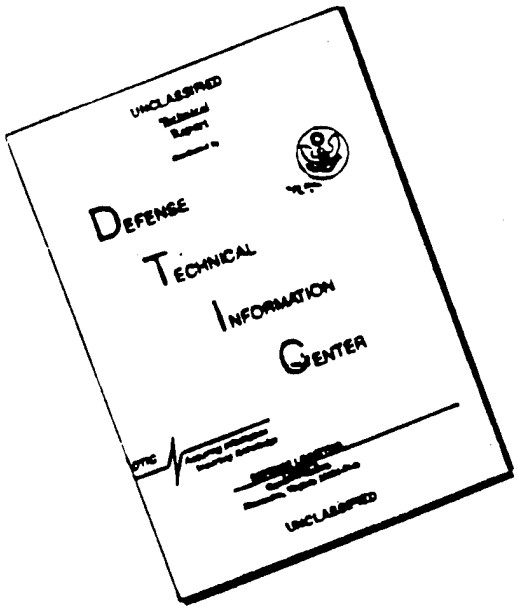

THIS DOCUMENT IS BEST QUALITY AVAILABLE. THE COPY FURNISHED TO DTIC CONTAINED A SIGNIFICANT NUMBER OF PAGES WHICH DO NOT REPRODUCE LEGIBLY.

Technical Report HL-95-14
November 1995

Montgomery Point Lock and Dam Gate Study

Report 1
Hydraulic Forces and Characteristics Acting on Spillway Gates

by Bobby P. Fletcher, Luis A. de Bejar

U.S. Army Corps of Engineers
Waterways Experiment Station
3909 Halls Ferry Road
Vicksburg, MS 39180-6199

Report 1 of a series

Prepared for U.S. Army Engineer District, Little Rock
P.O. Box 867, Little Rock, AR 72203-0867

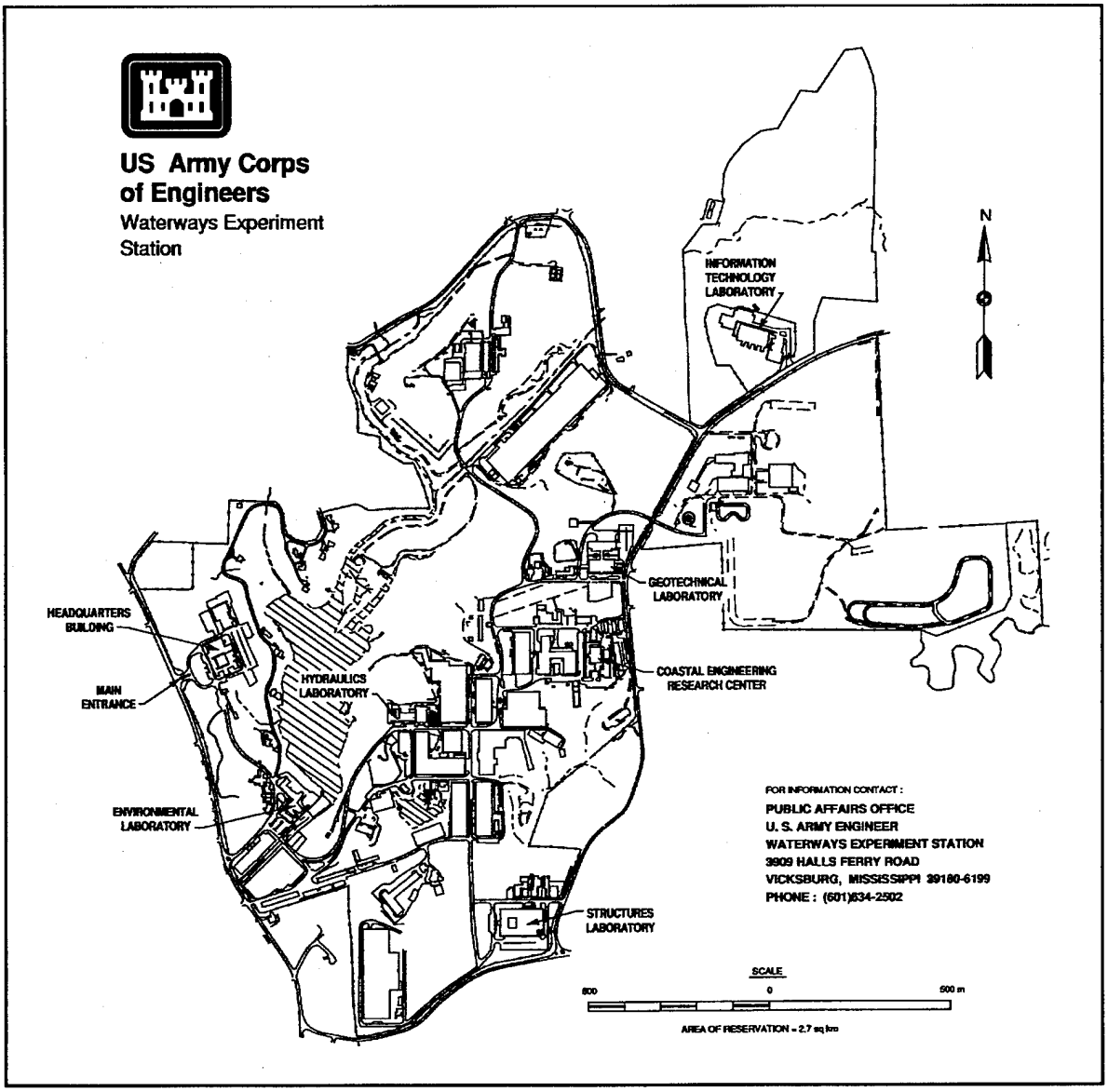

Waterways Experiment Station Cataloging-in-Publication Data

Fletcher, Bobby P.

Montgomery Point Lock and Dam Gate Study. Report 1, Hydraulic forces and characteristics acting on spillway gates / by Bobby P. Fletcher, Luis A. de Bejar ; prepared for U.S. Army Engineer District, Little Rock.

105 p. : ill. ; 28 cm. — (Technical report ; HL-95-14 rept.1)

Includes bibliographical references.

Report 1 of a series.

1. Locks (Hydraulic engineering) — Arkansas. 2. Hydraulic gates. 3. Dams — Arkansas. 4. Montgomery Point Lock and Dam (Ark.) I. Bejar, Luis A. de. II. United States. Army. Corps of Engineers. Little Rock District. III. U.S. Army Engineer Waterways Experiment Station. IV. Hydraulics Laboratory (U.S. Army Engineer Waterways Experiment Station) V. Title. VI. Series: Technical report (U.S. Army Engineer Waterways Experiment Station) ; HL-95-14 rept.1.

TA7 W34 no.HL-95-14 rept.1

Contents

Plates 1-51

SF 298

Preface

This model investigation was authorized by Headquarters, U.S. Army Corps of Engineers (HQUSACE), on 14 June 1993 at the request of the U.S. Army Engineer District, Little Rock. The studies were conducted by personnel of the Hydraulics (HL) and Structures (SL) Laboratories of the U.S. Army Engineer Waterways Experiment Station (WES) during the period June 1993 to November 1994. This is Report 1 of a series. Report 2 presents the results of the structural dynamics/finite-element studies on the torque-tube gate model.

The study was conducted under the direction of Messrs. F. A. Herrmann, Jr., Director, HL; B. Mather, Director, SL; R. A. Sager, Assistant Director, HL; and J. T. Ballard, Assistant Director, SL; and under the general supervision of Mr. G. A. Pickering, Chief, Hydraulic Structures Division (HSD), HL; Dr. J. P. Balsara, Former Chief, Structural Mechanics Division (SMD), SL; Dr. R. Mosher, present Chief, SMD; Mr. N. R. Oswalt, Chief, Spillways and Channels Branch (SCB), HSD; and Dr. R. L. Hall, Chief, Structural Analysis Group (SAG), SMD. Project engineers for the model studies were Mr. B. P. Fletcher, SCB, and Dr. L. A. de Bejar, SAG. The technican assisting the study was Mr. K. Pigg, SCB. Instrumentation and data analysis support were provided by Messrs. H. C. Greer, J. C. Ables, S. W. Guy, and T. W. Warren, Instrumentation Service Division, WES. This report was prepared by Mr. Fletcher and Dr. de Bejar.

During the investigation, Messrs. Sam Powell, HQUSACE; Raymond Veselka, Tom Plunkett, and Tasso Schmidgall, U.S. Army Engineer Division, Southwest; Jack Woolfolk, Estus Walker, Tom Clement, Ed Lofton, Jeff Stiles, Robert Young, Tom Papageorge, Larry Winters, Doug Eggburn, and Mitch Eggburn, Little Rock District; Wayne Coleman and Chander Sehgal, Harza Engineering, Chicago, IL; and Patrick March, Tennessee Valley Authority Engineering Laboratory, Norris, TN, visited WES to discuss the program of tests and observe the model in operation.

At the time of publication of this report, Director of WES was Dr. Robert W. Whalin. Commander was COL Bruce K. Howard, EN.

Conversion Factors, Non-SI to SI Units of Measurement

Non-SI units of measurement used in this report can be converted to SI units as follows:

Multiply	By	To Obtain
cubic feet	0.02831685	cubic meters
degrees (angle)	0.01745329	radians
degrees Fahrenheit	5/9	degrees Celsius or kelvins[1]
feet	0.3048	meters
feet of water (39.2° F)	2,988.98	pascals
inches	25.4	millimetres
kips (force)	4,448.222	newtons
kip-feet	1,355.8181	newton-meters
pounds (force)	4.448222	newtons
pounds (force) per square foot	47.88026	pascals
pounds (mass)	0.4535924	kilograms
pounds (mass) per cubic foot	16.01846	kilograms per cubic meter

[1] To obtain Celsius (C) temperature readings from Fahrenheit (F) readings, use the following formula: C = (5/9)(F - 32). To obtain kelvin (K) readings, use: K = (5/9) (F - 32) + 273.15.

1 Introduction

The Prototype

The proposed Montgomery Point Lock and Dam would be constructed at navigation mile 0.6 near the mouth of the White River. This portion of the White River, known as the White River Entrance Channel, is the initial segment of the McClellan-Kerr Arkansas River Navigation System (Figure 1). This project would consist of a 670-ft-long[1] (useable length 600 ft) by 110-ft-wide navigation lock (similar to other locks on the system), a 300-ft-wide controlled navigation pass spillway, and a 200-ft-wide fixed uncontrolled overflow spillway (Figures 2 and 3).

This model study focuses on the navigation pass spillway. The navigation pass spillway will be used to maintain the upper pool at a minimum stage of el 115.0.[2] The spillway would consist of 10 torque-tube gates operated by individual hydraulic cylinders. The operation sequence can be summarized as follows. When the tailwater is at el 115 and falling, the individual spillway gates will be raised completely until all are in the fully raised position with the upper edge of each gate at el 115.0. The fully raised gates will be at an angle of 70 degrees from horizontal. The depth of flow over the upper edge of the fully raised gates will vary, with the design upper pool level ranging from el 115.0 to el 119.0. At some point during the design life of the project, the tailwater is expected to drop as low as el 95.0. The gates will remain in the raised position during operations to control upper pool until the tailwater is again at el 115.0 and rising. At this point the gates will be lowered. During periods of controlled flow through the pass, and during periods of gate maintenance using the temporary cofferdam, all navigation will be conducted through the lock. An isometric view of a typical gate is shown in Plate 1.

Each of the 10 torque-tube gates will be operated by a hydraulic cylinder (Plate 2). The cylinder is oriented along the center line of the gate and is

[1] A table of factors for converting non-SI units of measurement to SI units is found on page vi.

[2] All elevations (el) cited herein are in feet referenced to the National Geodetic Vertical Datum (NGVD).

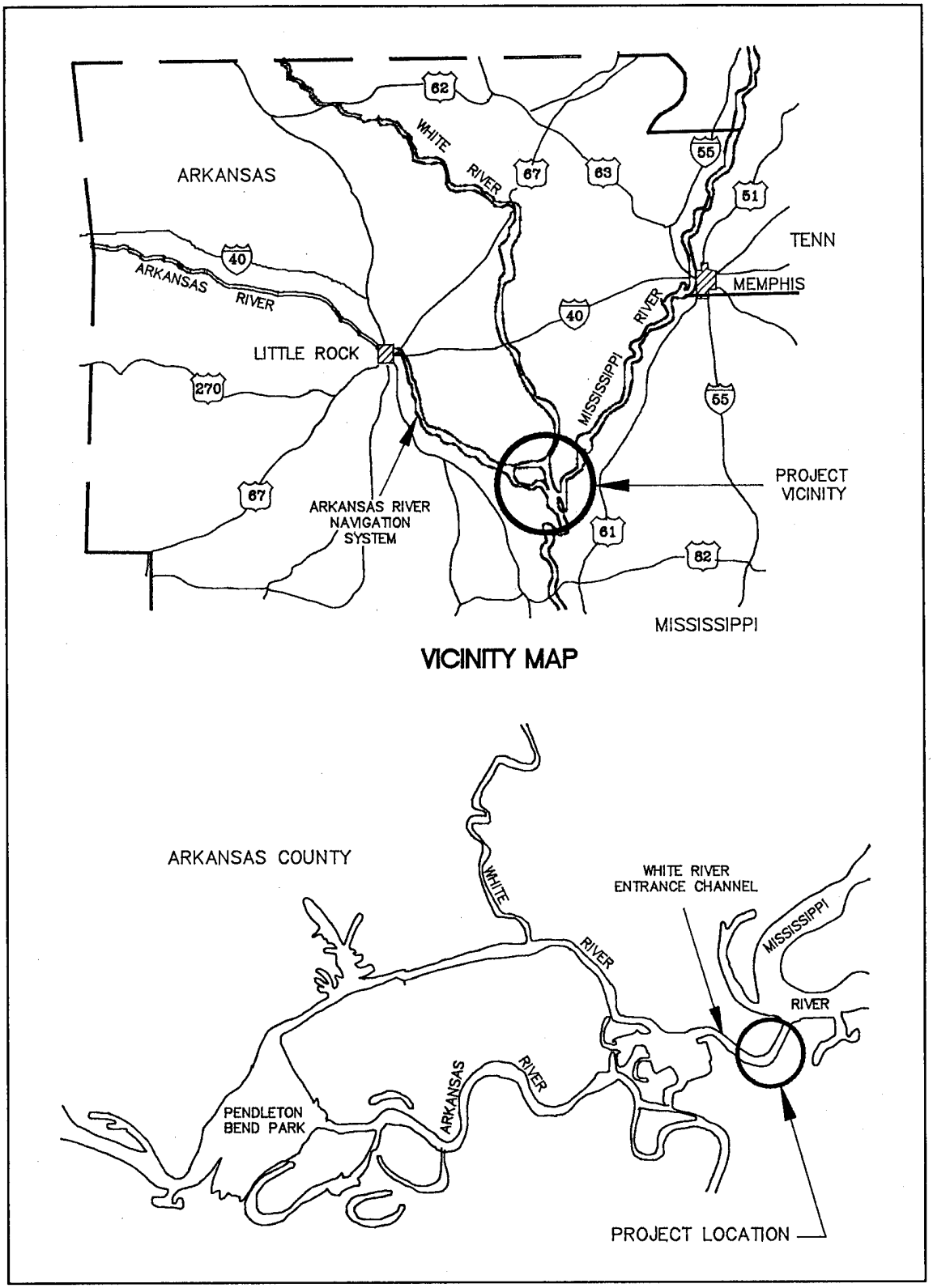

Figure 1. Vicinity and location maps

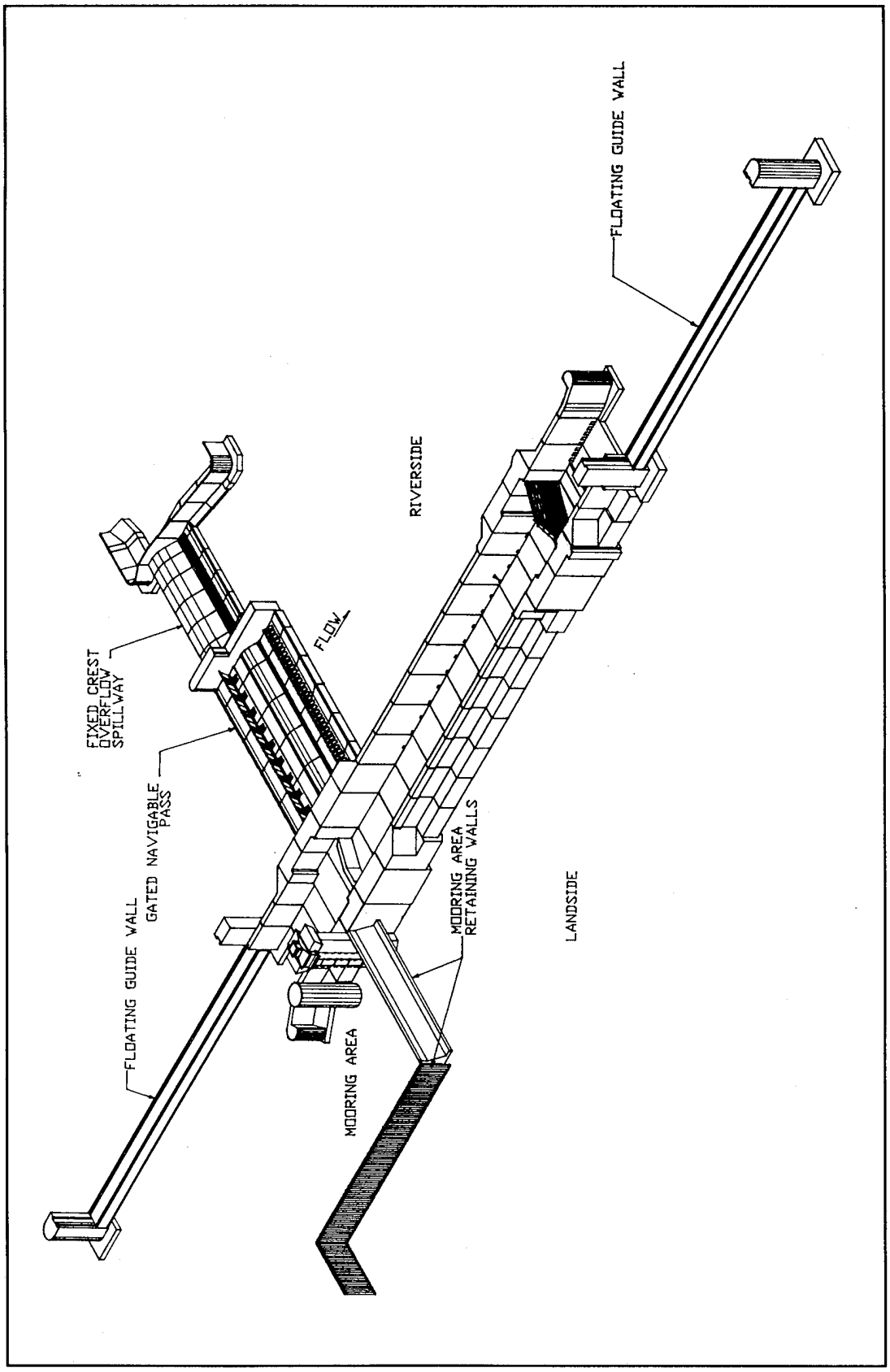

Figure 2. Montgomery Point lock and dam

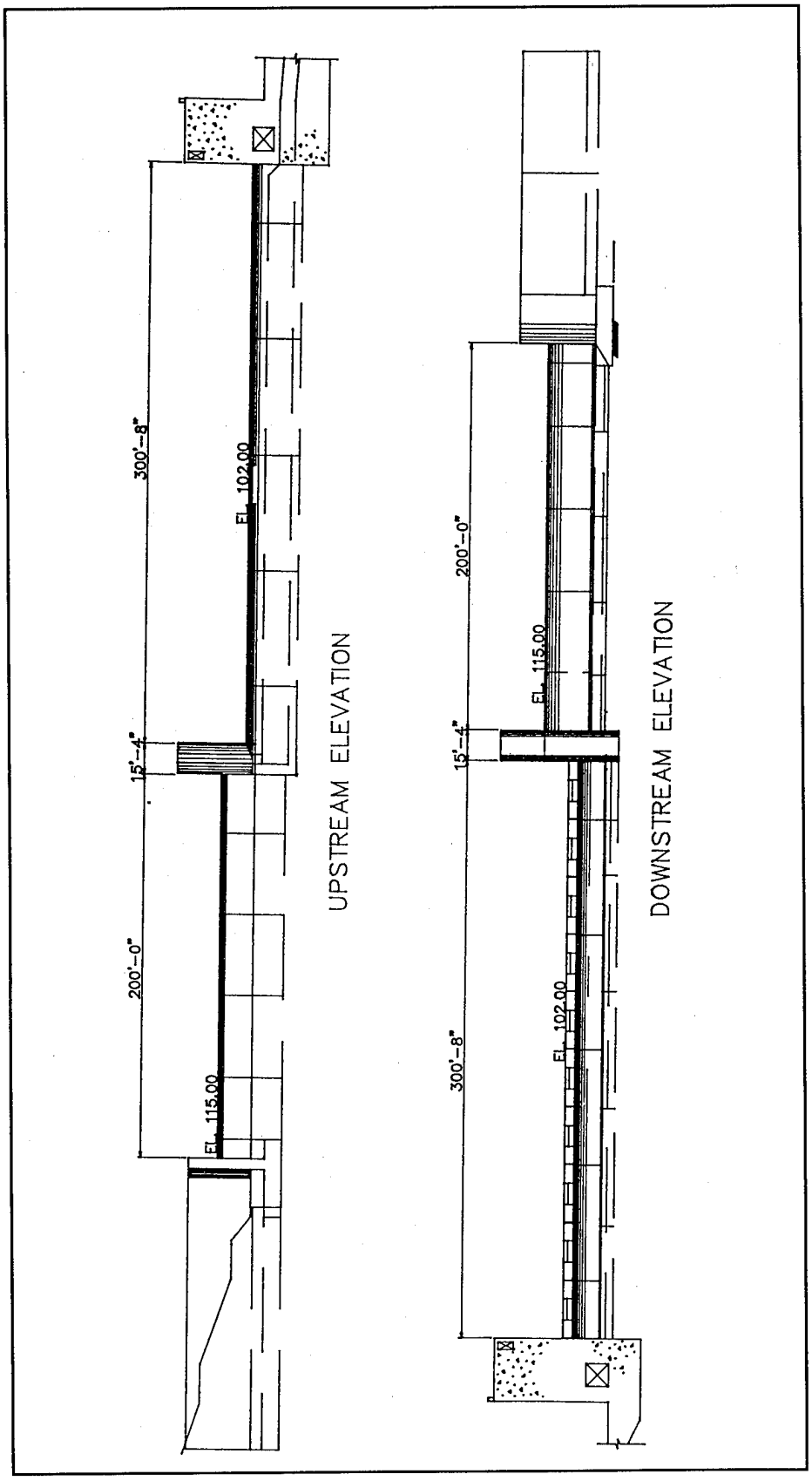

Figure 3. Upstream and downstream elevations

installed upstream from the center line of the torque-tube. The cylinder is supported on a horizontal trunnion to allow it to pivot in the vertical plane during movement of the operating arms. One gate will be operated at a time to reduce the electrical load.

Each gate will weigh about 89,200 lb. Upstream and downstream views of the gate with pressure gauges installed are shown in Plates 3 and 4. Because of the requirement that the gate cannot project above the top of the sill at el 102.0, the gate "wraps around" the concrete housing the drive shafts and operating arms as shown in Plate 1. Consequently the gate is constructed with two separate torque-tube segments (Plate 5) and one leaf attached to and transmitting loads to both torque-tube segments. Each torque-tube segment rests in two bearings and connects to a drive shaft segment (Plate 5). Each drive shaft segment is connected with a spline to a separate operating arm. The lower ends of the two operating arms are connected to a cross beam (Plate 2) which is engaged by the cylinder piston (Plate 2). The gate impact release mechanism is a hydraulic system which is integral with the gate operating cylinder.

The torque-tube segments and drive shaft segments for each gate are supported by a series of seven bearings situated along the torque-tube center line (Plate 5).

The torque-tube gate is supported in the fully raised position by the hydraulic cylinder. Upon impact from a runaway barge or some other large object, an abnormally high pressure in the bore end of the cylinder will be created, which will open hydraulic valves to vent the fluid from the bore. The gate will lower out of the way of the barge at a speed which will prevent a second impact from the barge.

Purpose and Scope of the Models

Two model studies were conducted for this project, a hydraulic model and a structures model, both by the U.S. Army Engineer Waterways Experiment Station (WES).

Hydraulic Model

The objectives of the hydraulic model testing were to determine the following for anticipated operation and flow conditions:

a. The magnitude and frequency of the static and dynamic hydraulic forces acting on the upstream and downstream side of the gate and bearing blocks.

b. Moment acting on the torque-tube.

c. Hydraulic performance of the spillway.

d. Potential for debris to circulate on the downstream side of the gate.

e. Uplift forces on the lowered gates resulting from barge and towboat passage over the gate.

f. Forces due to lateral approach flow.

g. Forces when the gate falls due to impact.

h. The need for a nappe venting system.

i. The size and extent of riprap required upstream and downstream from the spillway.

Tests were conducted for anticipated gate operations, discharges, and upper pool and tailwater elevations. Test results will provide design guidance for the project.

Structures Model

The objectives of the structures model testing were as follows:

a. Construct and instrument a rigid 1:15-scale physical model of the gate to experimentally determine (1) reaction forces for prototype design of the support bearings, and (2) time-histories of hydraulic pressure at selected discrete locations on both sides of the gate skin.

b. Determine a design representation of the net hydrodynamic pressure field acting on the gate under (1) regular operating conditions, and (2) extreme conditions of discharge and pool elevations and/or unusual operation. These semiempirical representations of the pressure field on the gate are based on sound theoretical principles and adjusted to fit the results from multiple automatically controlled tests.

c. Construct an analytical model of the gate for the finite element analysis of the structure subjected to the design hydraulic pressure field. This analysis renders design reaction forces at the support bearings to be compared with the experimental measurements.

d. Determine the gate natural frequencies, mode shapes, and parameters of energy dissipation mechanisms using (1) finite element analyses, and (2) nondestructive experimental techniques. Knowledge of the gate eigenproperties is necessary for effective assessments of structural safety during the useful life of the gate.

e. Development of a simple structural model for engineering analysis of the dynamic response of the gate under hydraulic flow. A random-vibration model for the stochastic description of the fluctuations of both the hydraulic pressure field and selected parameters of structural response about the respective steady-state mean components follows a simple deterministic representation of the gate system subjected to the hydraulic forces.

By spectral analysis, the study evaluates the safety of a typical torque-tube gate in service against fatigue from flow-induced vibrations over its design life.

2 The Hydraulic Model

Description

A sketch of the 1:15-scale section model is shown in Plate 6. The model was located inside a 6-ft-wide, 4-ft-deep, and 40-ft-long flume. A 90-ft-long section of the crest, three gates, stilling basin, 385-ft length of the approach channel, and a 372-ft length of the channel were simulated in the flume. The gates, drive shafts, operating arms, torque-tubes, and trashracks were constructed of brass. All external structural members were geometrically reproduced in the model to ensure simulation of flow patterns. The model components are shown in Figure 4. A sketch of a torque-tube, drive shaft, and operating arm is shown in Plate 7. Instrumentation of the center gate consisted of pressure cells on the upstream and downstream sides of the gate (Plates 3 and 4), force gauges on the seven bearing blocks (Plate 5) to measure vertical and horizontal forces, and force gauges on the operating arms (Figure 4c) to measure moment about the center line of the torque-tube.

Water used in the operation of the model was supplied by pumps, and discharges were measured by venturi meters. Steel rails set to grade along the sides of the flume provided reference planes for measuring devices. Water-surface elevations were measured with point gauges.

Interpretation of Model Results

The accepted equations of hydraulic similitude, based on the Froude criteria, were used to express the mathematical relations between the dimensions and hydraulic quantities of the model and prototype. The general relations expressed in terms of the model's scale or length ratio L_r are expressed in the following tabulation.

Characteristic	Dimension	Scale Ratio Model:Prototype
Length	L_r	1:15
Area	$A_r = L_r^2$	1:225
Velocity	$V_r = L_r^{1/2}$	1:3.873
Discharge	$Q_r = L_r^{5/2}$	1:871.4
Time	$T_r = L_r^{1/2}$	1:3.873
Force	$F_r = L_r^3$	1:3,375
Frequency	$f_r = 1/L_r^{1/2}$	1:0.258

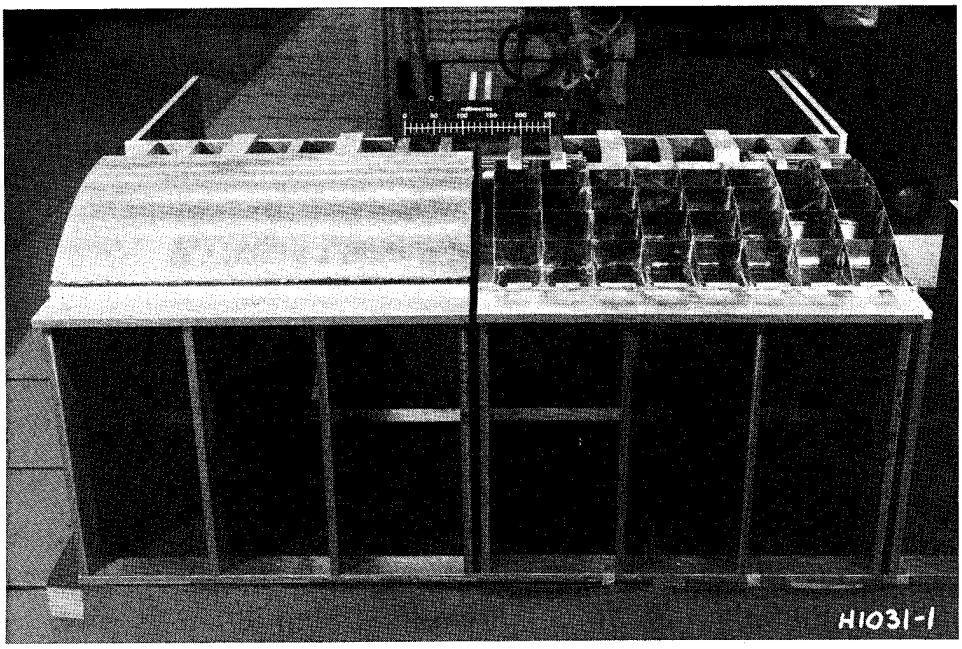

a. View looking upstream

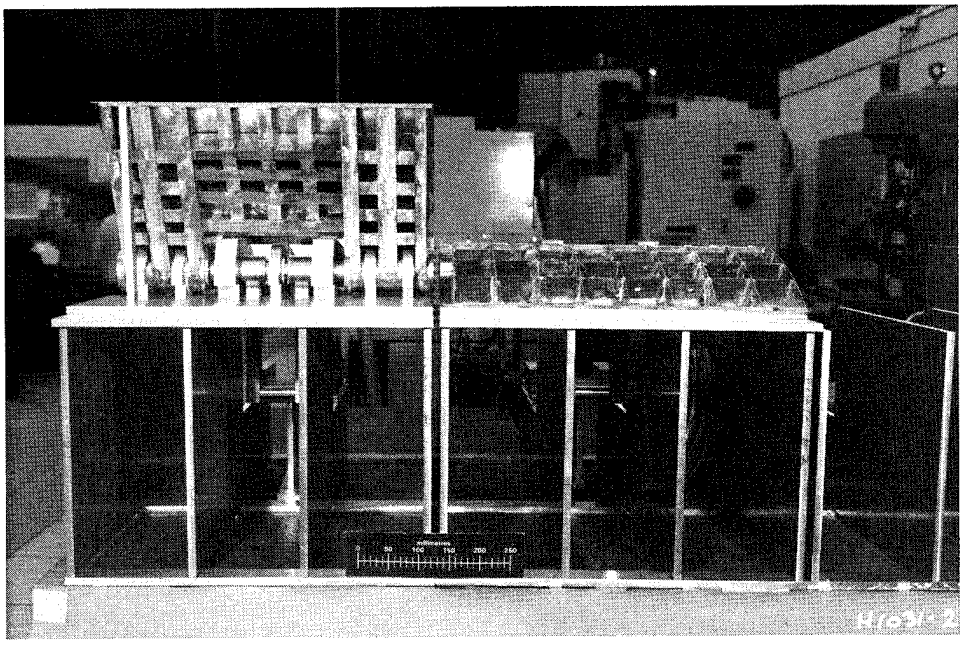

b. View looking upstream (raised gate)

Figure 4. Model components (Sheet 1 of 3)

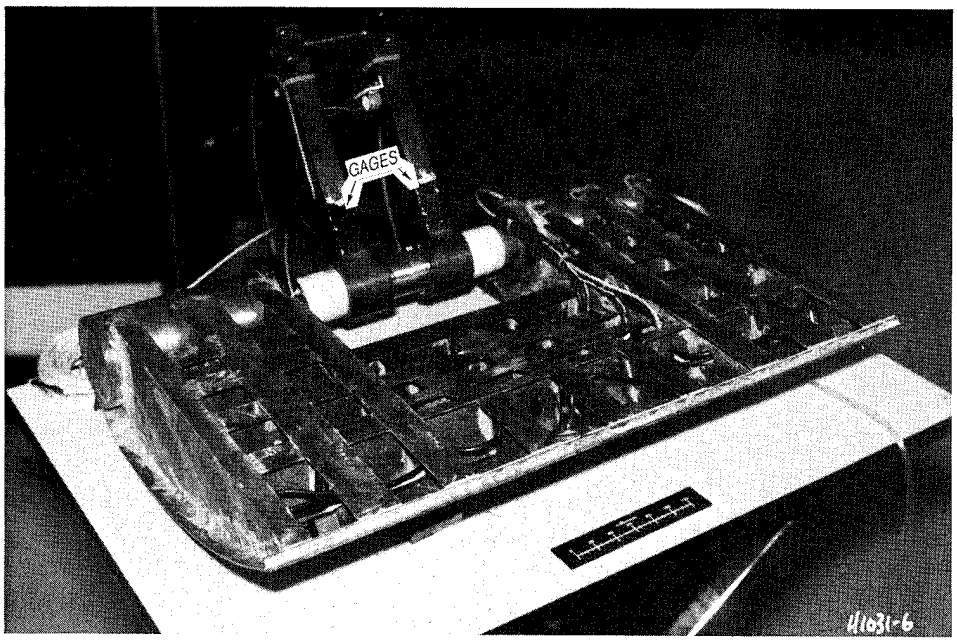

c. Instrumented gate

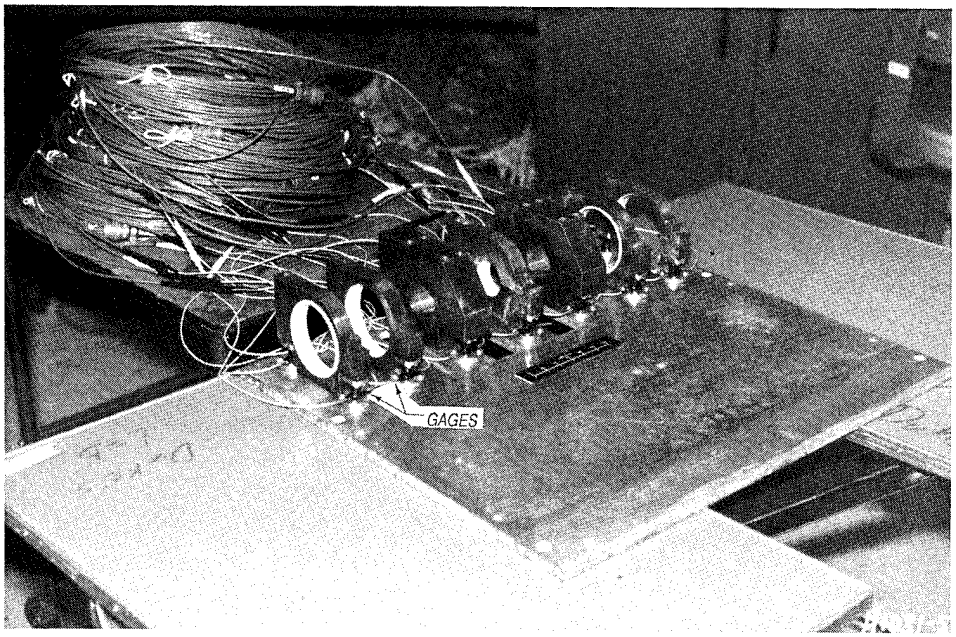

d. Instrumented bearing blocks

Figure 4. (Sheet 2 of 3)

e. Gate down

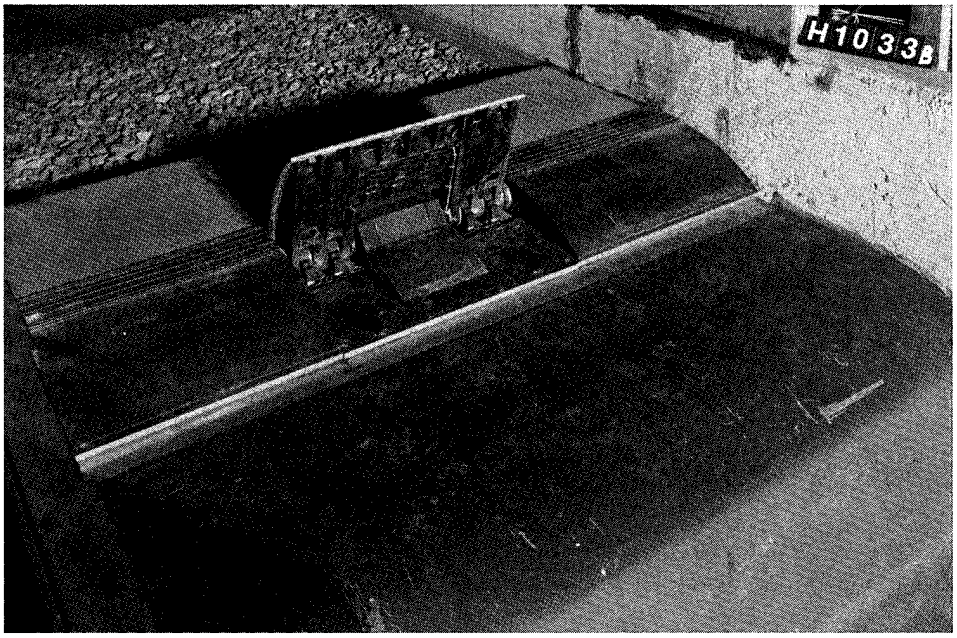

f. Gate up

Figure 4. (Sheet 3 of 3)

3 The Structural Model Studies

Description of Model

Due to numerous alignment difficulties encountered in the construction of a balanced 1:15-scale physical model of the gate standing on seven supports (refer to Report 2 for details[1]), the WES engineering team decided to conduct the experiments of the project on an instrumented gate to the required scale standing on only three supports (see page 16), and recommended reducing the number of supports in the final prototype gate to five (the construction process at a larger scale is more controllable).

The physical model of the gate was made out of bronze for convenience of construction. Bronze plates are easier to cut and assemble than structural steel plates and contribute to make the rigid gate model closer to a true Froude's model. Consequently, two separate finite element models were developed simultaneously: one bronze analytical model standing on three supports for the analysis of the 1:15-scale physical model, and another analytical model in structural steel standing on five supports for prototype analysis.

Parameters of force response were measured, in general, using automatically monitored strain gauges (Figure 4c). Support reactions were inferred from engineered strain gauges on load cells (i.e., force gauges), two structural aluminum tubes per support block (Figure 4d and Plate 7). The physical model of the gate was also instrumented with accelerometers to identify its natural structural properties from the forced experimentation (frequencies of natural vibration and the corresponding modal shapes). The corners of the gate were instrumented with triaxial accelerometers to identify spatial motions of the gate. Another six linear accelerometers were strategically installed over the rest of the gate skin area. Nine pressure cells on each side of the gate (Plates 3 and 4) continually monitored the variation of the hydraulic pressure field on the gate during the experiments.

---

[1] Luis A. de Bejar. "Montgomery Point Lock and Dam Gate study; Report 2, Montgomery Point torque tube gate, a structural model study," Technical Report HL-95-14, U.S. Army Engineer Waterways Experiment Station, Vicksburg, MS.

Test Procedure

The first phase of experiments intended to reproduce the effect of the net hydrodynamic pressure field acting on the gate under regular operating conditions. The maximum reaction response was obtained when a unit discharge of water of 50 cfs ran over the system of three fully raised gates with the tailwater pool maintained at 95 ft, prototype level (Plates 8 and 9 and Photos 1-6), and the headwater pool growing monotonically from about 114 ft to 119 ft, prototype level. Tests of various durations both with an integral nappe and with a ventilated nappe were conducted and contrasted with one another to determine the proper modification to the theoretical distribution of the hydraulic pressure field to provide an upper bound for design.

The design pressure field was used for separate finite element analyses of the 1:15-scale physical model and the prototype. Corresponding envelopes for the components of reaction at the supports were developed for bearing design, and the corresponding forces at the actuator cylinder were determined.

Using the pressure records obtained during the first phase of experiments, probabilistic models of extrapolation were applied to predict extreme-value pressure fields exerted on the gate in service during its useful life.

A second phase of experiments was devised to simulate the effect of the net hydrodynamic pressure field acting on the gate under extreme conditions of discharge and pool elevations and/or unusual operation. This set of tests provided a deterministic envelope to the hydraulic pressure field on the gate for ultimate analysis. Larger unit discharges are considered responsible for the substantial increase in the magnitude of the effective hydraulic forces acting on the gate during the second phase of the experiments.

The gate natural frequencies, modal shapes, and equivalent viscous damping ratio in both dry and submerged conditions were identified using finite element analysis and experimental analysis techniques. A variety of mutually checking methods were implemented in this exercise. Finite element analyses of the physical model standing on dry Teflon bearings on load-cell foundations provided the benchmarks for the results from free-vibration (Twang) tests, forced vibration tests (flow running over the gate in service), and laser vibrometry on the physical model. Results correlated well.

A simple structural model for engineering analysis of the gate under hydraulic forces was developed. This engineering model gives a quick and practical approximation of the fundamental natural frequency of vibration of the gate system and allows the expedient evaluation of its deterministic response to the steady-state component of hydraulic flow on the gate. The model is extended with a random-vibration description of the fluctuations of both the hydraulic pressure field and selected parameters of structural response about their respective steady-state mean values.

A spectral analysis of the test records evaluates the safety of a typical torque-tube gate in service against fatigue failure from flow-induced vibrations over the long run. These initial studies indicate no significant flow-induced vibration problems in the model, since the observed flow conditions produced no outstanding oscillation energy. Therefore, no evidence was detected pointing to flow-induced vibrations of such intensity to produce fatigue in components of the prototype; however, this does not ensure categoric safety against fatigue in the prototype.

4 The Hydraulic Model Studies

Symmetry and System Response

Verification tests to ensure that the model was capable of simulating and measuring the magnitude and frequency of the hydraulic forces were conducted. The first tests consisted of measuring the symmetry of the hydraulic load distribution to the seven bearing blocks supporting the torque-tube, drive shaft, spool, and two operating arms (Plate 7). Next, the frequency response of the model was measured by the force gauges installed in the bearing blocks and the operating arms.

Initial tests for symmetry revealed that either a dry load or water load applied uniformly to the center of the gate was transferred and measured compositely by the gauges in the bearing blocks and operating arms. The applied load was symmetrically distributed to the two operating arms but asymmetrically distributed to the seven bearing blocks. Further investigation indicated that symmetry between the seven bearing blocks (Plate 7) could not be achieved because the drive shaft and torque-tube were constructed and aligned with the bearing blocks with a tolerance of 0.001 in., and the force gauges were sensitive to a deformation of 0.0001 in. Attempts to achieve symmetry with the seven bearing blocks were unsuccessful with a solid brass shaft that simulated the torque-tube and drive shaft (gate was not attached). Two bearing blocks were disconnected and the solid shaft was supported by bearing blocks 2, 3, 4, 5, and 6 (Plate 7). A uniform load applied to the shaft was transferred asymmetrically to the bearing blocks. Following these tests, it was decided to support the torque-tube with bearing blocks 2, 4, and 6 (Plate 7). Tests proved that symmetry within 10 percent could be achieved and that the three-bearing system would be acceptable for measuring hydraulic-induced forces.

Tests to evaluate frequency response were conducted to ensure that the measured frequencies of the hydraulic-induced forces were not contaminated by the frequency response of the model. The frequency response was obtained by exciting the model with a sudden impact force on the gate. These tests were conducted in the dry and with water on one or both sides of the raised

gate. Time-history plots of the horizontal and vertical frequency response and a spectrum of the frequencies for bearing block 2 with water on the upstream side of the raised gates are shown in Plate 10. Plate 10 is typical of the natural frequencies measured at each bearing block and operating arm. Plate 10 shows predominant natural frequencies occurring between 30 and 50 Hz. This should be significantly higher than any hydraulic-induced frequency. The natural frequencies of the model were considered too high to significantly influence either the magnitude or frequency of the hydraulic forces measured. Tests also indicated no significant damping of the hydraulic pulsations. The model had acceptable symmetry and frequency response and was then a viable tool for measuring the magnitude and frequency of the hydraulic-induced forces.

Data Acquisition

The data acquisition system was capable of simultaneously measuring all forces and pressures detected by the force gauges and pressure transducers. Data could be collected for various time periods and sampling rates.

Typical Tests to Measure Forces

A typical test to measure forces involved pretest zeroing of the force gauges and pressure transducers, setting the discharge and tailwater, and collecting data with all gates stationary or while raising or lowering the center gate at a simulated speed of 8 min. Since the weight of the gate was zeroed out, only the hydraulic-induced forces were measured. Following data collection, the posttest zeros were compared with the pretest zeros to determine if there was significant mechanical and/or electronic drift. If the drift was significant, the test was rerun.

Hydraulic Forces

Hydraulic-induced forces and pressures were measured for various anticipated gate positions and hydraulic conditions. Various gate positions and hydraulic conditions are shown in Photos 1 and 2. Due to the large volume of data collected for the various gate positions and hydraulic conditions, only the conditions that generated the maximum hydraulic forces, pressure differentials, and moments are submitted in this report.

The maximum load on the three bearing blocks was generated when all three gates were up with the maximum regulated upper pool elevation of 119.0, a unit discharge of 50 cfs/ft (section model width 90 ft), and a tailwater elevation of 95.0. The following tests were conducted with the center gate raising from 0 to 70 deg and the two adjacent gates up. Plate 11 shows the

vertical and horizontal forces and moment about the center line of the torque-tube versus gate angle on bearing block 2. When the gate angle was 70 deg, the maximum average vertical and horizontal forces and moment of 120 and 119 kips and 130 kip-ft, respectively, occurred on bearing block 2 (Plate 11). Note that when the gate was in the down position, the force and moment curves indicated hydraulic uplift.

Tests were conducted to evaluate hydraulic forces with the nappe unvented and vented (Plates 12 and 13, respectively). Forces were measured when all gates were in a stationary raised position (70 deg) (Plate 12). The test shown in Plate 13 was the same as the test in Plate 12 except the nappe was vented. A comparison of the forces in Plates 12 and 13 indicates that venting the nappe reduces the amplitude of the static and pulsating forces on the bearing blocks. Unvented and vented nappes are shown in Photos 3 and 4. As shown in these photos, the water depth below the unvented nappe was 10.2 ft. The water depth below the vented nappe was 6.3 ft. The 6.3-ft depth of water under the vented nappe was caused by the upstream component of flow as the nappe plunged into the tailwater (Photo 4a). Pressure below the unvented nappe decreased as the air below the nappe was expelled as the nappe plunged into the tailwater. As the pressure decreased, the water beneath the nappe rose to an equilibrium depth of 10.2 ft. The increase from vented to unvented water depth of 3.9 ft was equivalent to the reduction in pressure below the nappe. Thus, the resultant hydraulic load on the gate was increased by this reduction in pressure on the downstream side of the gate (compare Plates 12 and 13). The depth of water under the nappe generated by the upstream component of the nappe plunging into the tailwater reduces the hydraulic differential load on the gate for either vented or unvented flow conditions.

The maximum pressure differential measured with the nine pressure transducers on each side of the gate during test 1108 (unvented nappe) is shown as pressure contours in Plate 14. The nappe was vented, and the vented pressure contours are also shown in Plate 14. This change in pressure from unvented to vented nappe correlates with the measurement of the change in water depth below the nappe (Photos 3 and 4). A comparison of the unvented and vented nappes relative to the differential forces (Plates 12 and 13) and pressures (Plate 14) indicates that the vented nappe provides only a slight reduction in the differential forces and pressures. Thus there is no significant reason for venting the nappe with nappe deflectors.

Tests were conducted to determine if flow approaching a gate at an angle would affect the hydraulic loads on the gate. Angle approach flows in the section model were simulated by use of a vane in the approach channel. A comparison of forces measured without and with a 45-deg vane in the approach shows no significant change in magnitude of the hydraulic forces due to asymmetric flow approaching the gate. Various approach flow angles up to a maximum of 45 deg were investigated, and no significant change in force, moment, or pressure was detected.

Towboat Passage Forces

Tests to measure the hydraulic effects of a towboat passing over the center gate were conducted with a unit discharge of 50 cfs/ft and tailwater and pool elevations of 115.0 and 115.1, respectively. The simulated single-screw towboat had a length of 130 ft, a width of 30 ft, a draft of 9 ft, and an 8-ft-diam Kort nozzle. The towboat simulated a ground speed of about 7.0 ft/sec (prototype) upstream and about 9 ft/sec downstream. The towboat in the section model is shown in Figure 5.

As the towboat moved upstream over the lowered gates, hydraulic forces were measured by the force gauges mounted in the three bearing blocks. Plate 15 illustrates passage of the towboat bow, towboat, and propeller over the gate. The measured hydraulic moment about the center line of the torque-tube is also shown in Plate 15. The maximum uplift force and moment measured at bearing block 2 were 38 kips and 62 kip-ft (Plate 15).

Forces measured as the towboat moved downstream over the gates are shown in Plate 16. The measured hydraulic moment is also shown in Plate 16. A comparison of Plate 15 (upstream passage) and 16 (downstream passage) shows more of a gate uplift tendency generated by upstream passage of the towboat.

Debris Passage Forces

Debris trapped in the hydraulic turbulence downstream of the raised gates is shown in Photo 5. The debris simulated log lengths of 10, 20, and 30 ft and diameters of 1, 2, and 3 ft, respectively. Although the debris on the downstream side of the gates was retained in the roller generated by the return flow, it did not tend to collect on the gates. For a unit discharge q of 50 cfs/ft and a tailwater elevation of 110, there was no impact load due to debris. When the tailwater elevation was lowered 5 ft to el 105.0, there was a debris impact load on the downstream side of the gates of about 70 kips. A unit discharge of 50 cfs/ft provided sufficient depth to prevent impact as debris floating downstream passed over the top of the gates. For a unit discharge of 50 cfs/ft over the raised gates, debris was retained on the downstream side of gate, in the return flow, between tailwater elevations of 115.0 and 102.

Gate Free-Fall Forces

Tests were conducted with various hydraulic conditions to document the forces during and the time for free-fall of the center gate due to impact of a tow. Free-fall of the gate due to impact of a tow was simulated by supporting the gate at 70 deg by a wire attached to the top of the gate and permitting the gate to fall by cutting the wire. The gate free-fall time for a unit discharge of

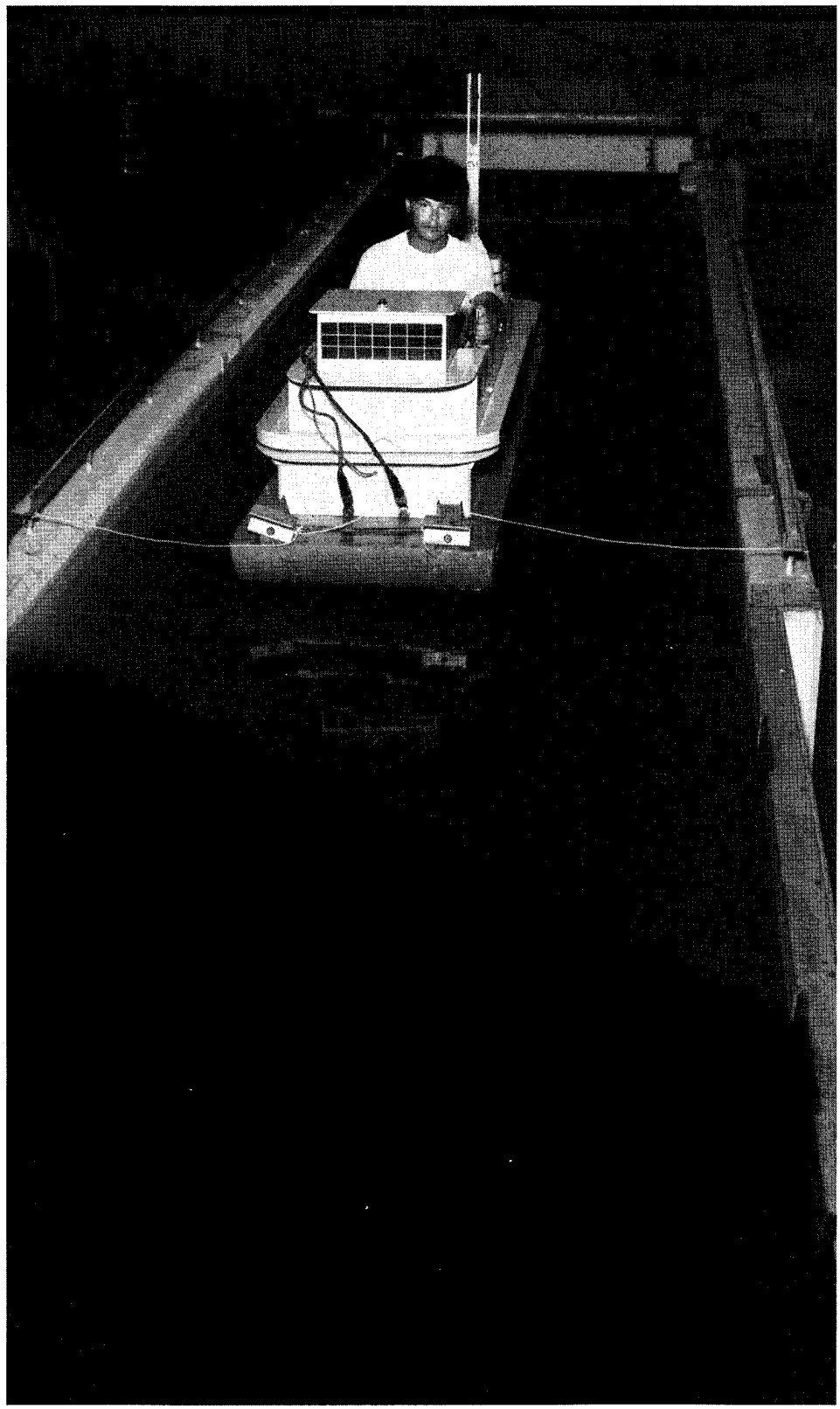

Figure 5. Simulated towboat

9.8 cfs/ft, pool el 116.0, and tailwater el 115.0 was 5.4 sec. Forces measured for these hydraulic conditions during free-fall of the gate are typical for unit discharges ranging from 9.8 to 133.3 cfs/ft. Horizontal and vertical forces and moment measured on bearing block 2 versus gate position during free-fall of the gate are shown in Plate 17. During free-fall of the gate, the maximum reaction at bearing block 2 occurred at a gate angle of about 10 deg (Plate 17). The vertical and horizontal forces and moment measured at the 10-deg gate angle were -80 and +25 kips and -45 kip-ft, respectively. The gate free-fall time for a unit discharge of 12.2 cfs/ft, pool el 116, and tailwater el 105 was 3.4 sec.

Spillway Discharge Characteristics

A spillway discharge rating curve for free-flow conditions with all gates down is shown in Plate 18. Free flow occurs when the upper pool is unaffected by tailwater. Flow over the spillway in Plate 18 is presented as unit discharge or discharge per foot of crest length q_c. The pool elevation in Plate 18 was measured 90 ft upstream from the center line of the torque-tube (Plate 8) and does not include velocity head. A head-discharge rating curve for free flow is presented in Plate 19. Head H is defined as the vertical distance from the pool elevation to the top of the trashrack (gates down), as illustrated in Plate 8. Plate 19 also includes an empirical equation for the head-unit discharge relationship.

The zone where free flow transitions to submerged flow (all gates down) was obtained by setting several constant discharges and raising the tailwater in increments from an elevation at which pool elevation was not affected to elevations where pool elevation was affected. Tailwater elevations were measured 300 ft downstream from the center line of the torque-tube. The pool and tailwater elevations for various unit discharges where free flow begins to transition to submerged flow are shown in Plate 20.

The three gates were rotated 70 deg to their full upright position. The top elevation of the gates was 115.0 (Plate 8). A spillway gate unit discharge rating curve for free-flow conditions with all gates up is shown in Plate 21. The pool and tailwater elevations for various unit discharges where free flow begins to transition to submerged flow are shown in Plate 22. The unit discharges shown in Plates 21 and 22 include leakage underneath and between the gates.

Tests were conducted to determine the amount of leakage under and between the gates when the tailwater elevation was below the bottom of the gates and when the pool elevation was equal to the elevation of the top of the gates. There were a 2-in. prototype gap between adjacent gates and a 2-in. prototype gap between the gate and flume sidewall. The leakage between gates was about the same as the leakage between the gate and sidewall. Measurement of total leakage L_t was accomplished by measuring the flow rate required to maintain a pool elevation of 115. The vertical gaps between each

gate and both end gates and sidewalls were sealed, and the flow rate required to maintain a pool elevation of 115 was measured. This measured unit flow rate, 5 cfs/ft, was equal to the leakage under the gates L_u. The leakage through the gaps L_g was determined by the following equation:

$$L_g = L_t - L_u \tag{1}$$

Model tests to determine leakage indicated the following leakage rates:

L_u = 5 cfs/ft

L_g = 20 cfs/gap

Therefore, total leakage rate L_t around 10 gates, each 30 ft long with a pool elevation of 115, would be computed as follows:

$$L_t = L_u(N_u)\ (G_L) + (N_g)\ (L_g) \tag{2}$$

where

N_u = number of gates up

G_L = gate length, ft

N_g = number of gaps, gaps = N_u + 1

Thus using Equation 2 to solve for L_t gives

L_t = 5 cfs/ft (10 gates) (30 ft/gate) + (11 gaps) 20 cfs/gap
= 1,720 cfs

Leakage through the gates for pool elevations above 115.0 can be determined by comparing the rating curves in Plate 23.

Tests were conducted to determine the change in effective crest length due to flow concentration around the side or sides of a raised gate. Normally, flow contraction around a gate raised 90 deg would reduce the effective crest length. However, the gate or gates sloping at an angle of 70 deg permit an increase in effective crest length that offsets the loss in crest length due to flow contraction around the side of a gate. This is illustrated by a comparison of the calibration data in Plate 20 (all gates down) with the calibration data in Plate 24 (two gates down and one gate up). For a given pool and tailwater elevation, Plate 20 predicts about the same unit flow rate as Plate 24. Flow contraction around the sides of a gate is illustrated in Photo 2.

An example of how to compute discharge through the structure is presented.

a. Given: pool el 116.0, tailwater el 110,
six gates up and four gates down

b. Unit discharge:

q_c = 205 cfs/ft (Plate 20)

q_g = 10 cfs/ft (Plate 22)

where

q_c = unit discharge (gates down) over crest, cfs/ft

q_g = unit discharge over raised gates, cfs/ft

c. Total discharge:

$$Q_t = q_c\,(N_D)(G_L) + q_g\,(N_u)(G_L) \qquad (3)$$

where

Q_t = total discharge, cfs

N_D = number of gates down, gates

Thus using Equation 3 to solve for Q_t gives

Q_t = 205 cfs/ft (4 gates) (30 ft/gate) + 10 cfs/ft (6 gates) (30 ft/gate)
= 26,400 cfs

Water-Surface Profiles

Tests were conducted to determine the water-surface profile over the center spillway gate.

Water-surface profiles measured along the center line and right side of the center gate bay with the center gate down and the two adjacent gates up, an upper pool elevation of 119.0, and tailwater elevations of 95.0 and 115 are shown in Plate 9. A water-surface profile measured with all gates up is also shown in Plate 9.

Stilling Basin and Riprap

The stilling basin performance was evaluated for various anticipated flow conditions with various gate openings, discharges, and pool and tailwater elevations. Various flow conditions are illustrated in Photo 6. The stilling basin design is satisfactory and provides sufficient energy dissipation for all anticipated flows.

Riprap stability upstream and downstream of the spillway was evaluated for anticipated flow conditions. The riprap in the model is shown in Figures 6 and 7. The riprap was subjected over 5 hr (prototype) to each of the most adverse flow conditions. The prototype riprap gradation limits and the riprap gradation simulated in the model upstream (LRD 5) and downstream (LRD 6) from the spillway are shown in Plate 25. These gradation curves show that the model riprap gradation was designed to be conservative. The riprap used in the model had a unit weight of 160 pcf.

The upstream and downstream riprap was stable for all anticipated gate positions and flow conditions.

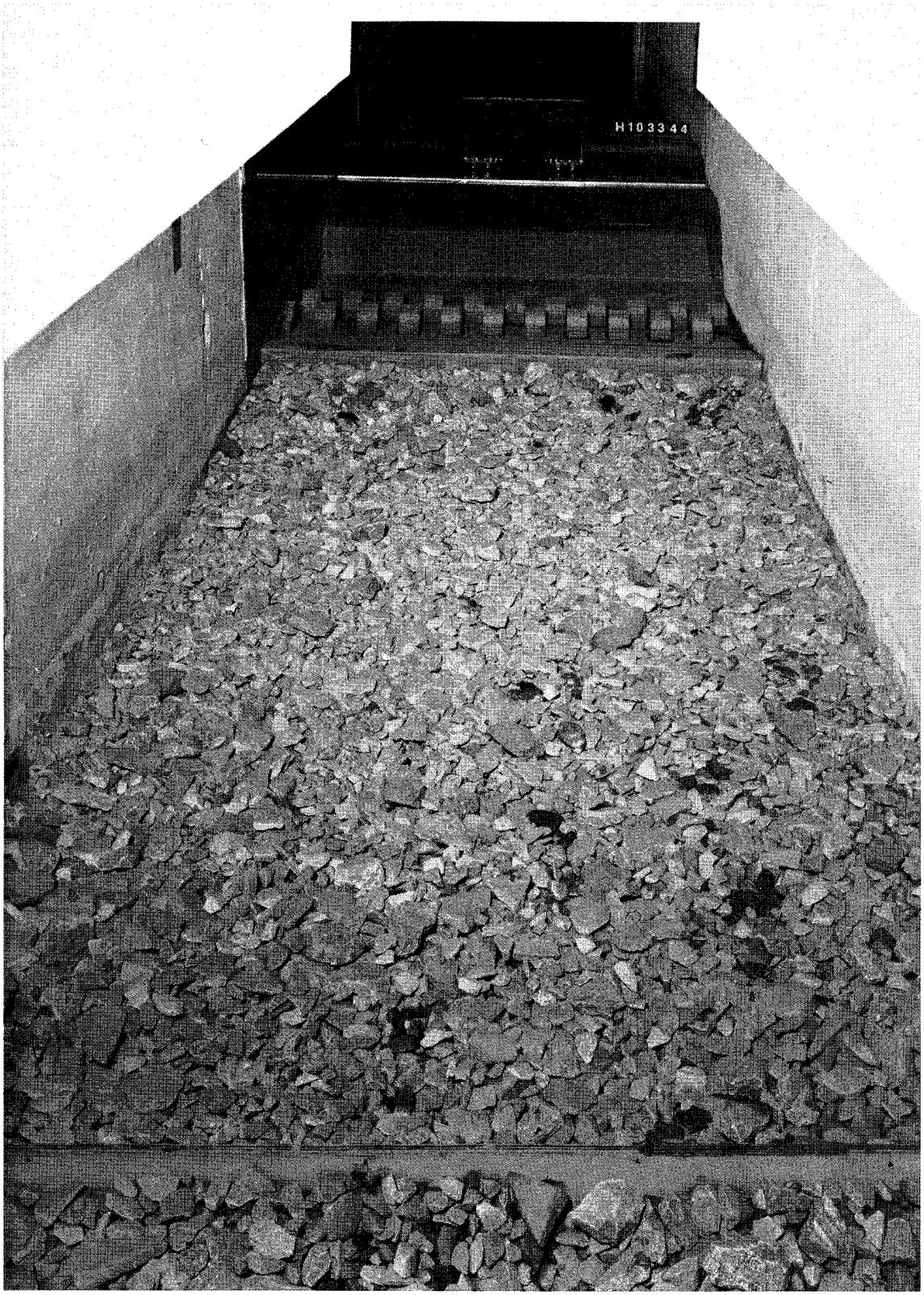

Figure 6. Riprap looking upstream

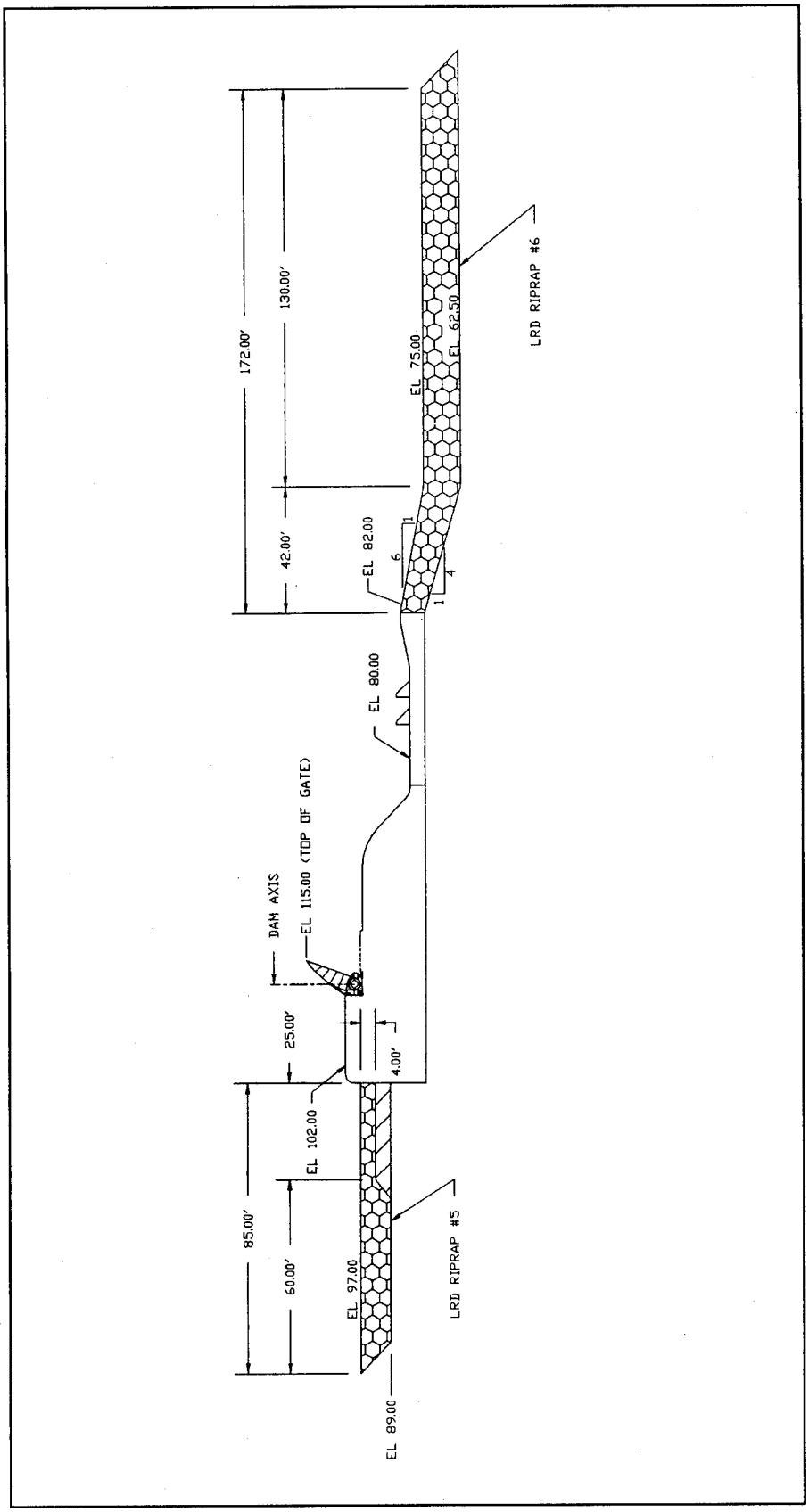

Figure 7. Riprap protection plan

5 Structural Model Analysis

General results of structural analyses and information pertinent to design hydraulic forces are discussed in this volume. Fundamental formulations of analyses of the gate system under hydrodynamic flow are discussed in Report 2.[1]

Phase 1, Design Reactions for Regular Operation

During the experiments with the physical model at WES, the maximum reaction response for regular operation was obtained when a unit discharge of water of 50 cfs ran over the system of fully raised gates (70-deg elevation) with the tailwater pool maintained at 95 ft (prototype level) and the headwater pool growing monotonically from about 114 to 119 ft (prototype level).

Semiempirical design values for the reactions at the bearing supports of the spillway gate and at the actuator cylinder were calculated for both the 1:15-scale physical model and the prototype. These design forces were obtained through finite element analyses of the corresponding structural idealizations subjected to a design distribution of the operational hydrodynamic pressure field acting on the fully raised gate.

Initially, the pressure field on the skin plate of the gate in operation was estimated analytically using two separate methods: a direct application of the theorem of moment of momentum and an implementation of the two-dimensional potential theory of hydrodynamics. Both techniques rendered similar results and were compared with the experimental pressure measurements. Plates 3 and 4 indicate the location of the 18 pressure cells (referred to prototype dimensions) equally distributed on the upstream (9 cells) and downstream (9 cells) sides of the gate to automatically record the time-histories of exerted pressures during the tests.

The first objective of the analysis was to formulate a plausible design

[1] Luis A. de Bejar. "Montgomery Point Lock and Dam Gate study; Report 2, Montgomery Point torque tube gate, a structural model study," Technical Report HL-95-14, U.S. Army Engineer Waterways Experiment Station, Vicksburg, MS.

pressure field to be applied to analytical models of the gate for finite element analyses, as schematically depicted by the displaced configuration in Plate 26. The pressure field is described along three different gate arcs: the left edge, the right edge, and the middle arc, looking in the downstream direction into the upstream side of the gate (Plate 27). Plate 28 shows the minimum and maximum values of the experimental pressure acting on the upstream side of the gate during the controlling 100-sec test. Notice that the curves represent polynomial fits on three data points, which explains the intersection between the upper and the lower bound curves for the middle arc toward the gate base. These minimum and maximum curves delimit narrow bands suggesting very little fluctuation of the pressure at a given location during the test. Notice also that the theoretical estimation of the pressure field is an upper bound over most of the domain, except on a small region toward the gate base.

The proposed design pressure line AB in Plate 29 represents a compromise between safety against the 100-sec tests and total safety against the pressure cell readings in the 200-sec tests. As the plate shows, during the 200-sec tests without nappe ventilation, some unconservative readings took place toward the gate ridge. However, due to certain practical difficulties during the installation of the pressure cells, there is reason to believe that these readings are slightly off their correct value, and therefore, to introduce further conservatism against them may not be justified. The following design pressure line was proposed as a reasonable envelope for both the theoretical estimations and the maximum readings during the experiments on the physical model:

$$p = 40 + 3.9\,s \quad [psf], \tag{4}$$

where s is the curvilinear coordinate, in., along the 1:15-scale gate arc and p is in lbf/ft^2.

This design pressure field was used as input for separate finite element analyses of the 1:15-scale physical model and the prototype. The physical model was built out of brass, for constructional convenience, on one central and two external supports, whereas the prototype will be constructed in structural steel, on five supports (one support under each external and internal edge of the torque-tubes and a central support). Plate 30 describes the labels attached to the various supports in the respective models. The structural geometries were constructed analytically using the preprocessor PATRAN-3, the finite element processes were executed by ABAQUS, and the postprocessing of output information was again effected by PATRAN-3.

Plate 31 shows the displaced shape of the 1:15-scale physical model subjected to the design pressure field given by Equation 4, and Table 1 reports the reaction forces acting on the three bearings. The upstream and downstream load cells at each support are labeled in Table 1 with numbers 1 and 2, respectively (refer to Report 2 for details on the instrumentation setup). Notice that

the results for only one edge support are reported in the table, since the results for the other edge support are identical, due to symmetry. The magnitude of total resultant bearing reaction turned out 50 percent higher than experimentally measured. The corresponding force in the actuator f_{CYL} was 131.4 lbf.

The prototype was next subjected to the design pressure field properly scaled (λ_p = 15), and Table 2 reports the reactive forces required for the actual design of the bearings. These reactions are for ideal conditions and do not consider any misalignment in the torque-tubes or imperfections in the construction. The corresponding force in the actuator cylinder F_{CYL} was 1,699.4 kips.

No indication of local yielding was detected during the finite element analysis of either gate.

Phase 2, Hydraulic Pressure Field for Unusual/Extreme Operations

In phase 2 of the experimental project, design total pressure lines were constructed for additional tests involving unusual/extreme loading conditions. Table 3 describes the characteristics of each test. Plates 32-51 present the most relevant deterministic information for the individual tests in the series (analytical expressions for each design pressure line appear at the bottom of each plot, referred to prototype dimensions). In general, for each reference longitude in the gate (i.e., right edge, middle arc, and left edge), two bound pressure fields are determined for each region, as measured experimentally. The upper bound curve is obtained from the maximum total pressure on the upstream side of the gate alone. The lower bound curve represents the maximum net pressure on the upstream side of the gate, obtained as the algebraic summation of the maximum and minimum pressure fields on the upstream and downstream sides of the gate, respectively. A parabolic polynomial was fitted to the three-point spectral data extracted from pressure cell time-histories of response along a given reference longitudinal arc of the gate during the experiments (100 sec per test).

In reviewing the data from this phase of the study, it was discovered that a key pressure cell had malfunctioned during the experiments. As indicated in Table 3, the controlling tests of the Phase 2 study were repeated and new design pressure fields on the gate generated.

The hydraulic pressure envelopes in Plates 50 and 51 refer to the prototype and are provided as information to the designer. They are expressed algebraically as follows:

a. For the right edge (Plate 51):

$$-80.0s + 1{,}000 \text{ lbf/ft}^2, \qquad 0 \le s < 5 \text{ ft}$$

$18.75s + 506.25$ lbf/ft^2, $5 \text{ ft} \le s < 13 \text{ ft}$,

$9.649s^2 - 169.1228s + 1{,}317.895$ lbf/ft^2, $13 \text{ ft} \le s < 20 \text{ ft}$

b. For the middle arc (Plate 50):

$16.2s^2 - 348.5s + 1{,}996.2$ lbf/ft^2, $0 \le s < 4.5$ ft,

$11.533s + 704.1$ lbf/ft^2, $4.5 \text{ ft} \le s < 15 \text{ ft}$,

$10.9s^2 - 193s + 1{,}319.6$ lbf/ft^2, $15 \text{ ft} \le s < 17.5$ ft.

c. For the left edge (Plate 51):

$-100.0s + 1{,}500$ lbf/ft^2, $0 \le s < 7$ ft,

$+ 800$ lbf/ft^2, $7 \text{ ft} \le s < 14.5 \text{ ft}$,

$127.27s - 1{,}045.46$ lbf/ft^2, $14.5 \text{ ft} \le s < 20 \text{ ft}$

These input forcing functions should be used in the context of allowable stress design for structural steel; i.e., there is no need for further factoring the loads since sufficient conservatism has already been built into the estimation procedure.

6 Discussion and Summary of Test Results

Initially, verification tests were conducted to ensure that the 1:15-scale section model would simulate and permit measurement of the magnitude and frequency of the hydraulic forces acting on the instrumented gate. Verification tests were accomplished by applying known forces to the gate and then evaluating the moment, magnitude, frequency, and symmetry of the forces detected by the gauges mounted in the operating arms and bearing blocks.

Hydraulic forces were measured during operation of the gate and for various gate positions and hydraulic conditions. The maximum force on the gate bearing blocks occurred with all gates in the raised position (70 deg). Maximum vertical and horizontal forces and moment of 120 and 119 kips and 130 kip-ft, respectively, were measured.

In general, the hydraulic forces in the tests of phase 2 of the experimental project were of larger magnitude than those in phase 1, due to larger unit discharges. The tests controlling the design hydraulic pressures are test 1192 (former test 1160), for the upper region of the gate, and tests 1179 and 1180 (former tests 1139 and 1140), for the intermediate and deep regions of the gate. All these tests feature the central and left gates in raised position. In tests 1179 and 1192, the right gate was also held raised; but in the case of test 1179, the central gate (instrumented) was kept stationary, whereas in test 1192, the central gate was lowered during the test (with the upstream pool maintained above the normal level, simulating improper operation). In test 1180, the right gate was held steadily in lowered position (with the upstream pool maintained at the peak level, simulating extreme normal operation).

Forces measured with the nappe vented and unvented revealed that venting the nappe only slightly reduced the magnitude of the static and pulsating forces. Forces on the gate derived from pressure measurements on the upstream and downstream faces of the gate were similar to those measured at the bearing blocks. Installation of nappe deflectors to vent the nappe and thereby reduce the differential pressure acting on the gate may not be justified.

Tests were conducted to measure the uplift forces acting on the gate due to

the passage (upstream and downstream) of a towboat over the lowered gates. Upstream passage of the boat generated more uplift on the gate than downstream passage. The maximum uplift force and moment measured at bearing block 2 were 38 kips and 62 kip-ft.

Evaluation of debris passage over the raised gates indicated that, for tailwater elevations between 102 and 115, debris would be retained on the downstream side of the gates in the hydraulic roller generated by the return flow. The debris did not attached to the downstream side of the gates. Debris circulating in the hydraulic roller would occasionally strike the gate, and impart a force that was detected by the gauges in the bearing blocks and operating arms. The tests indicated that debris was not a significant factor in hydraulic performance of the structure.

Forces and time-histories were documented for various flow conditions due to free-fall of the center gate. Free-fall of the gate due to barge impact was simulated by cutting a wire supporting the gate in the raised position. During free-fall of the gate the maximum reaction at bearing block 2 occurred at a gate angle of 10 deg. The vertical and horizontal forces and moment measured at the 10-deg gate angle were -80 and +25 kips and -45 kip-ft, respectively.

Hydraulic performance of the spillway was satisfactory and was documented for various gate openings, discharges, and upper and lower pool elevations. The spillway was calibrated for free and submerged flow conditions.

Tests were conducted with the pool elevation at the top of the raised gates (el 115.0) to determine the amount of leakage under and between the gates. Computations based on empirical results from the model indicated that the total leakage for the 10 prototype gates would be 1,720 cfs when the tailwater is below the bottom of the gates.

Water-surface profiles measured along the center line and right side of the center gate with the gate down for an upper pool of 119.0 and various tailwater elevations were documented.

Hydraulic performance of the stilling basin and the stability of riprap upstream and downstream of the spillway were evaluated. Stilling basin performance was documented with photographs and was satisfactory for all anticipated flow conditions, including single gate operation. Energy dissipation for all anticipated flow conditions was sufficient to prevent displacement of riprap downstream from the stilling basin. Riprap upstream of the spillway and downstream from the stilling basin was stable for all anticipated flow conditions.

The information provided in this report describes for the most adverse anticipated flow conditions the frequency and magnitude of the pulsating hydraulic force acting on the spillway gate. Also provided is hydraulic

performance relative to towboat and debris passage, spillway performance, and adequacy of the stilling basin and riprap located upstream and downstream from the spillway. The information in this report can be used to evaluate the safety of the structure, predict hydraulic performance of the structure, and to make structural improvements as necessary.

Table 1
Summary of Finite Element Analysis Bearing Reactions, 1:15-Scale Model (Three Supports)

Support Type	Force on Edge, lbf		Force on Center, lbf		Algebraic Sum of Components, lbf
	Load Cell 1	Load Cell 2	Load Cell 1	Load Cell 2	
Vertical component	25.32	-83.40	46.90	-91.73	-160.99
Horizontal component	41.00	41.00	41.90	41.90	247.80
Resultant force	48.19	92.93	62.89	100.85	295.50

Note: A minus sign indicates compressive force on the support.

Table 2
Summary of Finite Element Analysis Bearing Reactions, Prototype (Five Supports)

Support Type	Force, kips			
	External Edge	Internal Edge	Center	Algebraic Sum of Components, kips
Vertical component	-200.87	-221.61	-376.19	-1,221.15
Horizontal component	388.00	444.29	1,259.54	2,924.12
Resultant force	436.91	496.49	1,314.52	3,168.86

Note: A minus sign indicates compressive force on the support.

Table 3
Phase 2 Test Descriptions

Test	Head-Water El	Tail-Water El	Left Gate Position	Initial Center Gate Position	Center Gate Position	Right Gate Position	Remarks
1129-30	115.0	115.0	Lowered/ Lock wall	Lowered	Raising	Lowered	Raising first gate during normal operation when tailwater is falling. Test for interior gate and end gate.
1164-65	115.0	115.0	Lowered/ Lock wall	Raised	Lowering	Lowered	Lowering last gate during normal operation when tailwater is rising. Test for interior gate and end gate.
1133-34	119.0	115.0	Raised	Lowered	Raising	Raised/ Lock wall	Raising last gate during normal operation when tailwater is falling. Test interior gate and end gate.
1166-67	119.0	115.0	Raised	Raised	Lowering	Raised/ Lock wall	Lowering first gate during normal operation when tailwater is rising. Test interior gate and end gate.
1136	119.0	115.0	Raised	Raised	Hold	Raised	Normal operation
1137	119.0	115.0	Raised	Raised	Hold	Lowered	Normal operation
1138	119.0	115.0	Lowered	Raised	Hold	Lowered	Normal operation
(1139)[1] 1179	119.0	95.0	Raised	Raised	Hold	Raised	Normal operation
(1140) 1180	119.0	95.0	Raised	Raised	Hold	Lowered	Normal operation
(1141) 1181	116.8	95.0	Lowered	Raised	Hold	Lowered	Normal operation
(1143) 1183	119.0	95.0	Raised	Raised	Lowering	Raised	Normal operation. Lowering gate(s) to maintain maximum headwater el 119.0.
(1144) 1184	117.0	95.0	Raised	Raised	Lowering	Lowered	Normal operation. Lowering gate(s) to maintain maximum headwater el 119.0.
(1145) 1187	116.8	95.0	Lowered	Raised	Lowering	Lowered	Normal operation. Lowering gate(s) to maintain maximum headwater el 119.0.

(Continued)

[1] Number in parentheses refers to previous test label (tests were rerun).

Table 3 (Concluded)

Test	Head-Water El	Tail-Water El	Left Gate Position	Initial Center Gate Position	Center Gate Position	Right Gate Position	Remarks
1147	119.0	95.0	Raised	Lowered	Hold	Raised	Normal operation. Gate has been lowered to maintain maximum headwater el 119.0.
1148	119.0	95.0	Raised	Lowered	Hold	Lowered	Normal operation. Gate has been lowered to maintain maximum headwater el 119.0.
1149	119.0	95.0	Lowered	Lowered	Hold	Lowered	Normal operation. Gate has been lowered to maintain maximum headwater el 119.0.
1170-77	115.0	115.0	Lowered	Lowered	Hold	Lowered	Measure uplift during high stages.
1150	120.0	120.0	Lowered	Lowered	Hold	Lowered	Measure uplift during high stages. If uplift increases over 1170-77, increase height of flume and test elevations 125 and 130.
(1152) 1188	115.0	95.0	Raised	Lowered	Raising	Raised	Raising gate which has been lowered to maintain maximum head-water el 119.0.
(1153) 1189	115.0	95.0	Raised	Lowered	Raising	Lowered	Raising gate which has been lowered to maintain maximum head-water el 119.0.
(1154) 1190	119.0	95.0	Raised	Lowered	Raising	Lowered	Raising gate after accident, operator error, etc.
(1155) 1191	117.0	95.0	Raised	Lowered	Raising	Raised	Raising gate after accident, operator error, etc.
1157	121.0	115.0	Raised	Raised	Hold	Raised	Pool above normal level due to improper operation.
1158	121.0	115.0	Raised	Raised	Hold	Lowered	Pool above normal level due to improper operation.
(1160) 1192	121.0	115.0	Raised	Raised	Lowering	Raised	Pool above normal level due to improper operation.
1161	121.0	115.0	Raised	Raised	Lowering	Lowered	Pool above normal level due to improper operation.

a. Unit discharge 16.7 cfs/ft; pool el 115.5; tailwater el 95.0

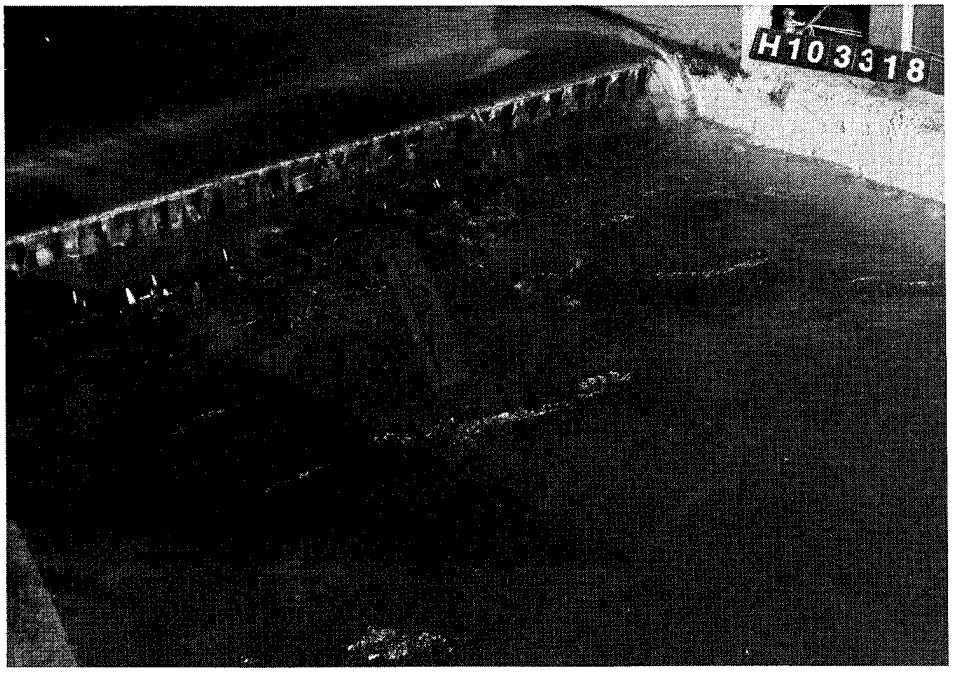

b. Unit discharge 50 cfs/ft; pool el 119; tailwater el 110

Photo 1. Various flow conditions, all gates 70 deg (Continued)

c. Unit discharge 50 cfs/ft; pool el 120; tailwater el 115

Photo 1. (Concluded)

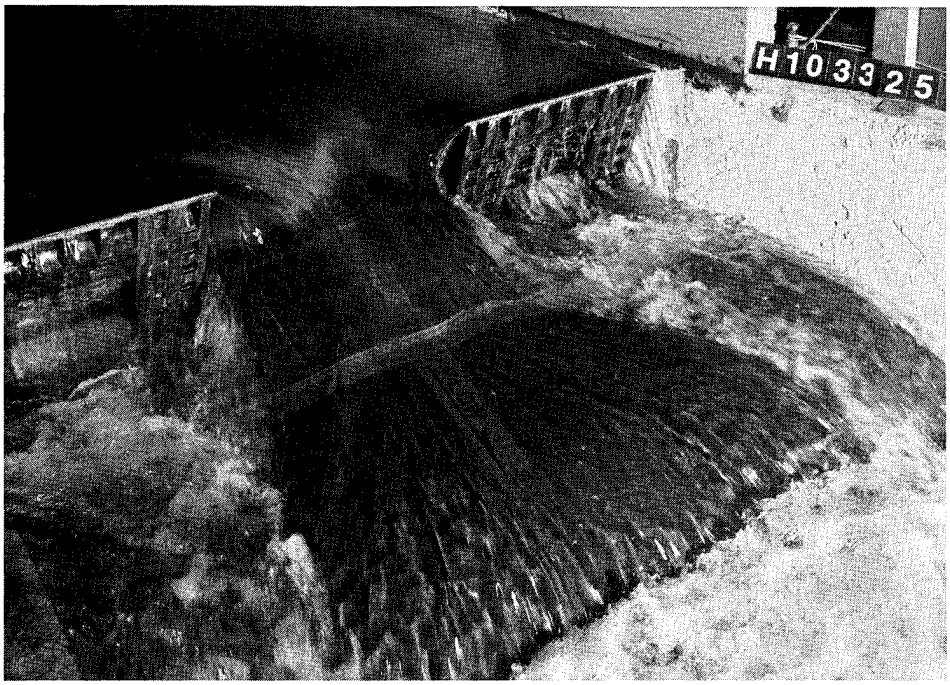

a. Pool el 115.0; center gate 0 deg; side gates 70 deg

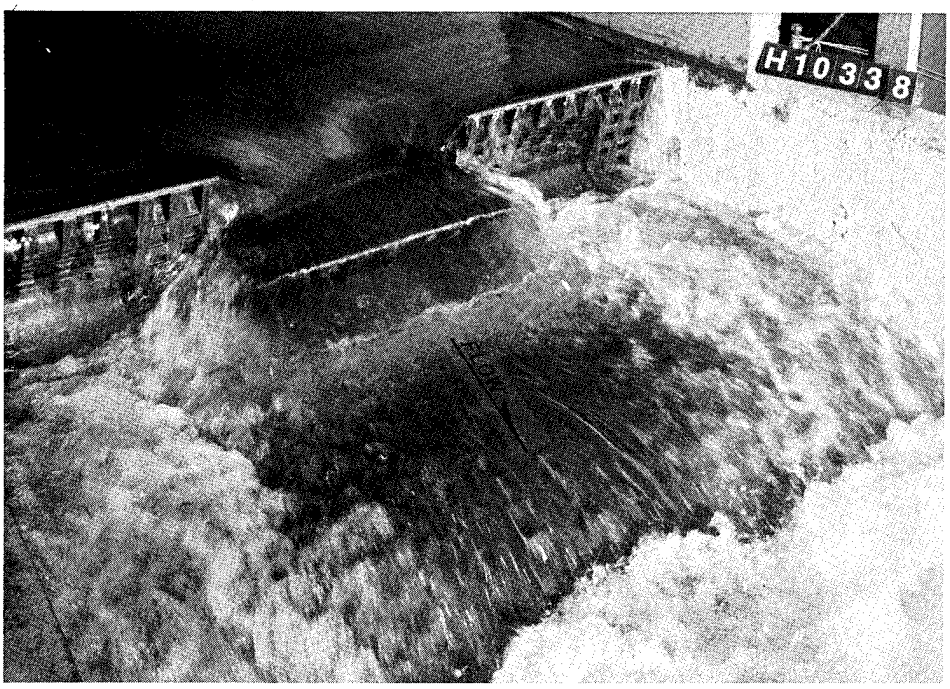

b. Pool el 118.2; center gate 60 deg; side gates 70 deg

Photo 2. Various gate positions, unit discharge 50 cfs/ft; tailwater el 95.0 (Continued)

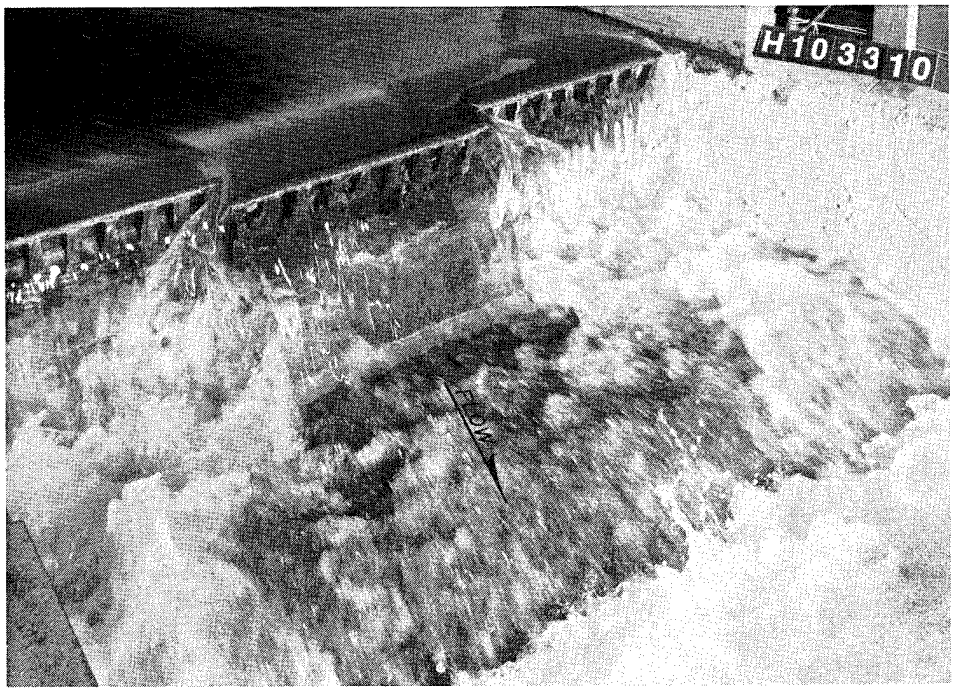

c. Pool el 118.2; center gate 60 deg; side gates 70 deg

Photo 2. (Concluded)

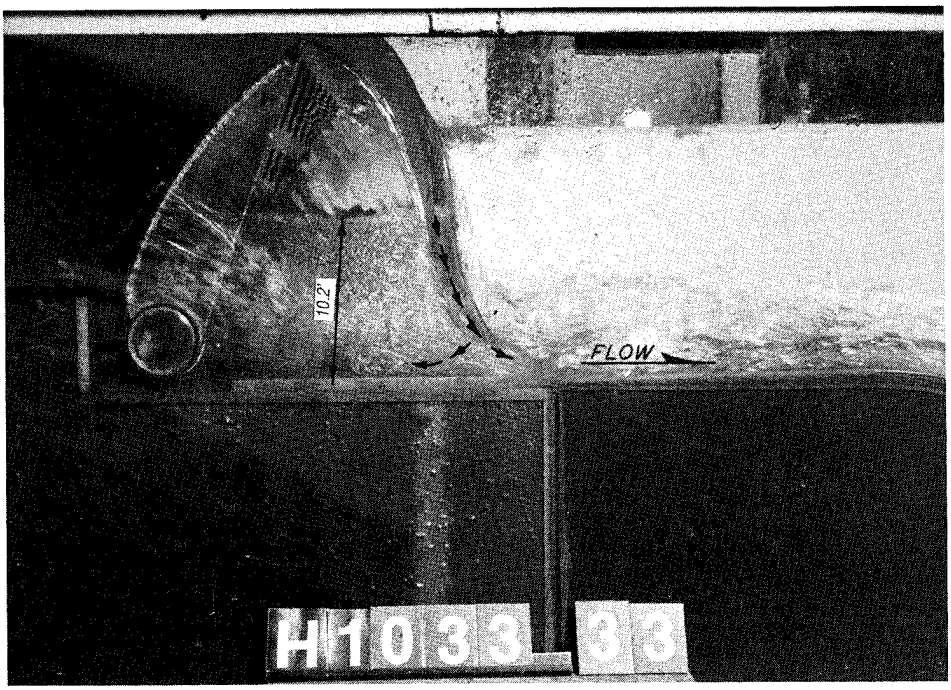

a. Profile

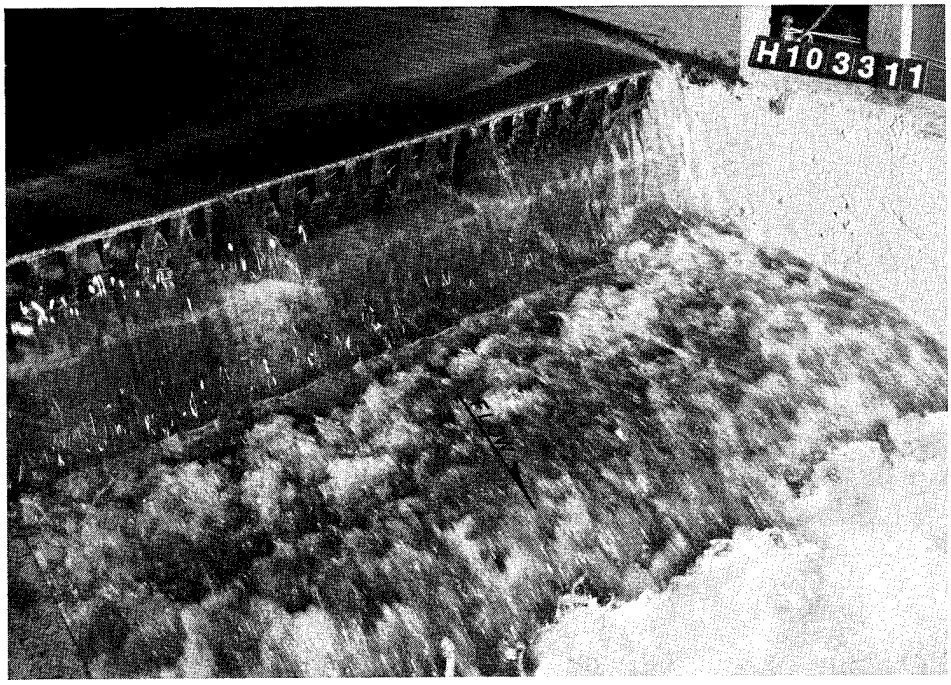

b. Downstream view

Photo 3. Unvented nappes, unit discharge 50 cfs; pool el 119.2; tailwater el 95.0; all gates open 70 deg

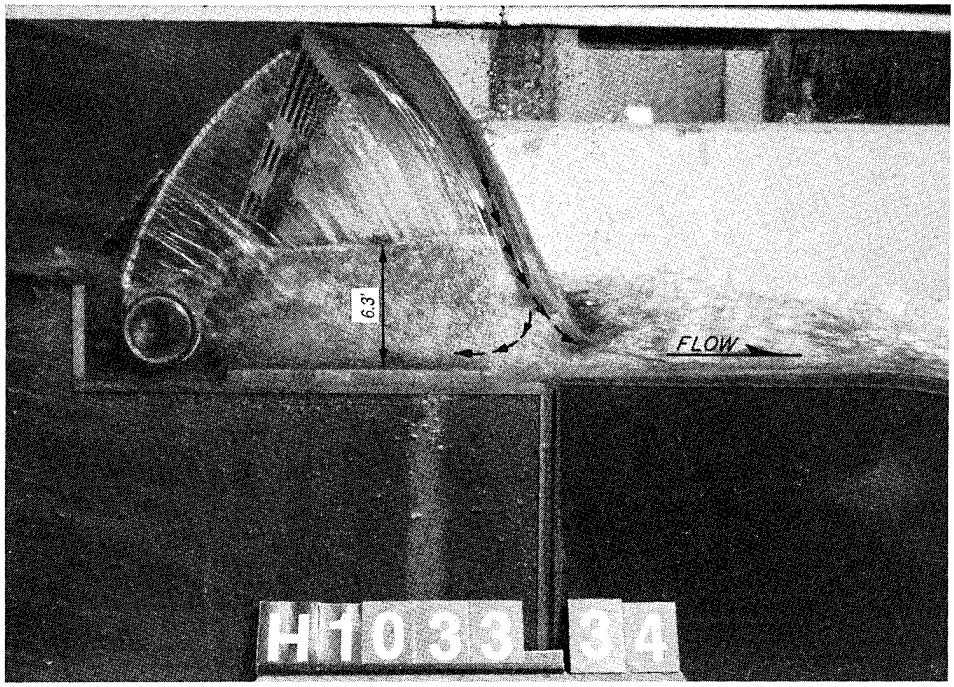

a. Profile

b. Downstream view

Photo 4. Vented nappes, unit discharge 50 cfs; pool el 119.2; tailwater el 95.0; all gates open 70 deg

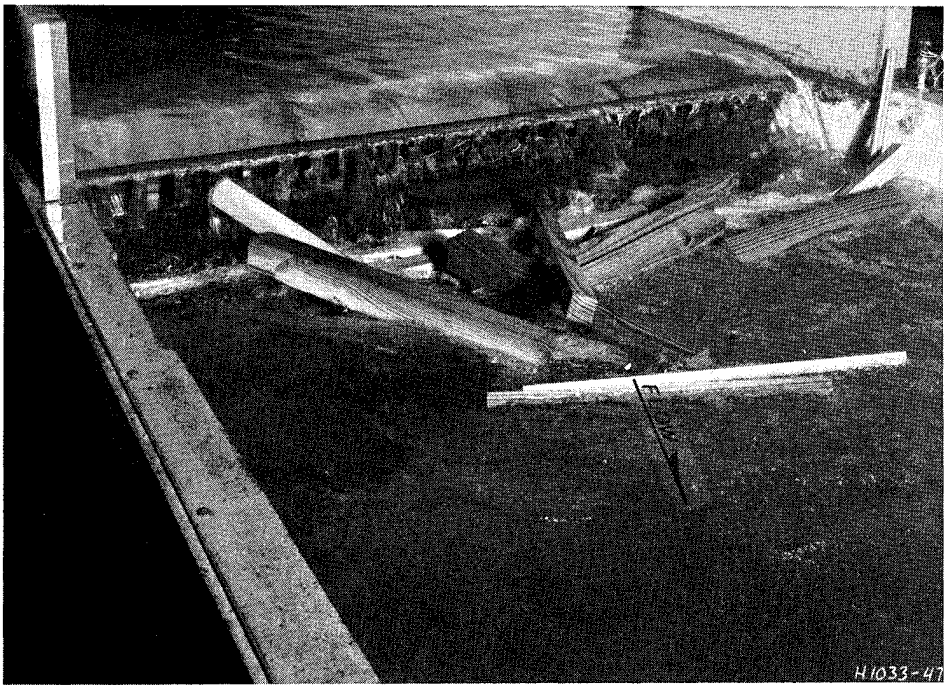

a. Viewed from downstream

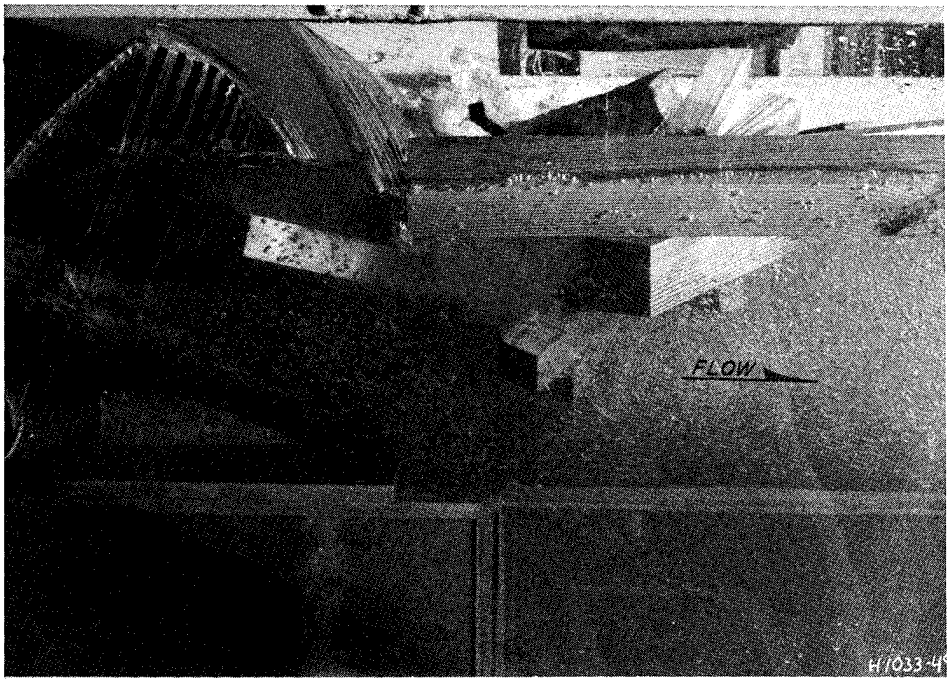

b. Profile

Photo 5. Debris passage, discharge 50 cfs/ft; pool el 119.3; tailwater el 110.0

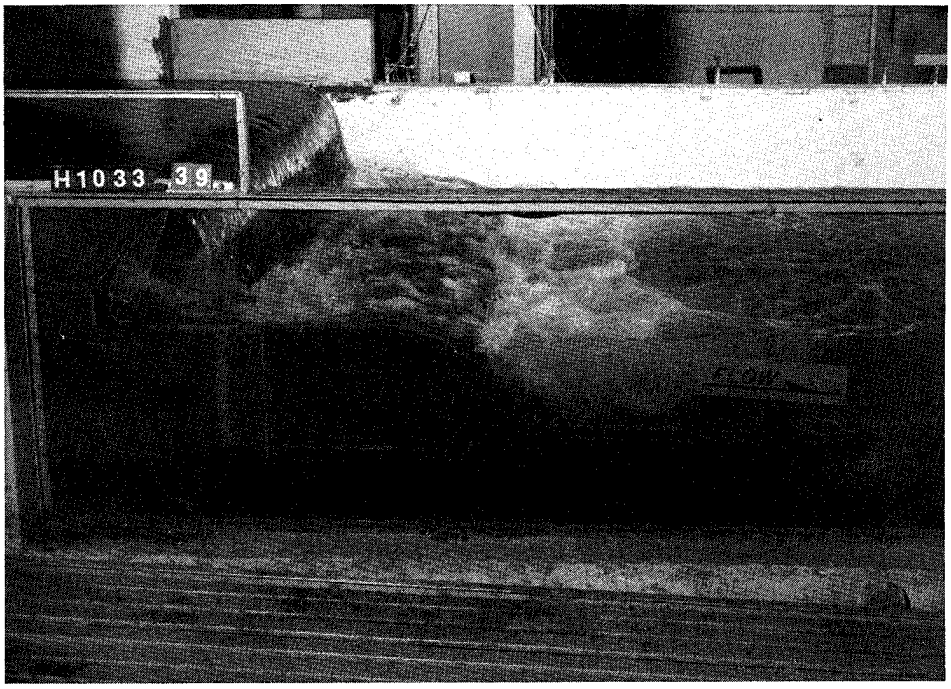

a. Unit discharge 50 cfs/ft; pool el 119.3; tailwater el 95.0; all gates 70 deg

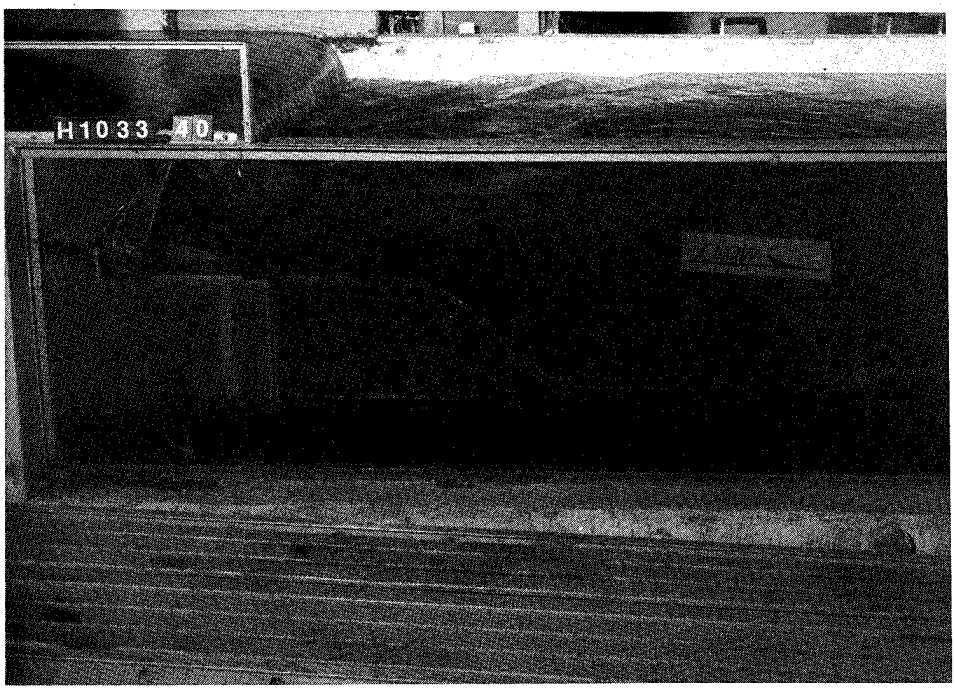

b. Unit discharge 50 cfs/ft; pool el 119.4; tailwater el 110.0; all gates 70 deg

Photo 6. Stilling basin performance (Sheet 1 of 3)

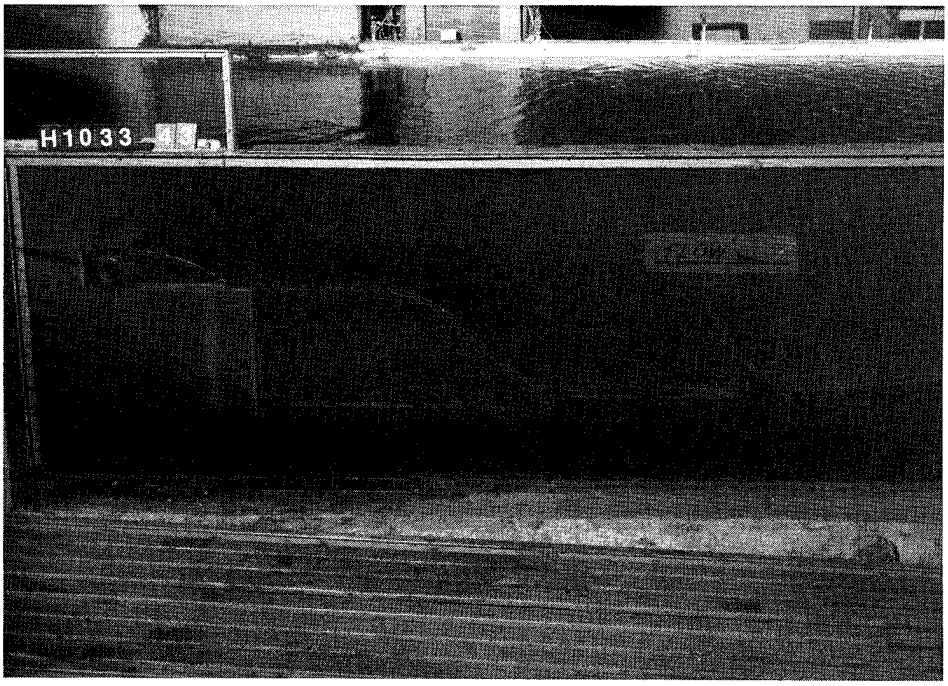

c. Unit discharge 50 cfs/ft; pool el 115.1; tailwater el 115.0; all gates 0 deg

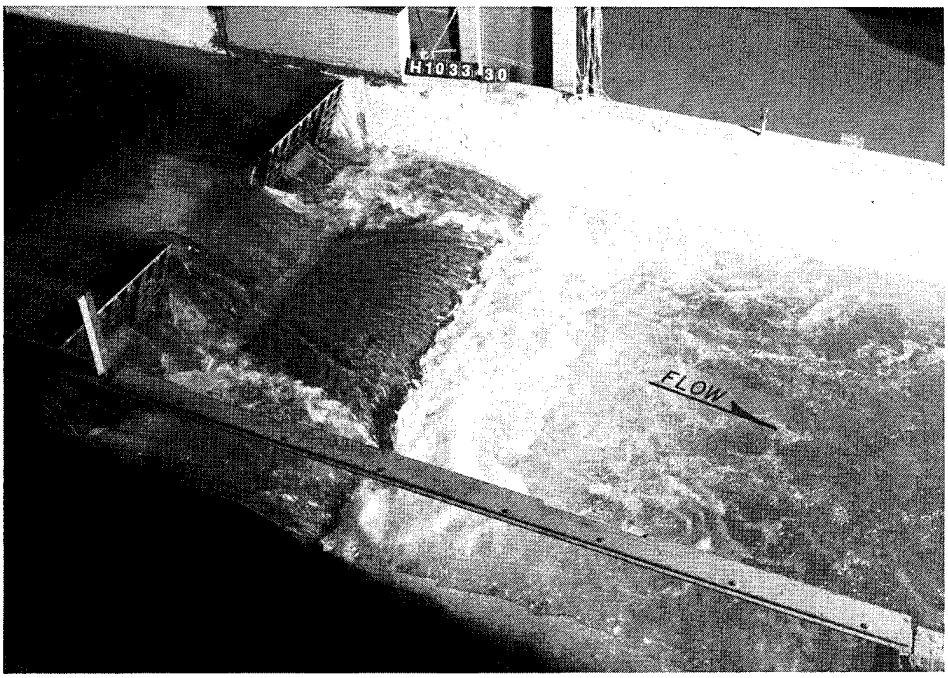

d. Unit discharge 58.9 cfs/ft; pool el 115.0; tailwater el 95.0; center gate 0 deg; side gates 70 deg

Photo 6. (Sheet 2 of 3)

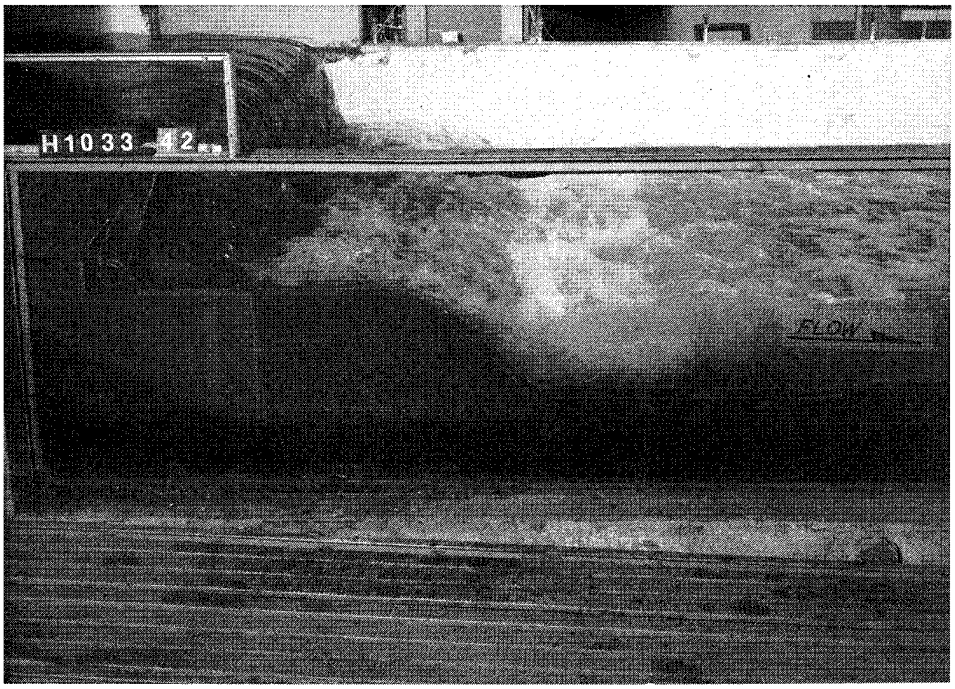

e. Unit discharge 83.3 cfs/ft; pool el 121.0; tailwater el 95.0; all gates 70 deg

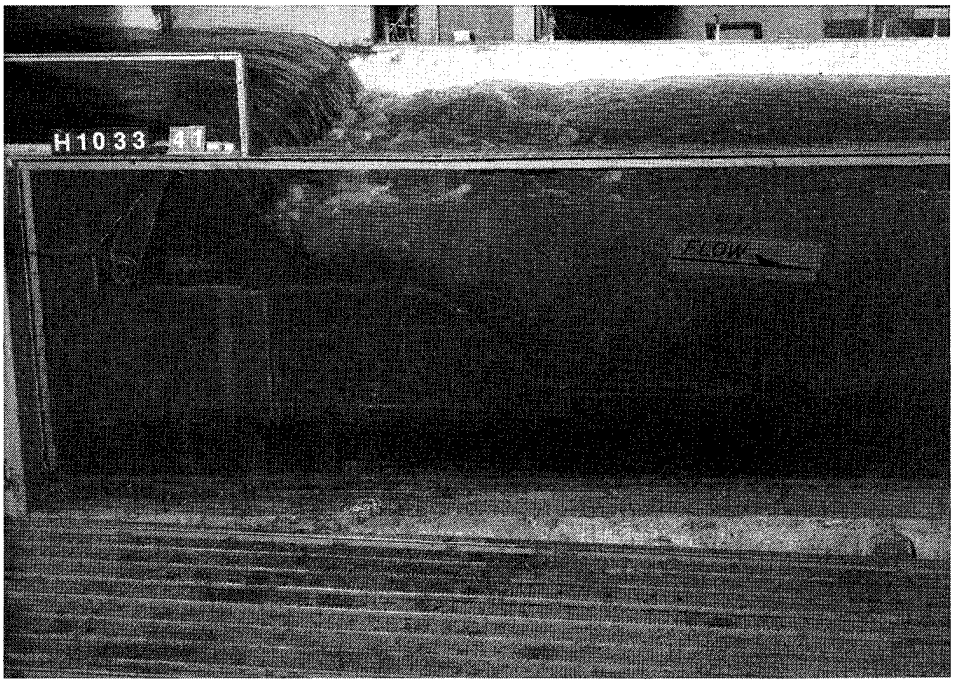

f. Unit discharge 100 cfs/ft; pool el 122.0; tailwater el 110.0; all gates 70 deg

Photo 6. (Sheet 3 of 3)

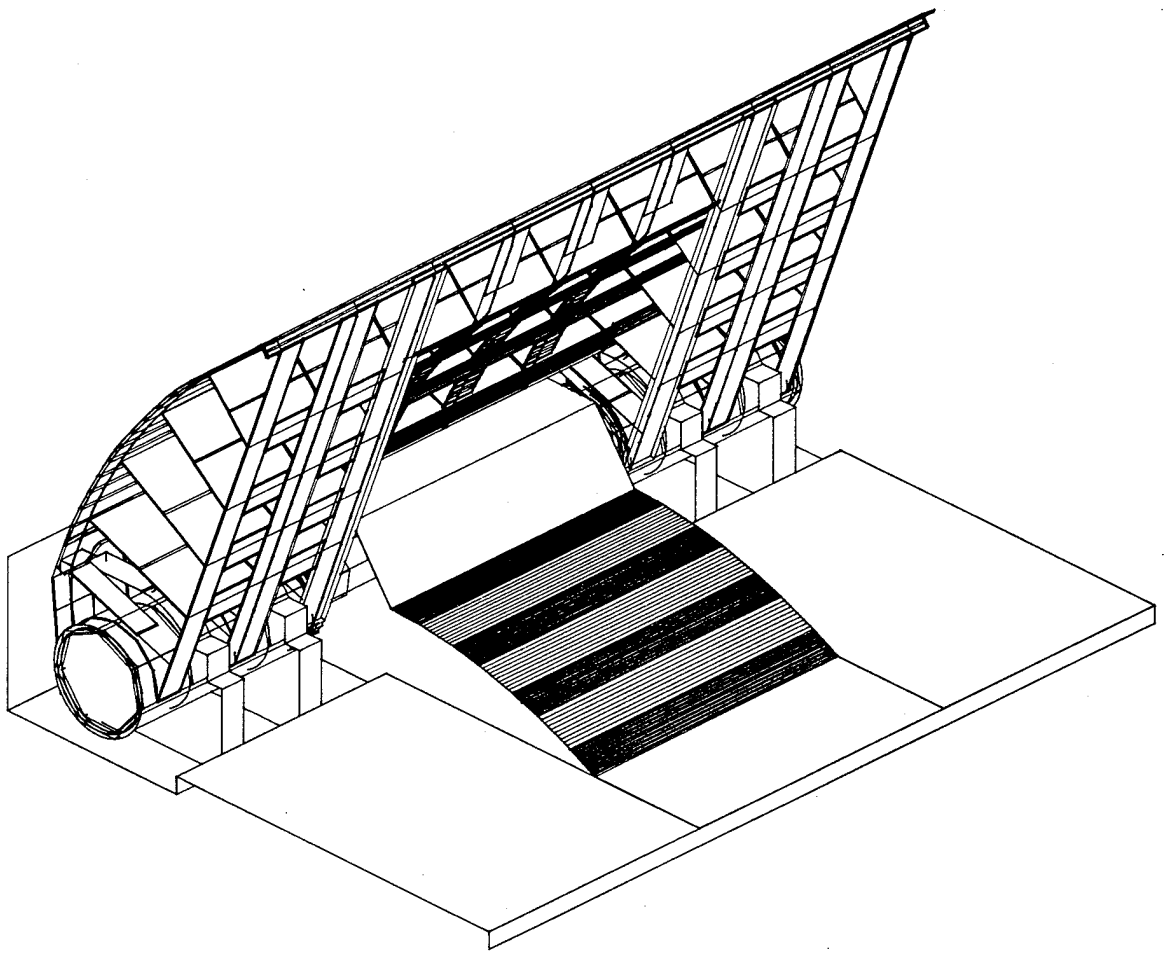

TYPICAL SPILLWAY GATE

Plate 1

Plate 2

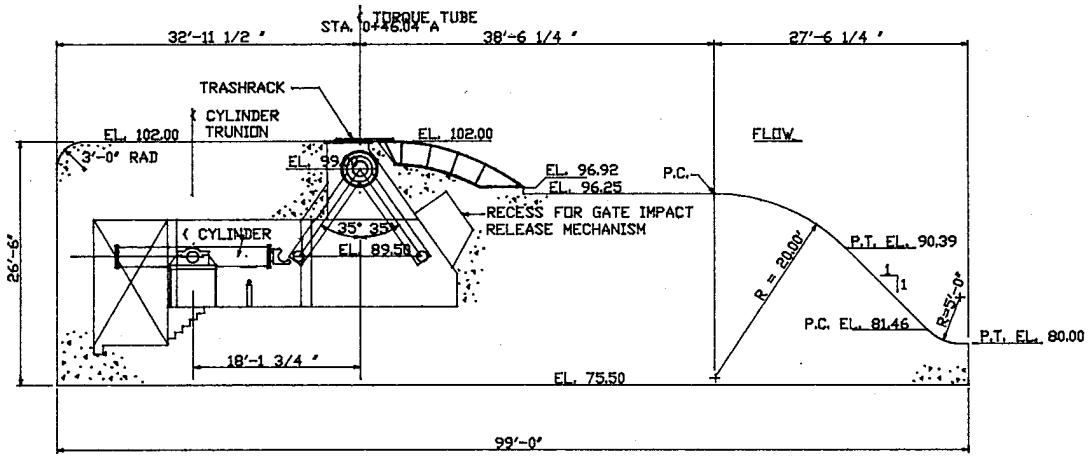

SECTION THRU NAVIGABLE PASS MONOLITH
(CENTER OF GATE)

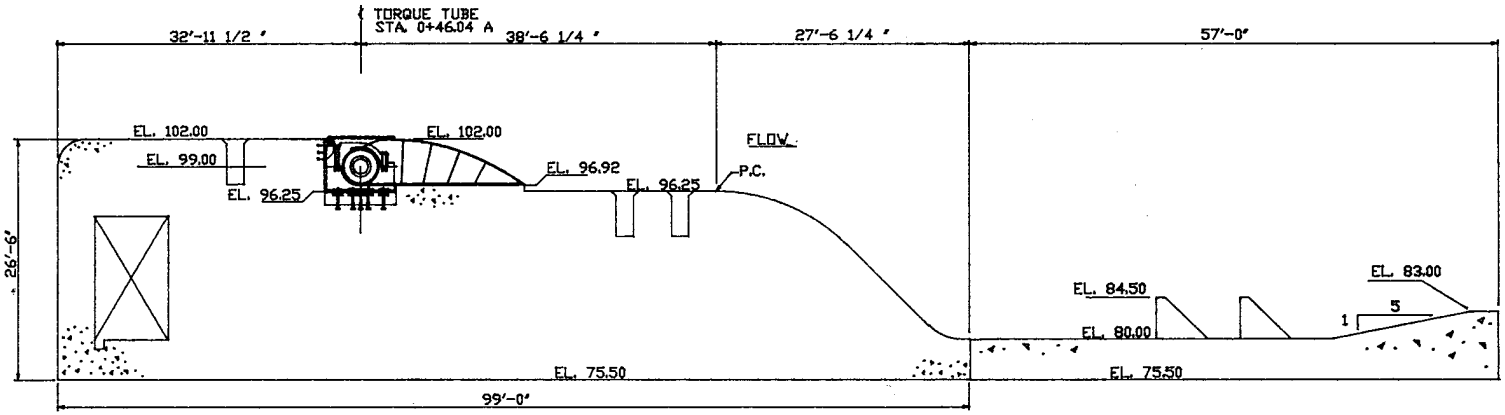

SECTION THRU NAVIGABLE PASS MONOLITH
(ENDS OF GATE)

CENTER AND END SECTIONS

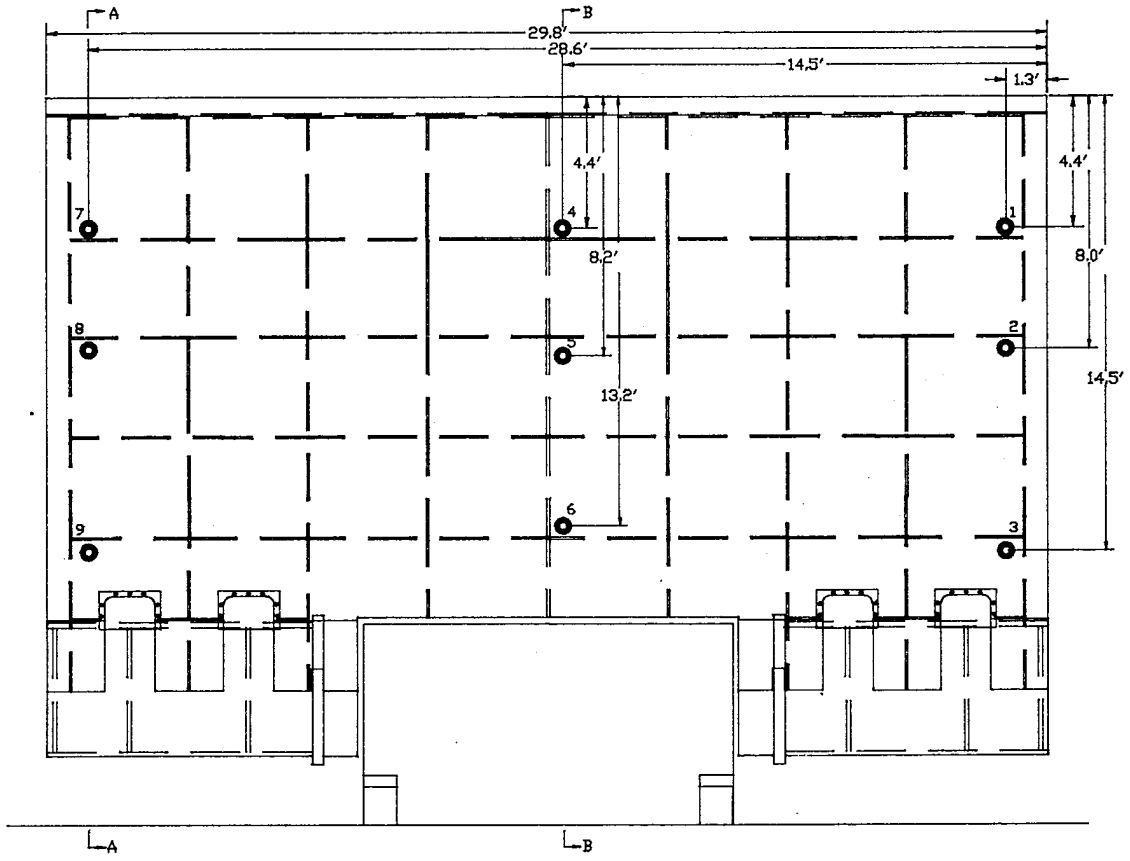

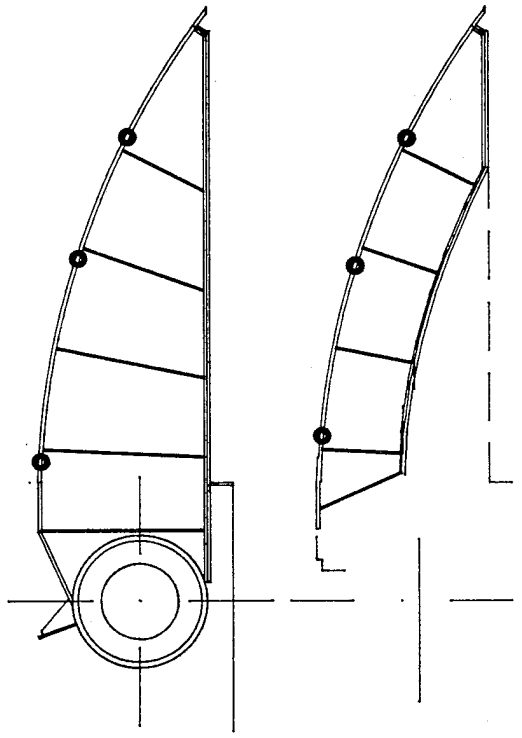

LEGEND

PRESSURE GUAGES

UPSTREAM VIEW OF GATE

Plate 3

Plate 4

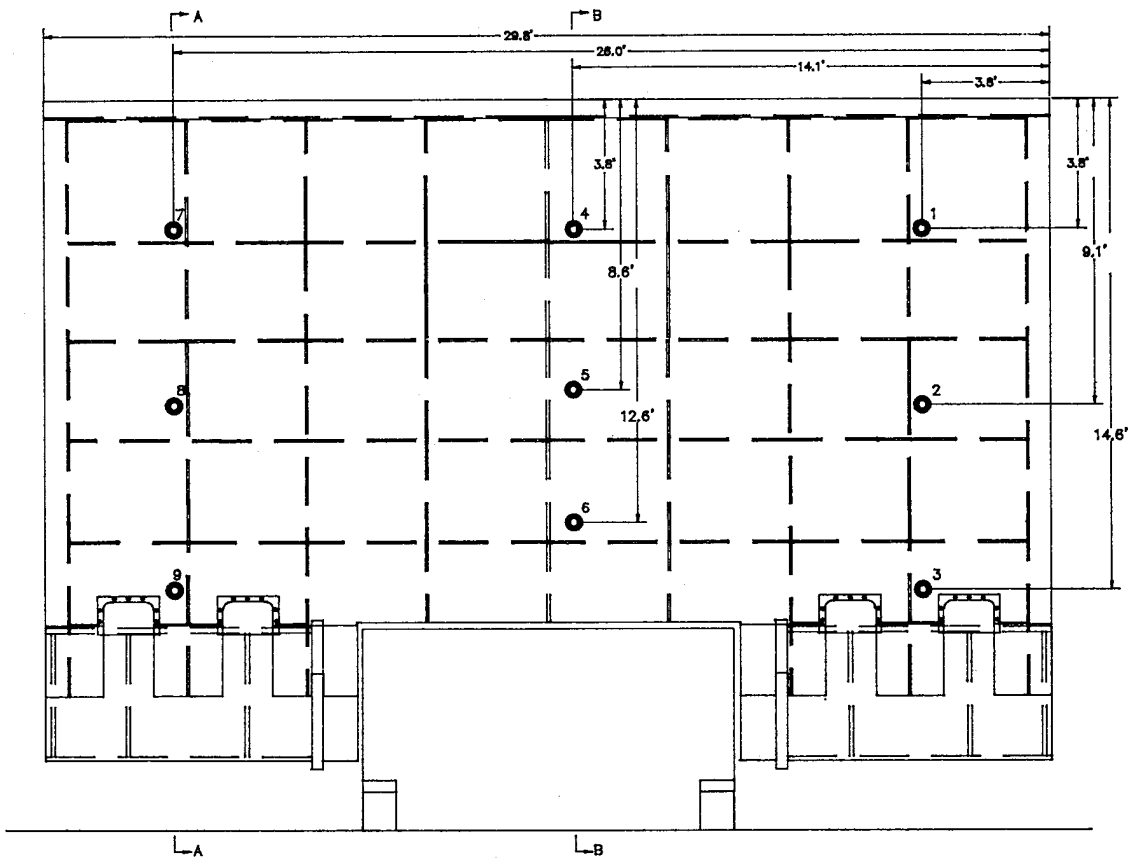

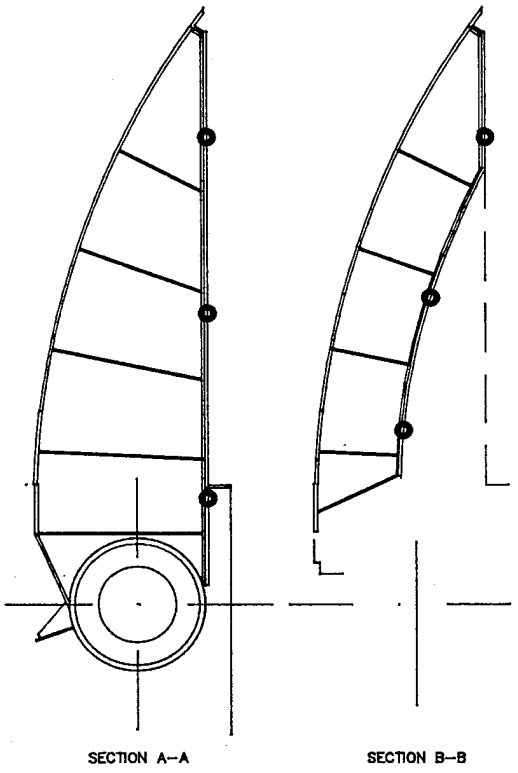

LEGEND

PRESSURE GUAGES

DOWNSTREAM VIEW OF GATE

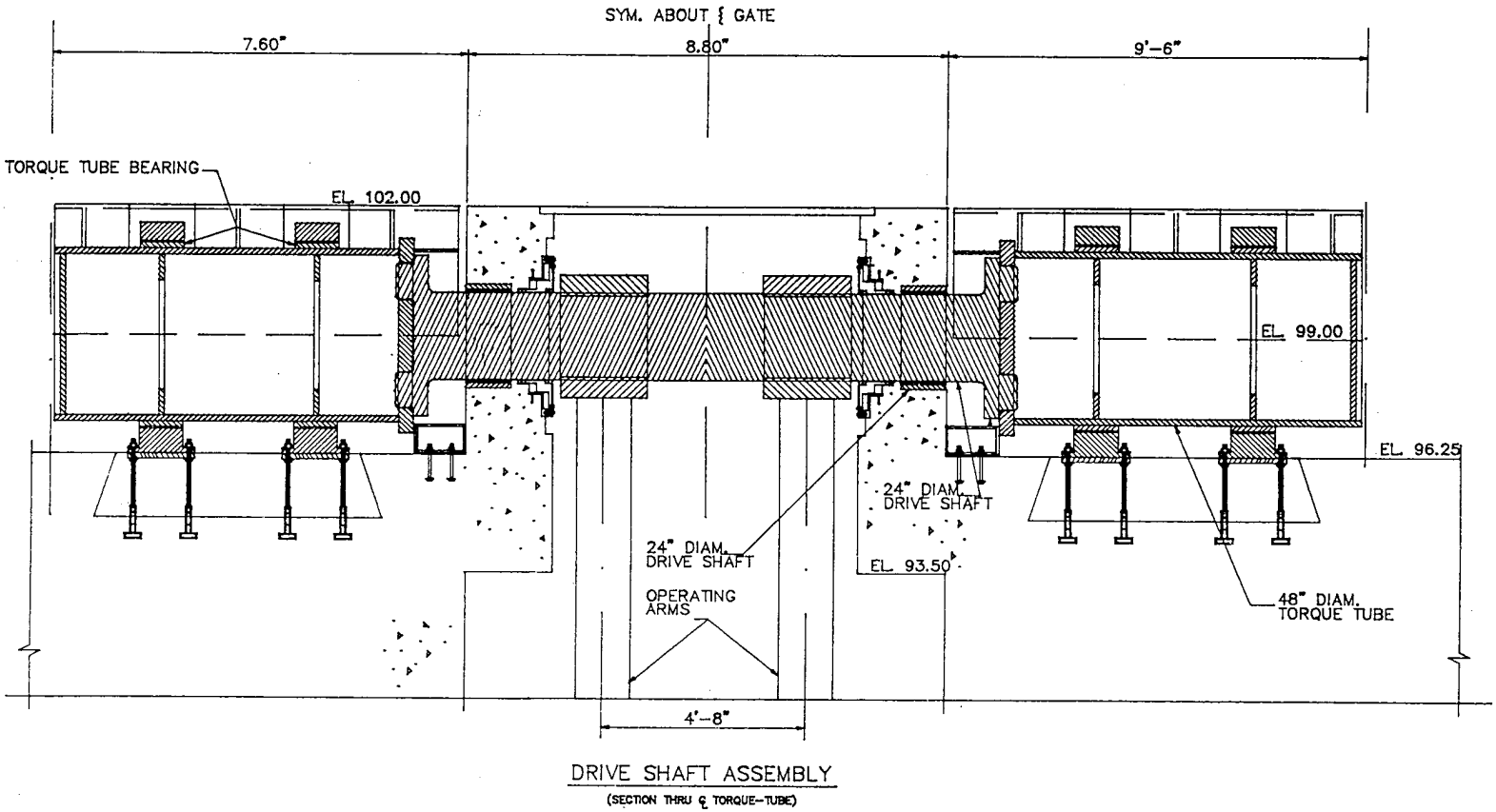

DRIVE SHAFT ASSEMBLY

(SECTION THRU ℄ TORQUE-TUBE)

SECTION THROUGH TORQUE TUBES

Plate 5

Plate 6

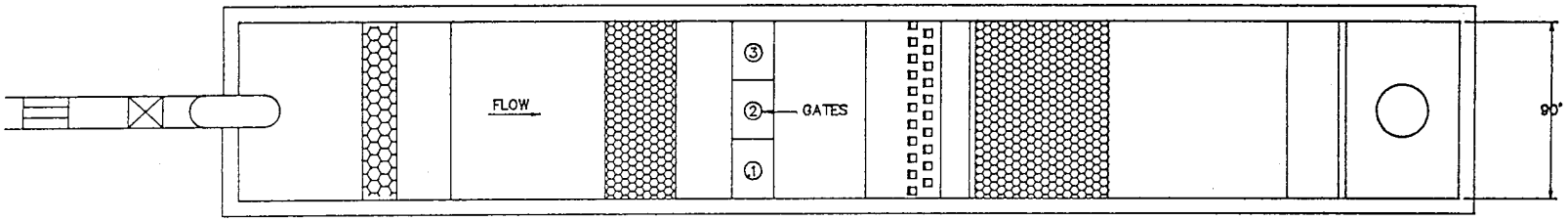

PLAN

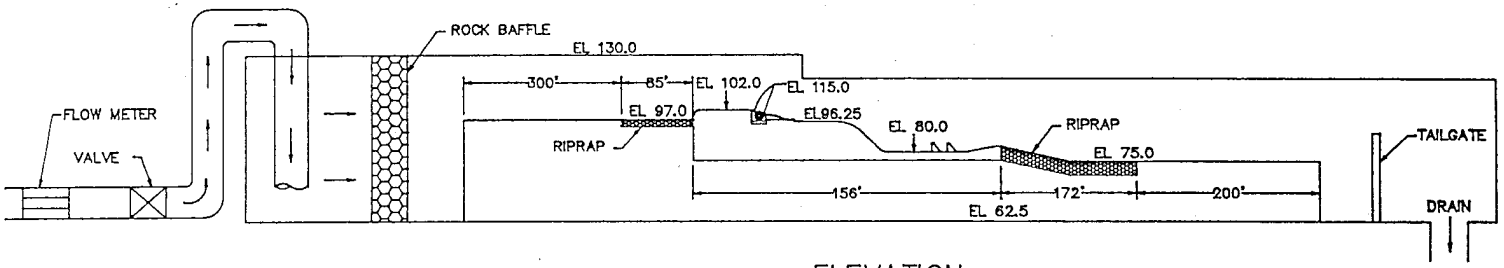

ELEVATION

1:15 SCALE SECTION MODEL
PLAN AND ELEVATION

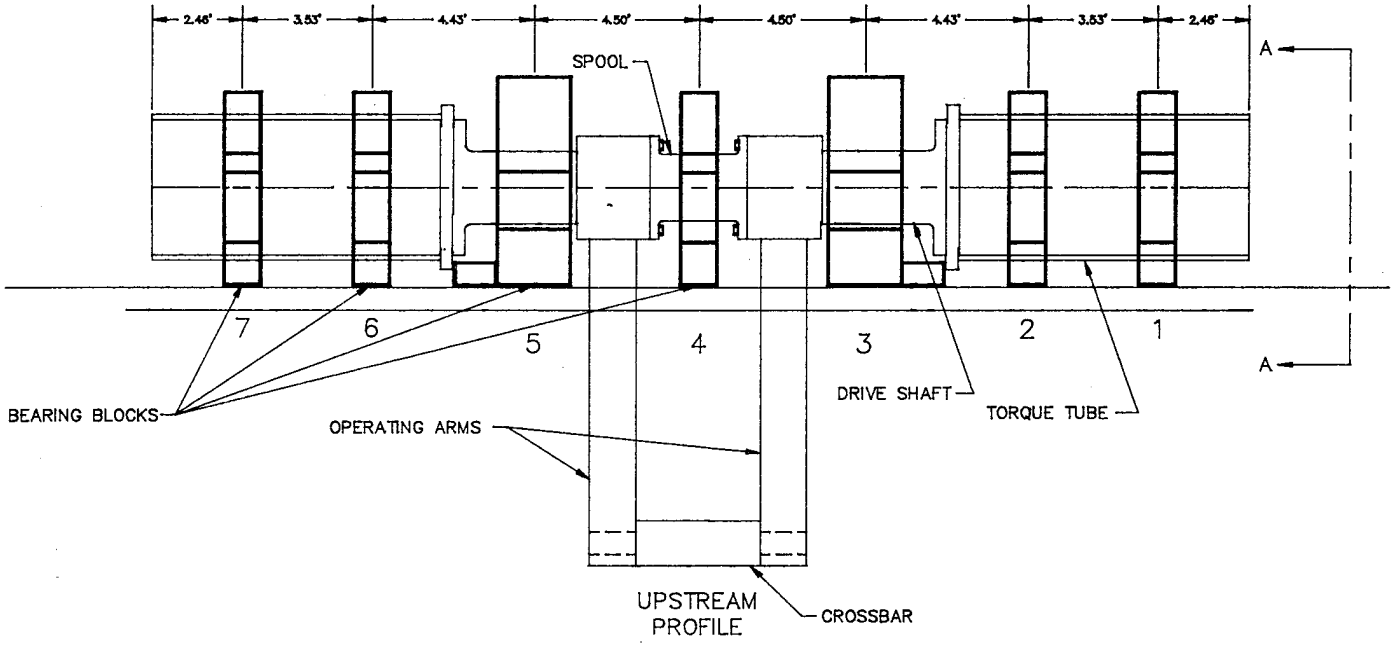

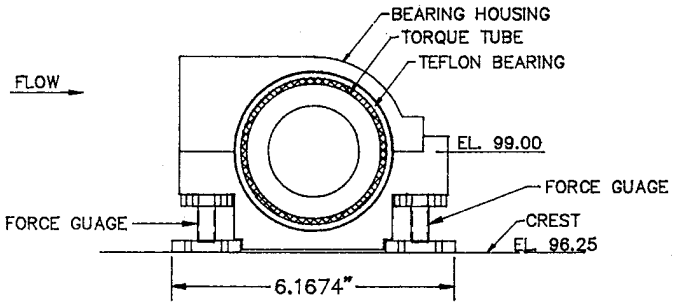

SECTION A–A

TORQUE TUBE, SPOOL, AND DRIVE SHAFT BEARING BLOCKS

Plate 7

Plate 8

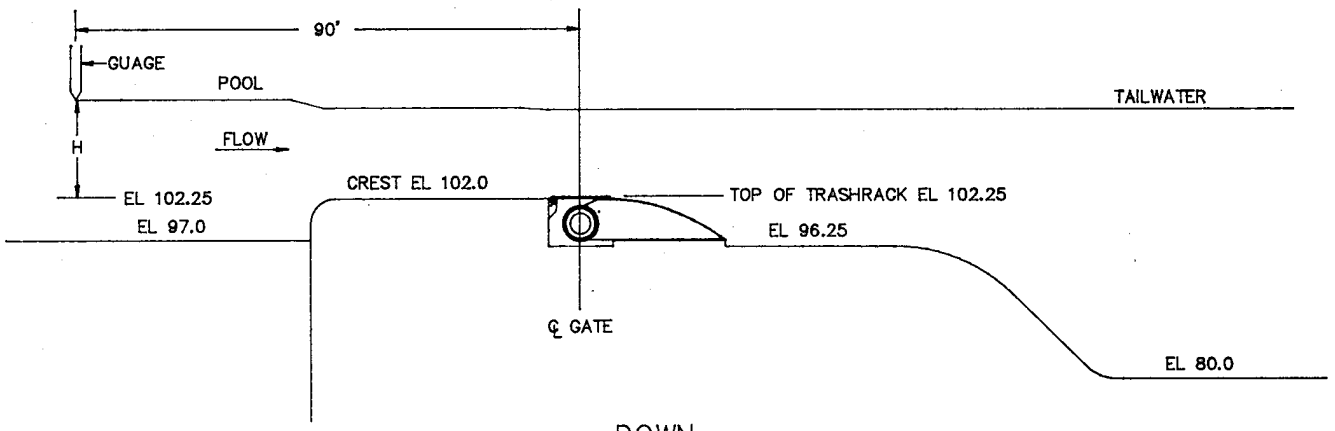

DOWN

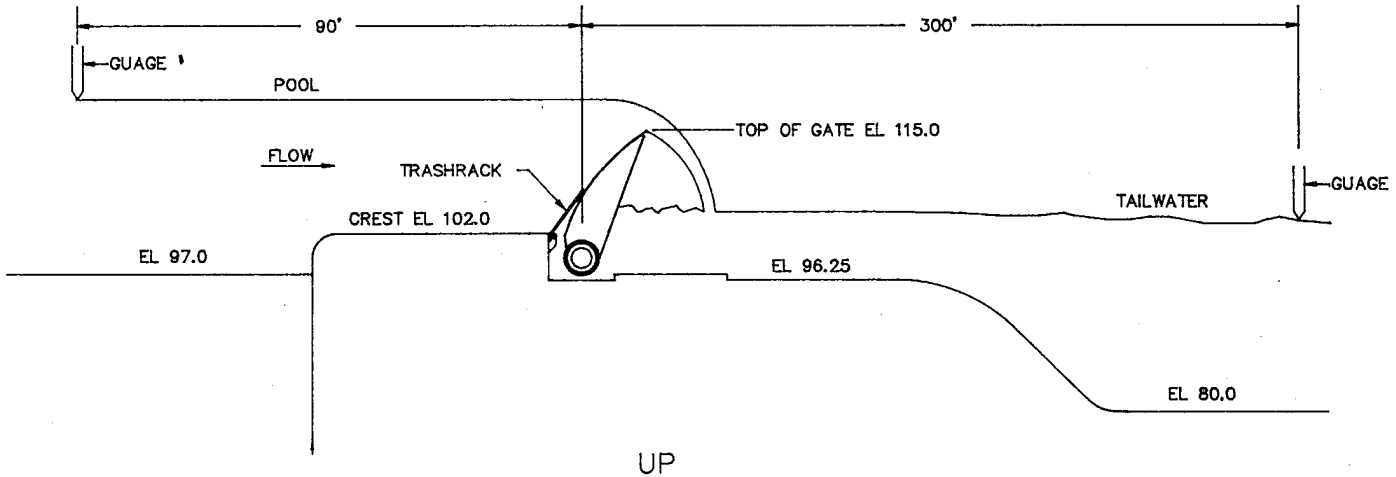

UP

GATE POSITIONS

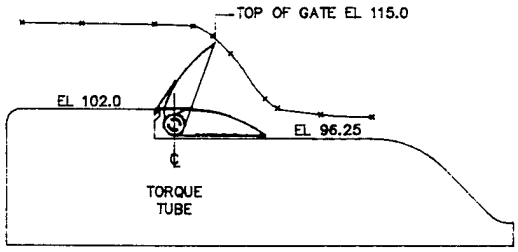

RIGHT SIDE OF CENTER BAY

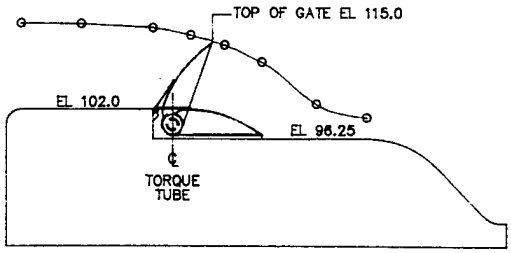

CENTER LINE OF CENTER BAY

a. TAILWATER EL 95
CENTER GATE DOWN
SIDE GATES UP

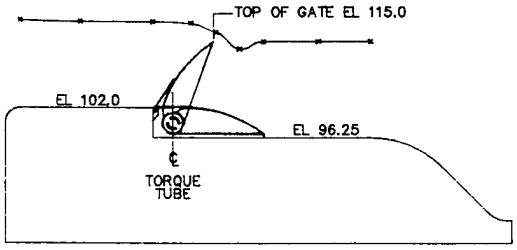

RIGHT SIDE OF CENTER BAY

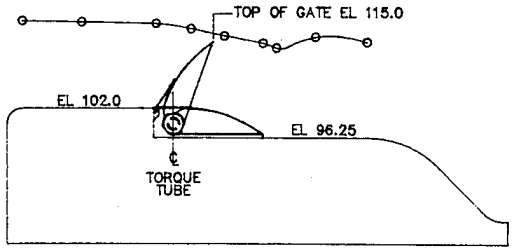

CENTER LINE OF CENTER BAY

b. TAILWATER EL 115
CENTER GATE DOWN
SIDE GATES UP

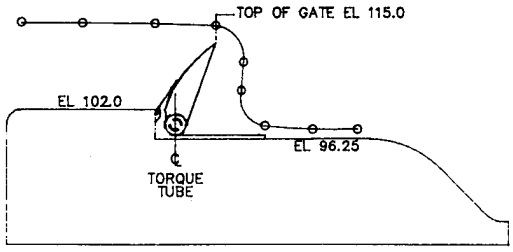

CENTER LINE OF CENTER BAY

c. TAILWATER EL 95
ALL GATES UP

WATER-SURFACE PROFILES
CENTER GATE BAY
POOL EL 119.0

Plate 9

Plate 10

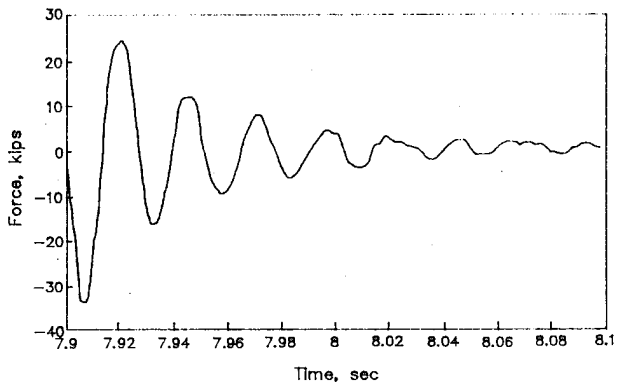

TIME-HISTORY

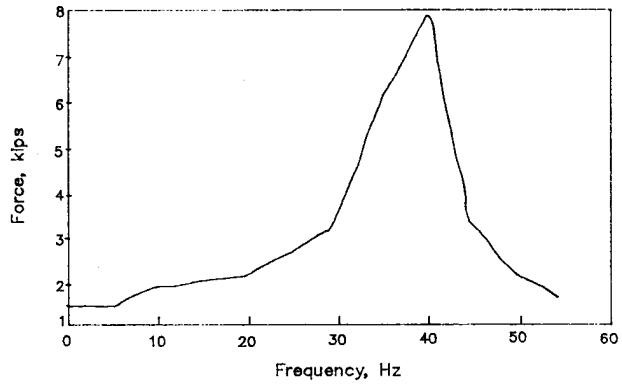

FREQUENCY RESPONSE

HORIZONTAL

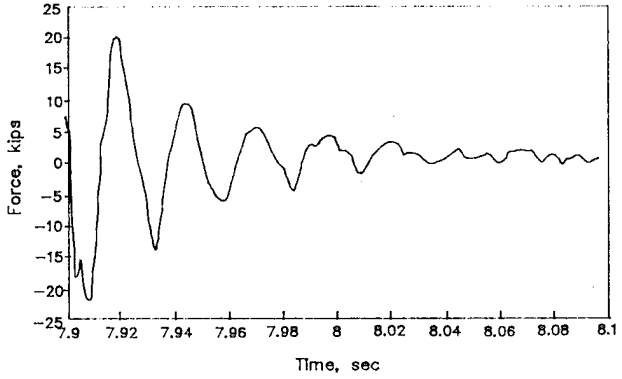

TIME-HISTORY

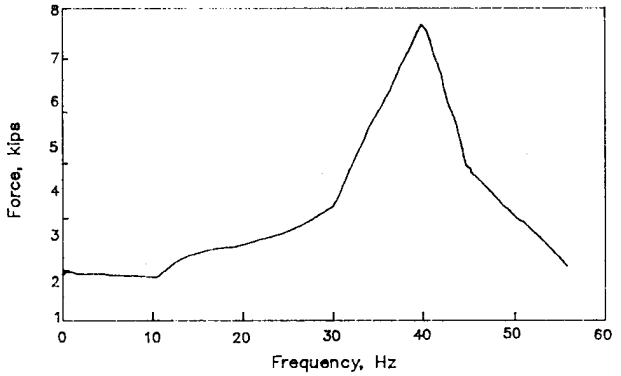

FREQUENCY RESPONSE

VERTICAL

TIME-HISTORY AND FREQUENCY RESPONSE BEARING BLOCK 2

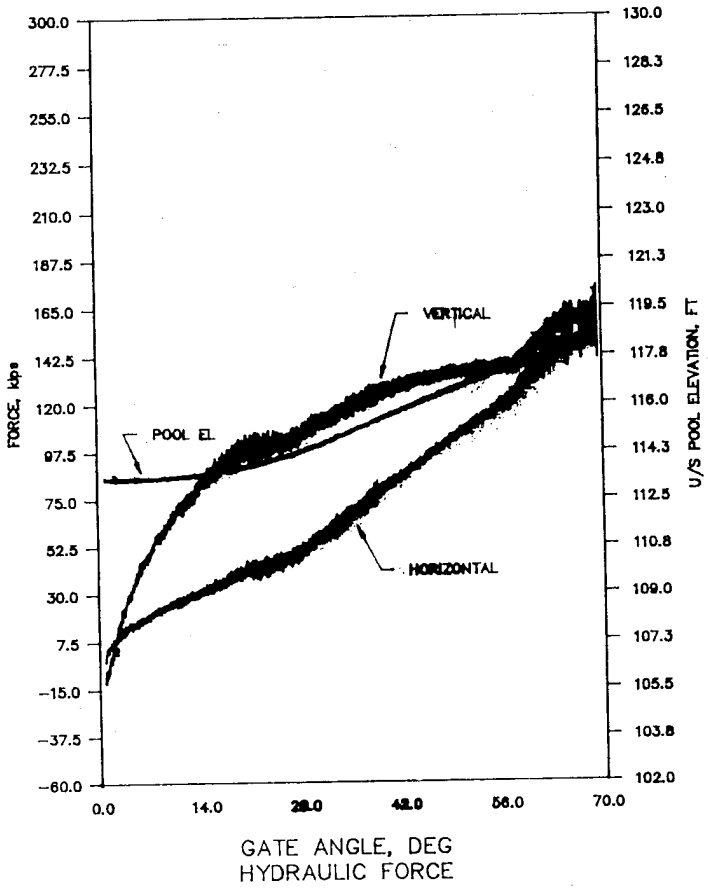

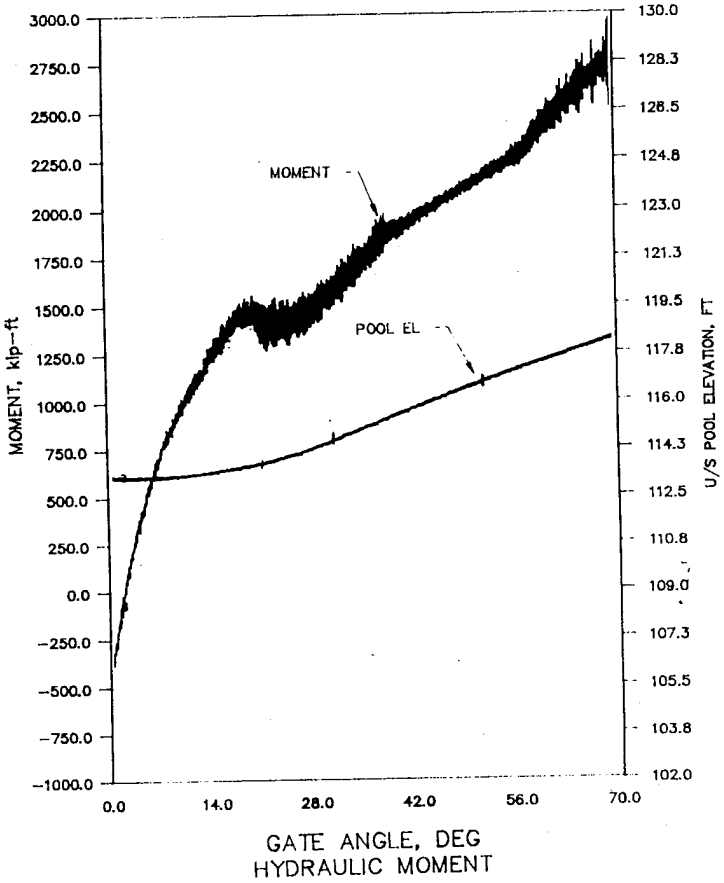

GATE OPERATION:
CENTER GATE ROTATING FROM 0 TO 70 DEG
IN 8 MIN, SIDE GATE
FIXED AT 70 DEG

HYDRAULIC FORCE AND MOMENT

ROTATING CENTER GATE
BEARING BLOCK 2
UNIT DISCHARGE 50 CFS/FT
TAILWATER EL 95

Plate 11

Plate 12

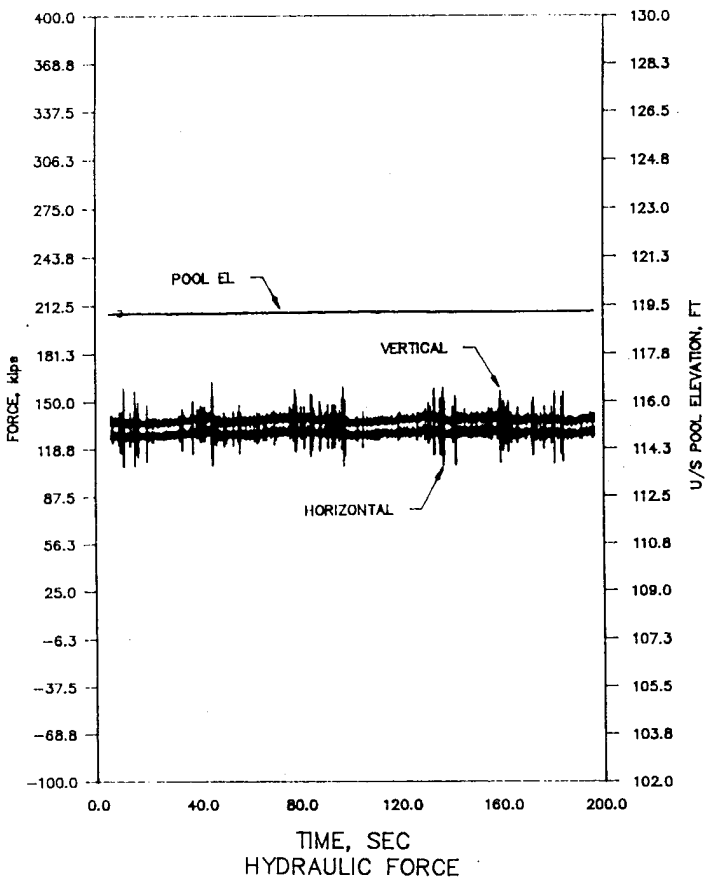

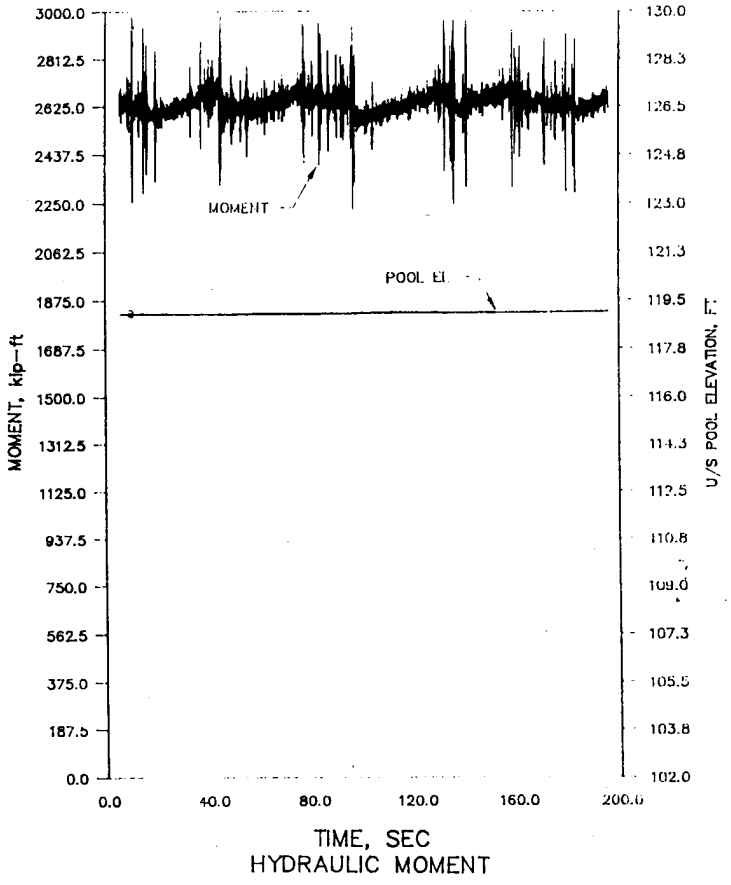

GATE OPERATION:
ALL GATES 70 DEG

HYDRAULIC FORCE AND MOMENT
UNVENTED NAPPE
BEARING BLOCK 2
UNIT DISCHARGE 50 CFS/FT
TAILWATER EL 95

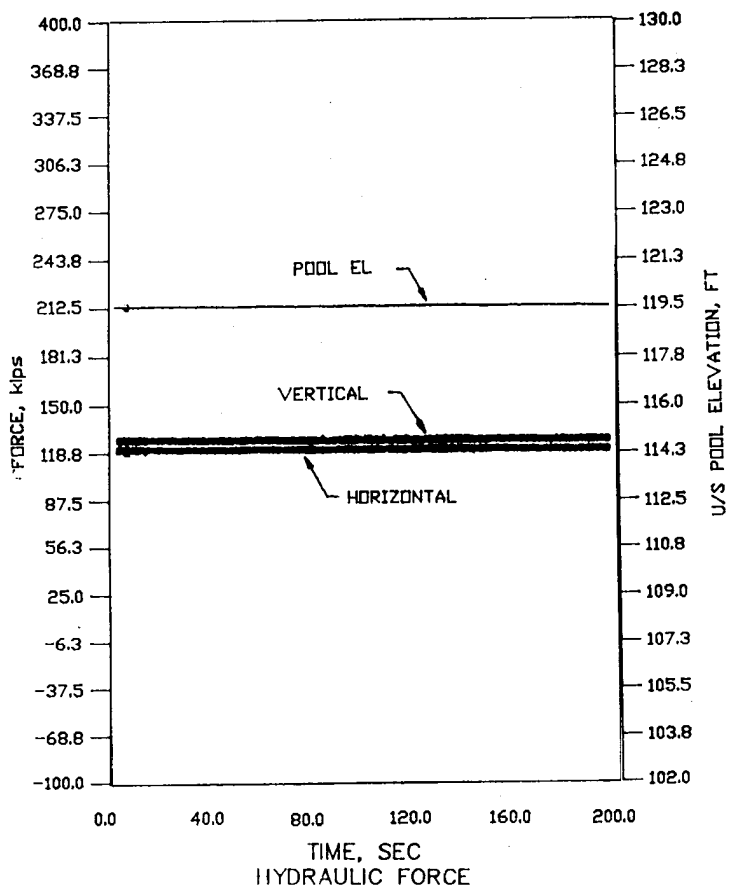

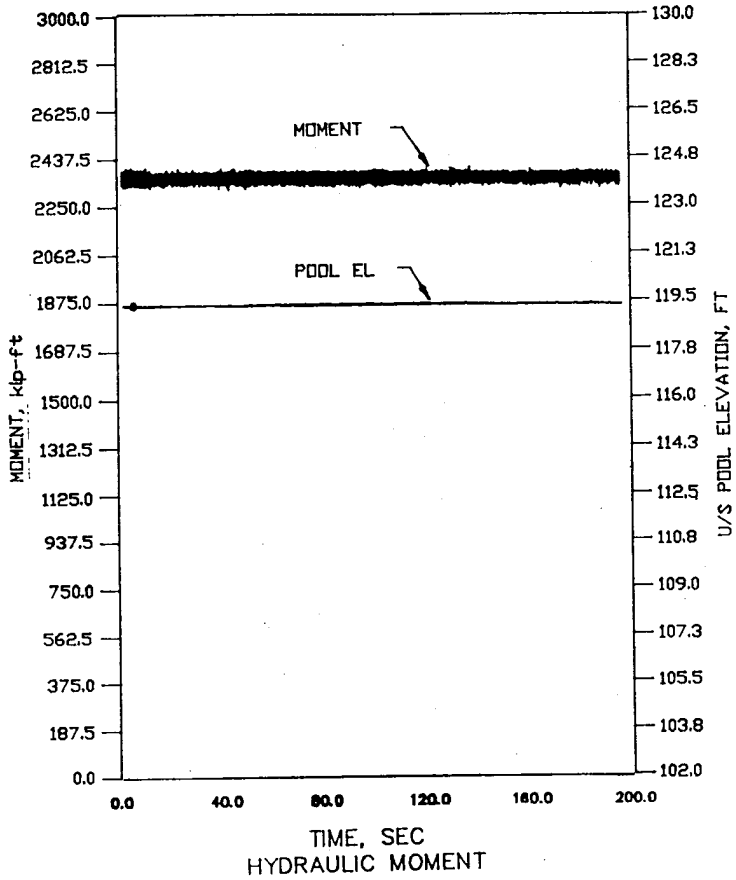

GATE OPERATION:
ALL GATES 70 DEG

HYDRAULIC FORCE AND MOMENT

VENTED NAPPE
BEARING BLOCK 2
UNIT DISCHARGE 50 CFS/FT
TAILWATER EL 95

Plate 13

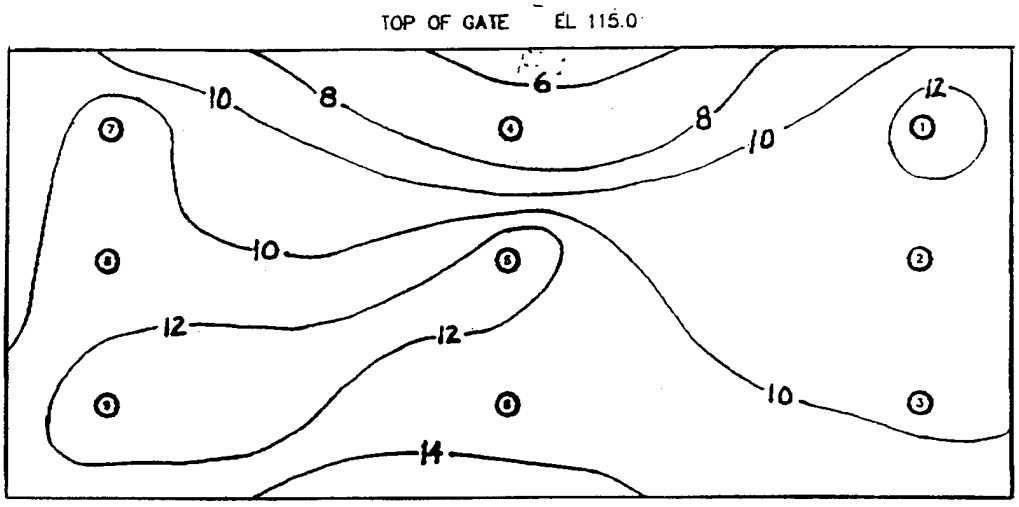

NAPPE UNVENTED

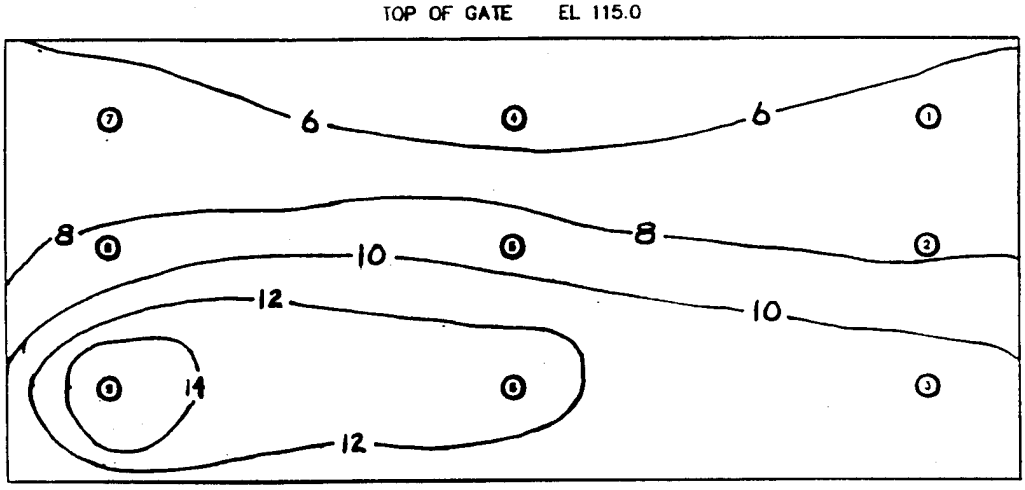

NAPPE VENTED

LEGEND

⑤ PRESSURE TRANSDUCER

NOTE: PRESSURES GIVEN IN FEET OF WATER

PRESSURE DIFFERENTIAL CONTOURS

Plate 14

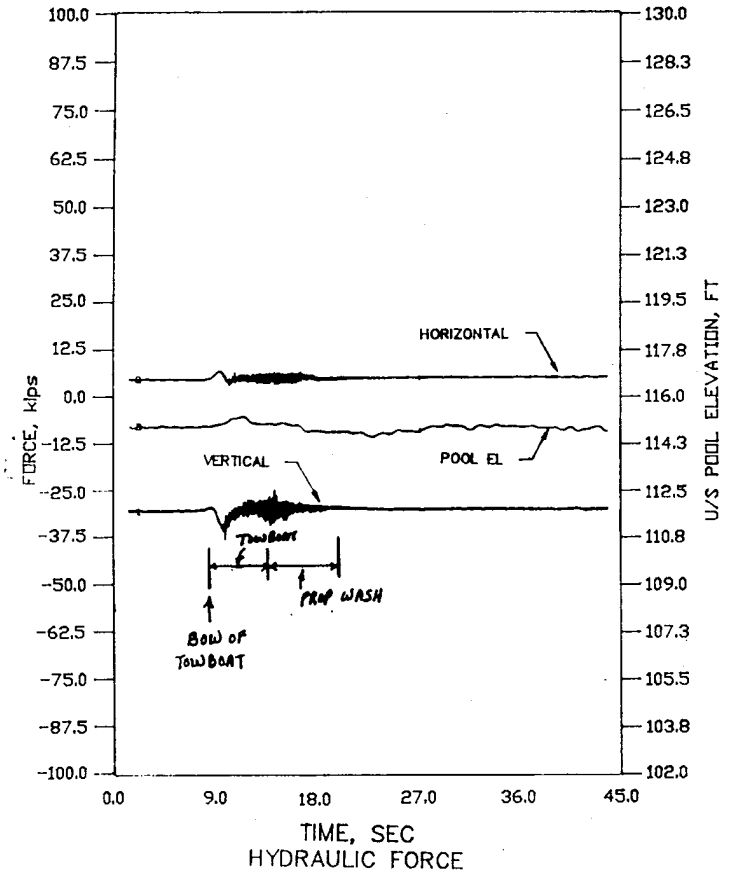

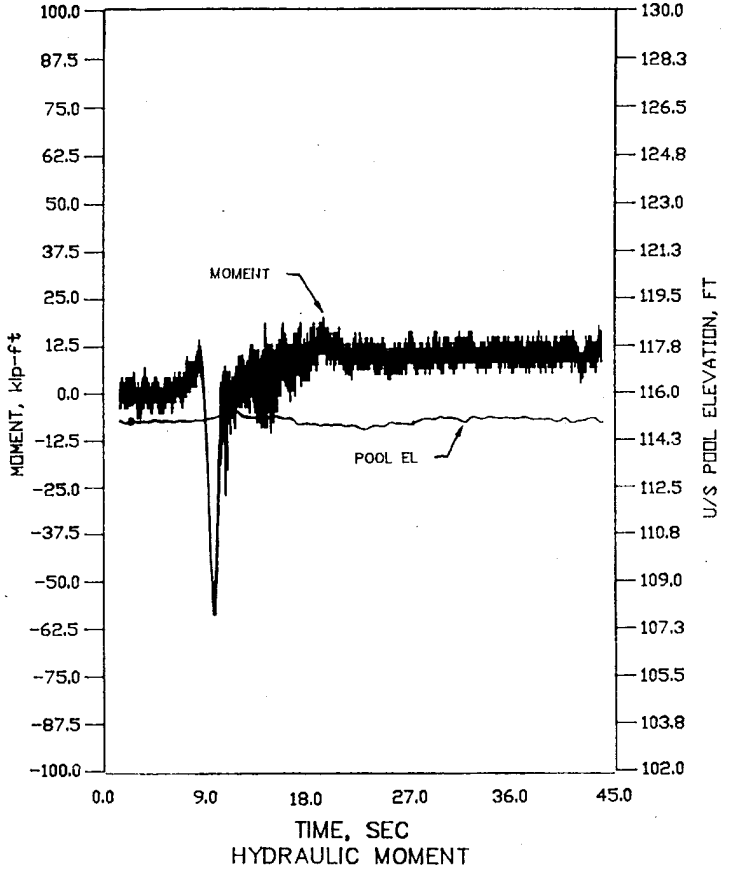

HYDRAULIC FORCE AND MOMENT

UPSTREAM TOWBOAT PASSAGE
BEARING BLOCK 2
UNIT DISCHARGE 50 CFS/FT
TAILWATER EL 115.0

Plate 15

Plate 16

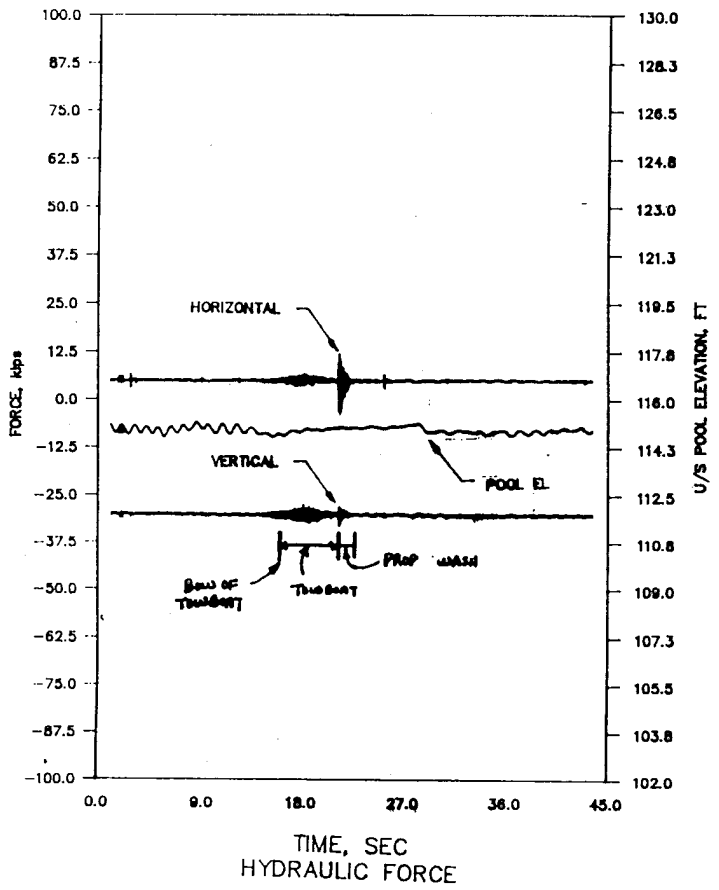

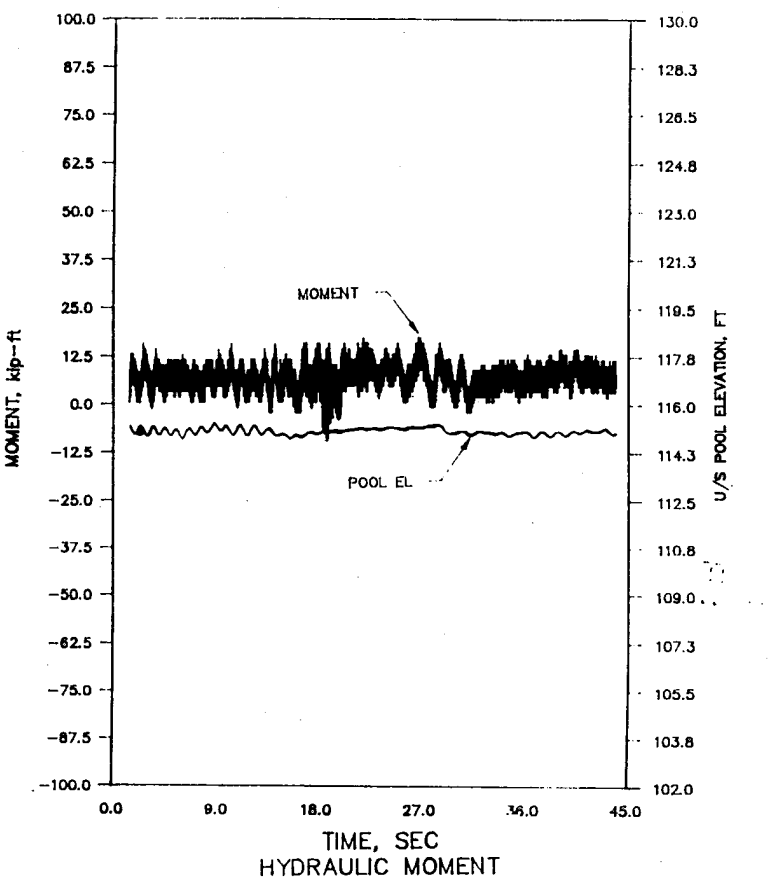

HYDRAULIC FORCE AND MOMENT
DOWNSTREAM TOWBOAT PASSAGE
BEARING BLOCK 2
UNIT DISCHARGE 50 CFS/FT
TAILWATER EL 115.0

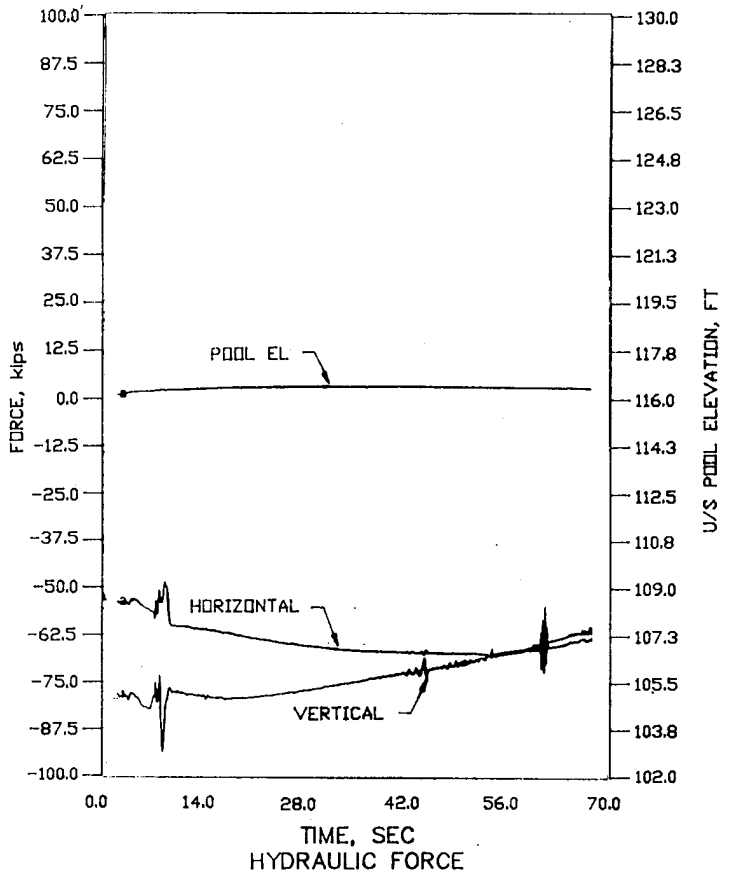

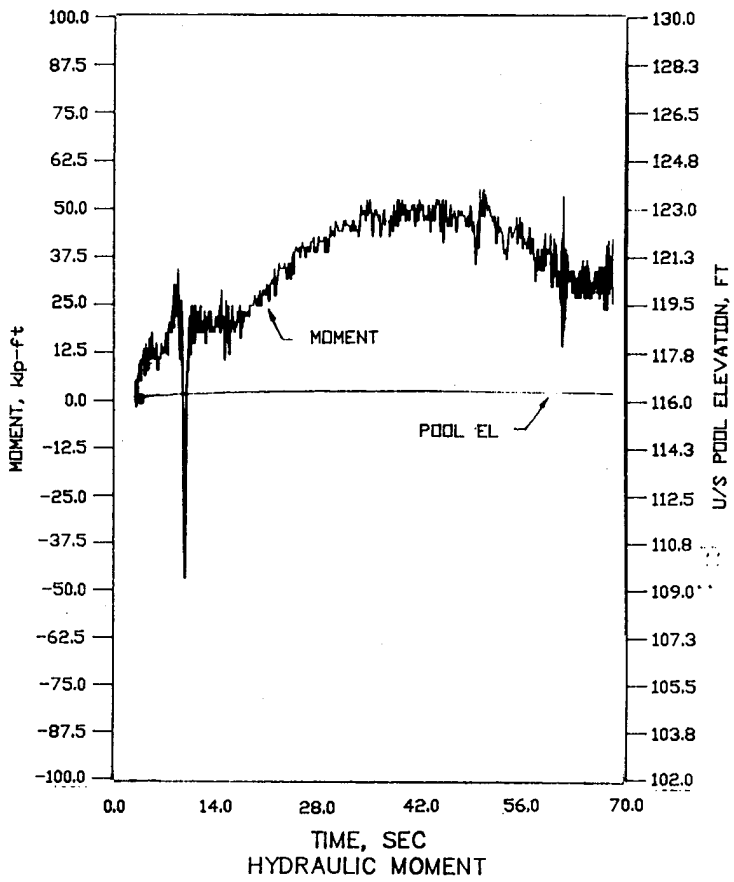

HYDRAULIC FORCE AND MOMENT
FREE-FALL CENTER GATE
BEARING BLOCK 2
UNIT DISCHARGE 9.8 CFS/FT
TAILWATER EL 115.0

Plate 17

Plate 18

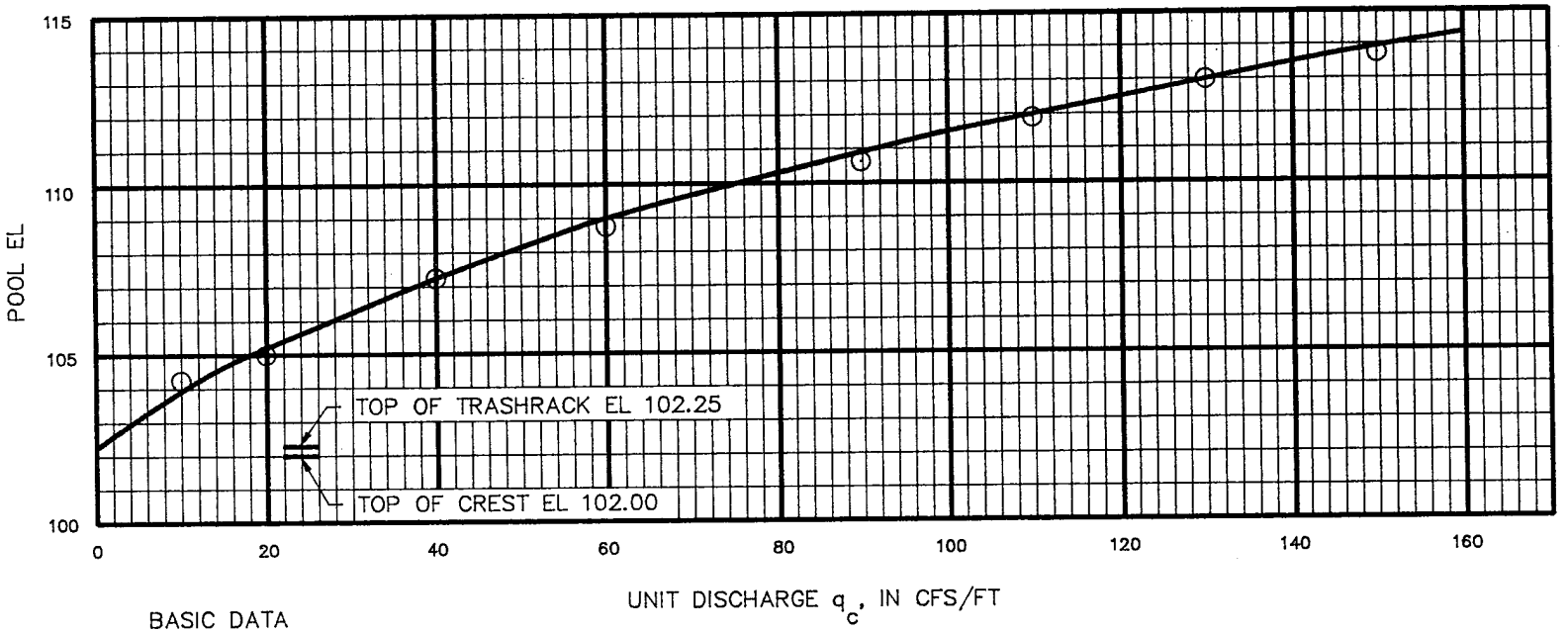

BASIC DATA

q_c	POOL EL
10	104.3
20	105.2
40	107.3
60	108.6
90	110.6
110	111.8
130	113.0
150	113.8

SPILLWAY RATING CURVE
ALL GATES DOWN
FREE FLOW

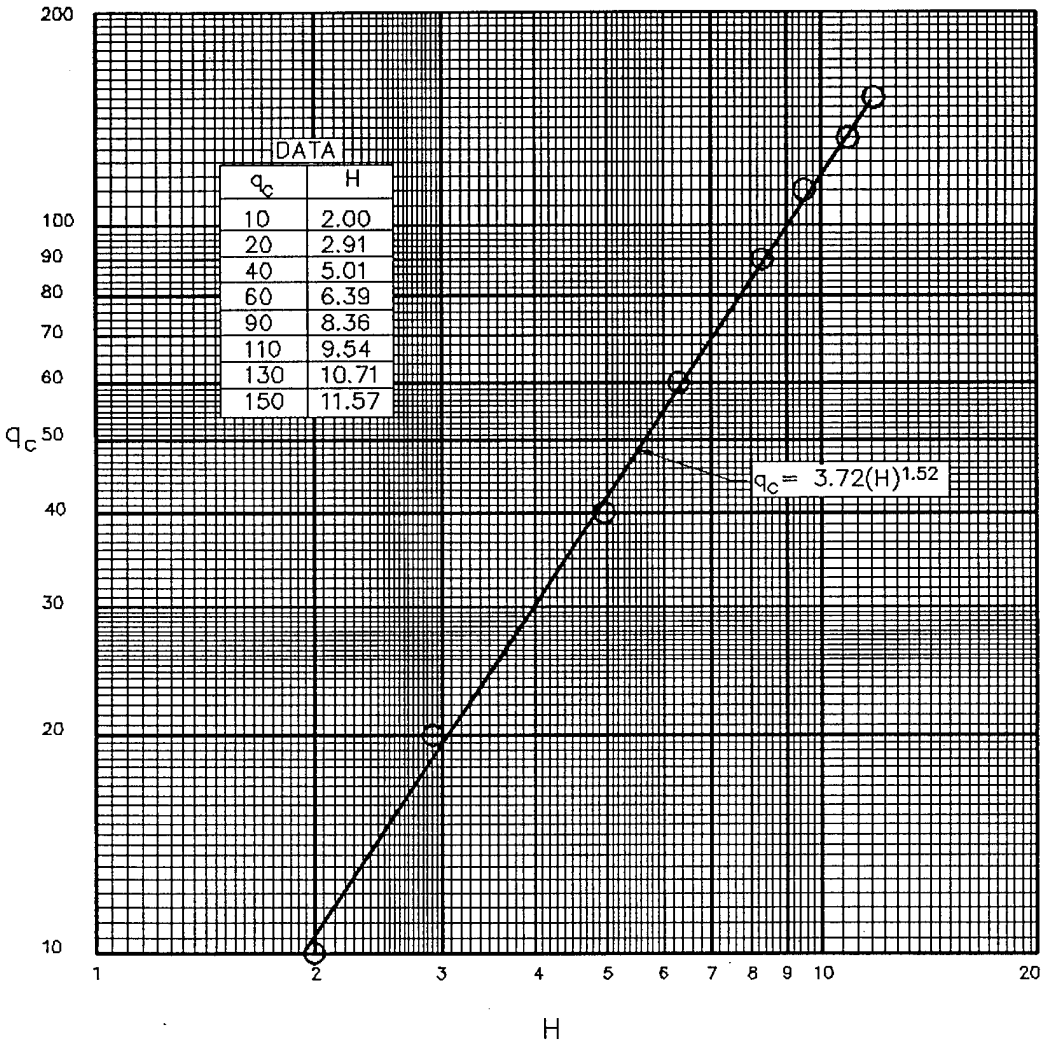

NOTE: TOP OF TRASHRACK EL 102.25

HEAD DISCHARGE RATING CURVE
ALL GATES DOWN
FREE FLOW

Plate 19

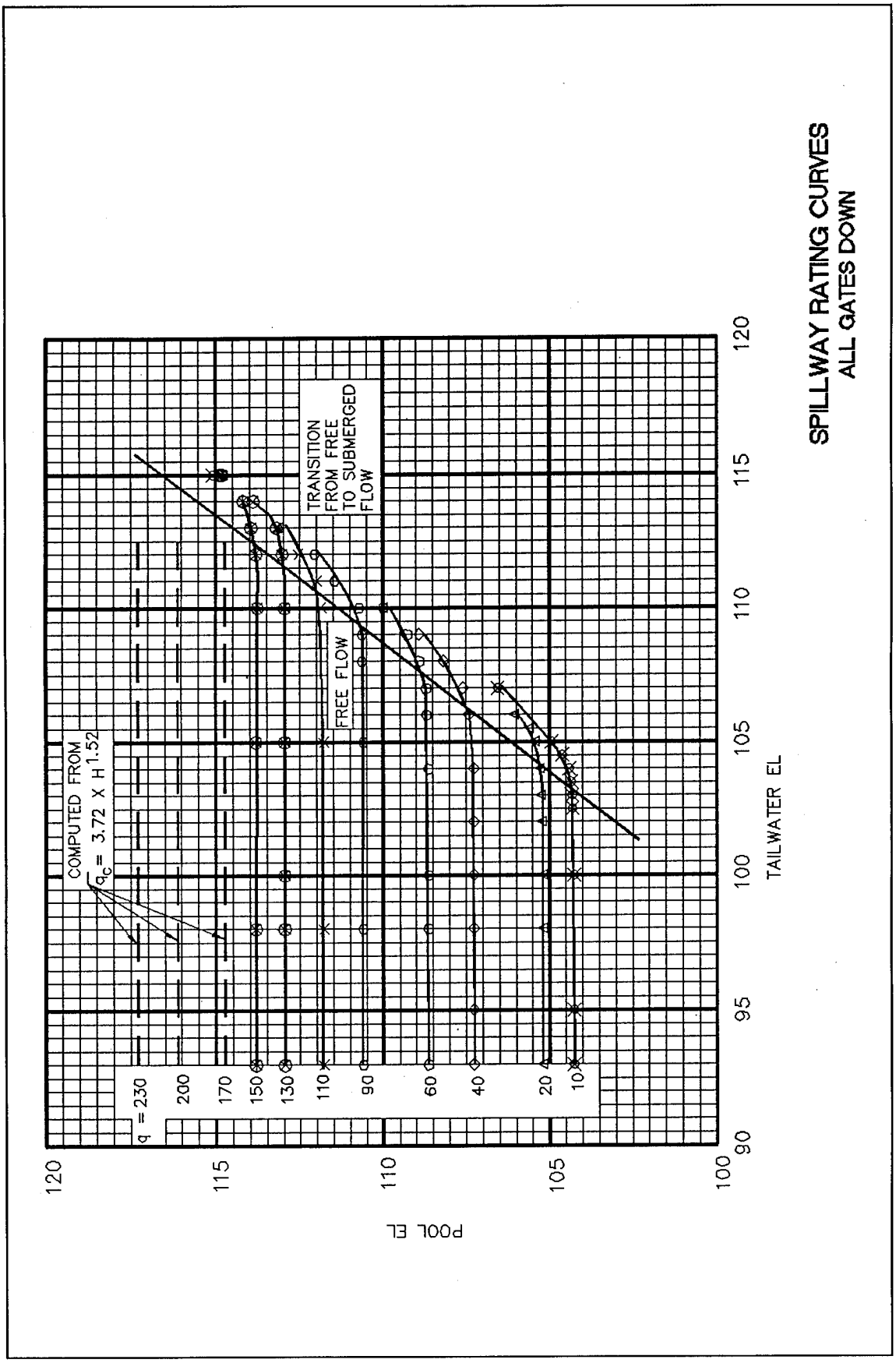
SPILLWAY RATING CURVES
ALL GATES DOWN
POOL EL
TAILWATER EL
120
115
110
105
100
90
95
100
105
110
115
120
COMPUTED FROM
$Q_c = 3.72 \times H^{1.52}$
TRANSITION
FROM FREE
TO SUBMERGED
FLOW
FREE FLOW
q = 230
200
170
150
130
110
90
60
40
20
10

Plate 20

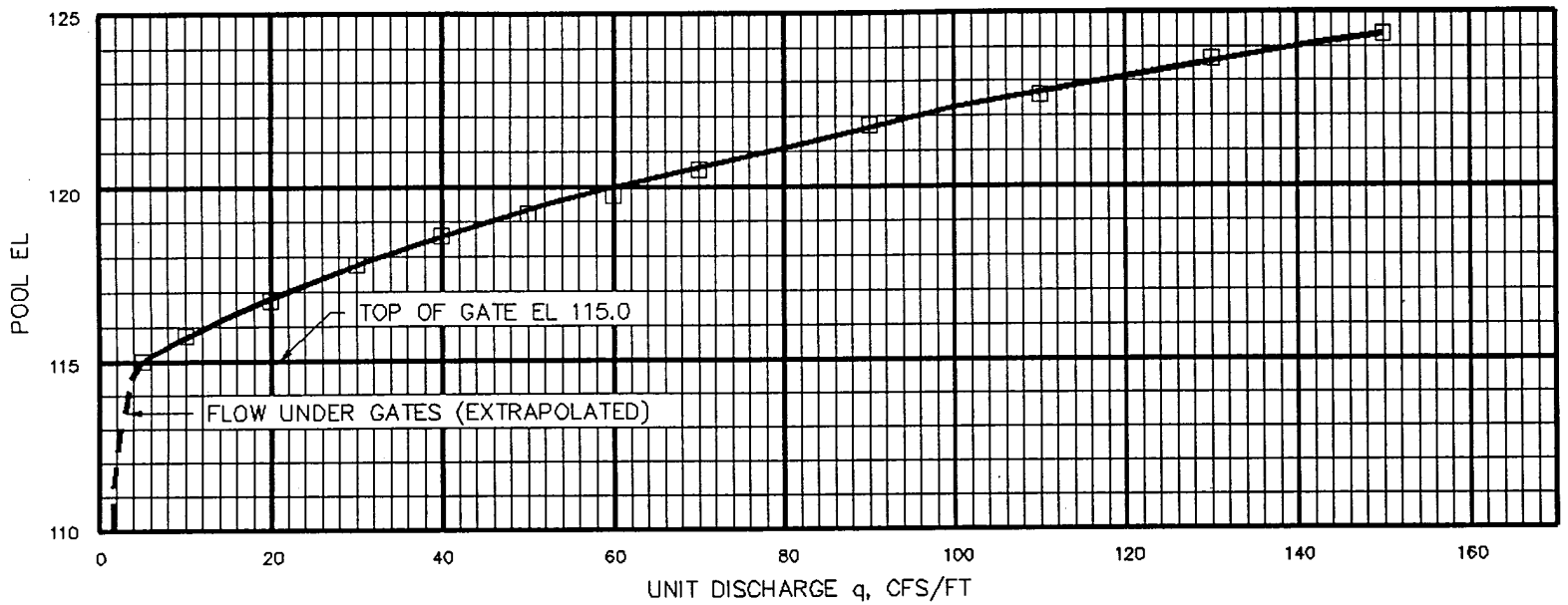

BASIC DATA

q	POOL EL
* 5.7	115.0
10	115.6
20	116.7
30	117.8
40	118.6
50	119.3
60	119.8
70	120.5
90	121.7
110	122.6
130	123.6
150	124.3

* ALL LEAKAGE

SPILLWAY RATING CURVE
ALL GATES UP
FREE FLOW

Plate 21

Plate 22

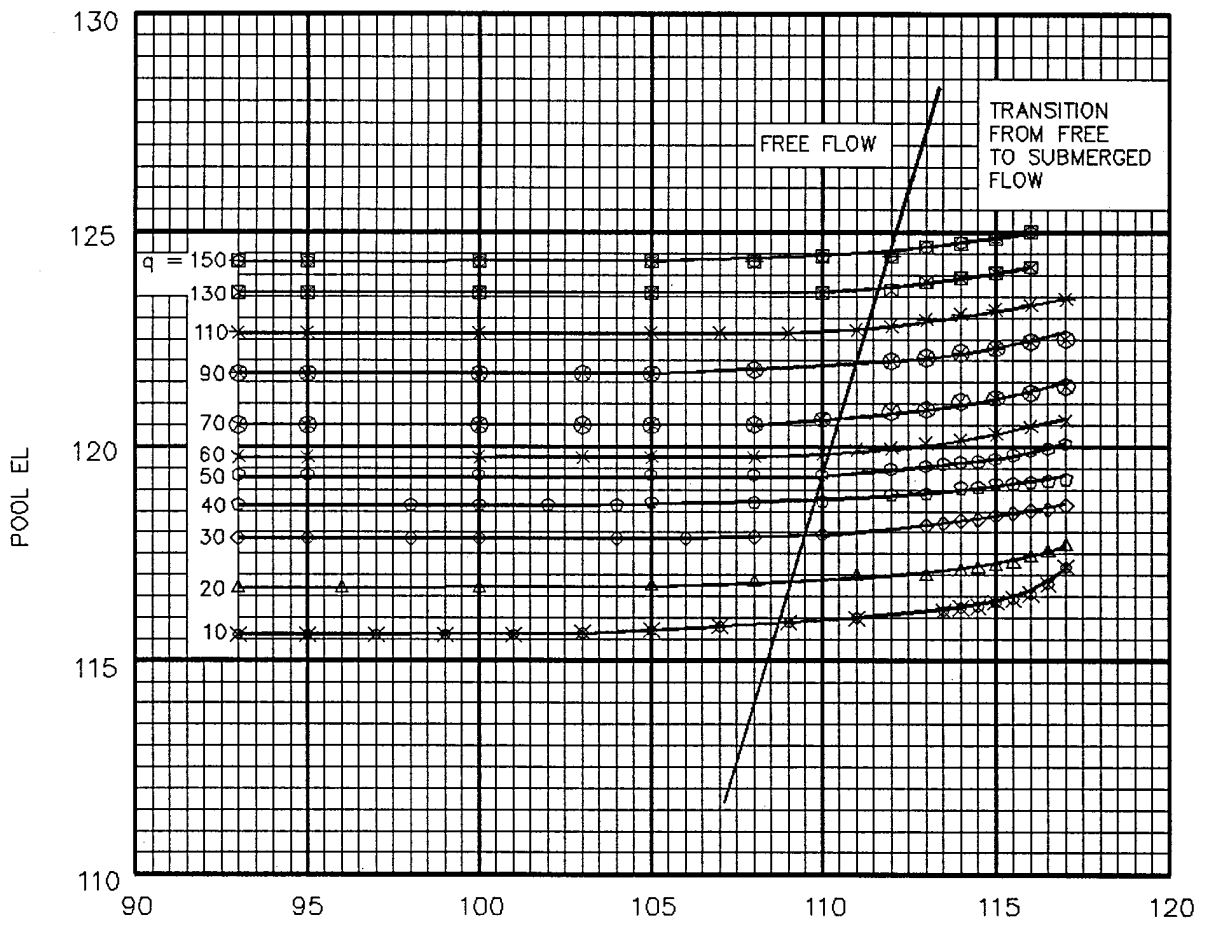

SPILLWAY RATING CURVES
ALL GATES UP

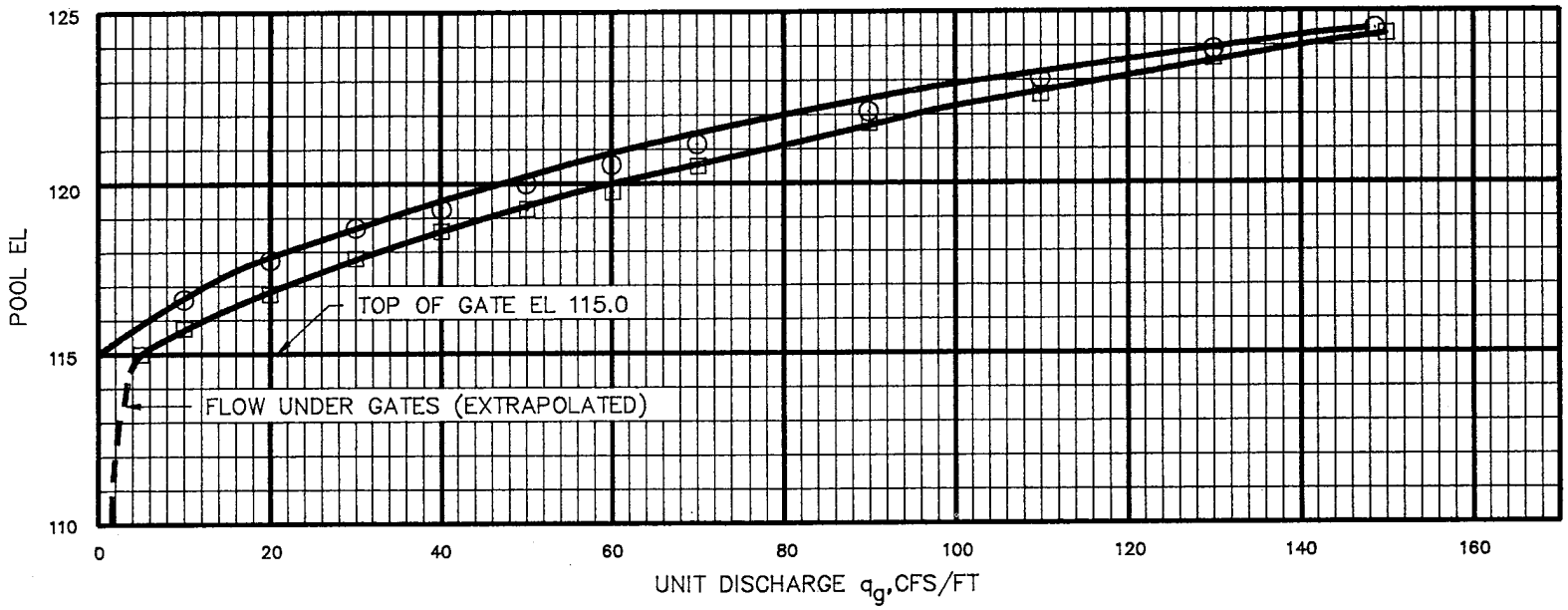

NO LEAKAGE ⊙
BASIC DATA

q_g	POOL EL
10	116.7
20	117.6
30	118.7
40	119.4
50	120.0
60	120.6
70	121.3
90	122.2
110	123.1
130	123.8
150	124.5

LEAKAGE ⊡
BASIC DATA

q_g	POOL EL
* 5.7	115.0
10	115.6
20	116.7
30	117.8
40	118.6
50	119.3
60	119.8
70	120.5
90	121.7
110	122.6
130	123.6
150	124.3

* ALL LEAKAGE

SPILLWAY RATING CURVES
ALL GATES UP
FREE FLOW
WITH AND WITHOUT LEAKAGE

Plate 24

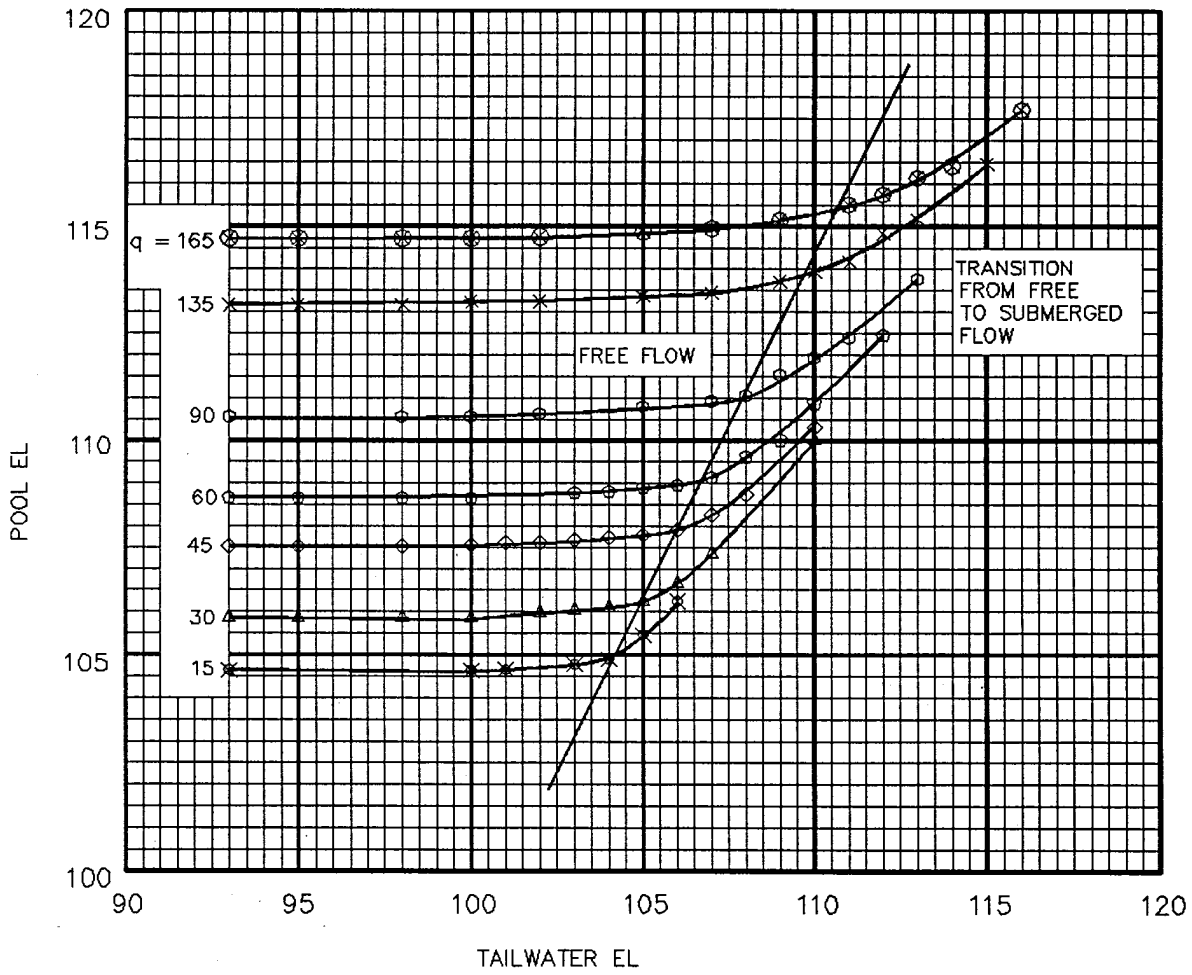

SPILLWAY RATING CURVES
GATE 1 UP, GATES 2 AND 3 DOWN

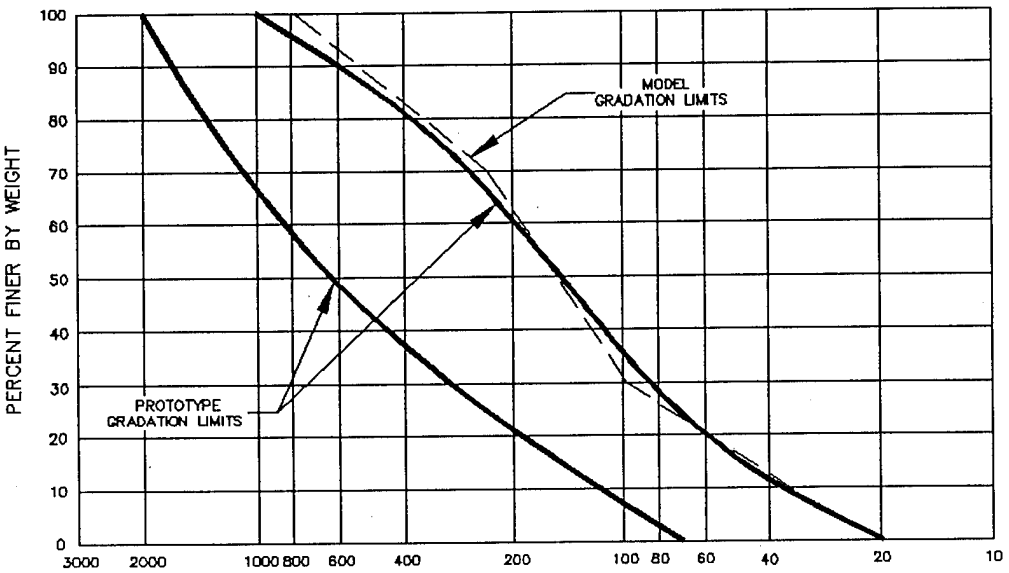

UPSTREAM OF SPILLWAY (LRD RIPRAP 5)

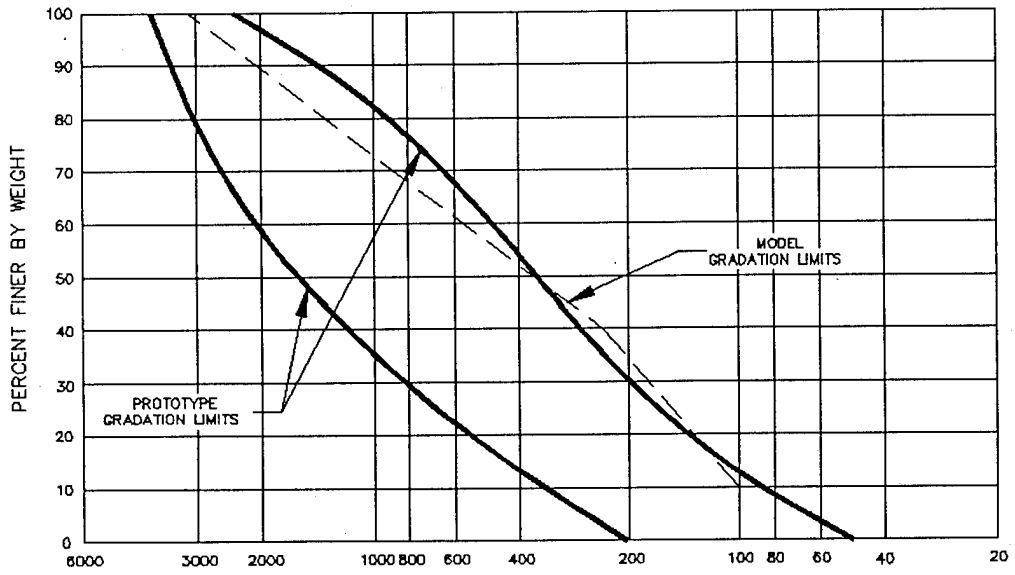

DOWNSTREAM FROM SPILLWAY (LRD RIPRAP 6)

RIPRAP GRADATION CURVES

Plate 25

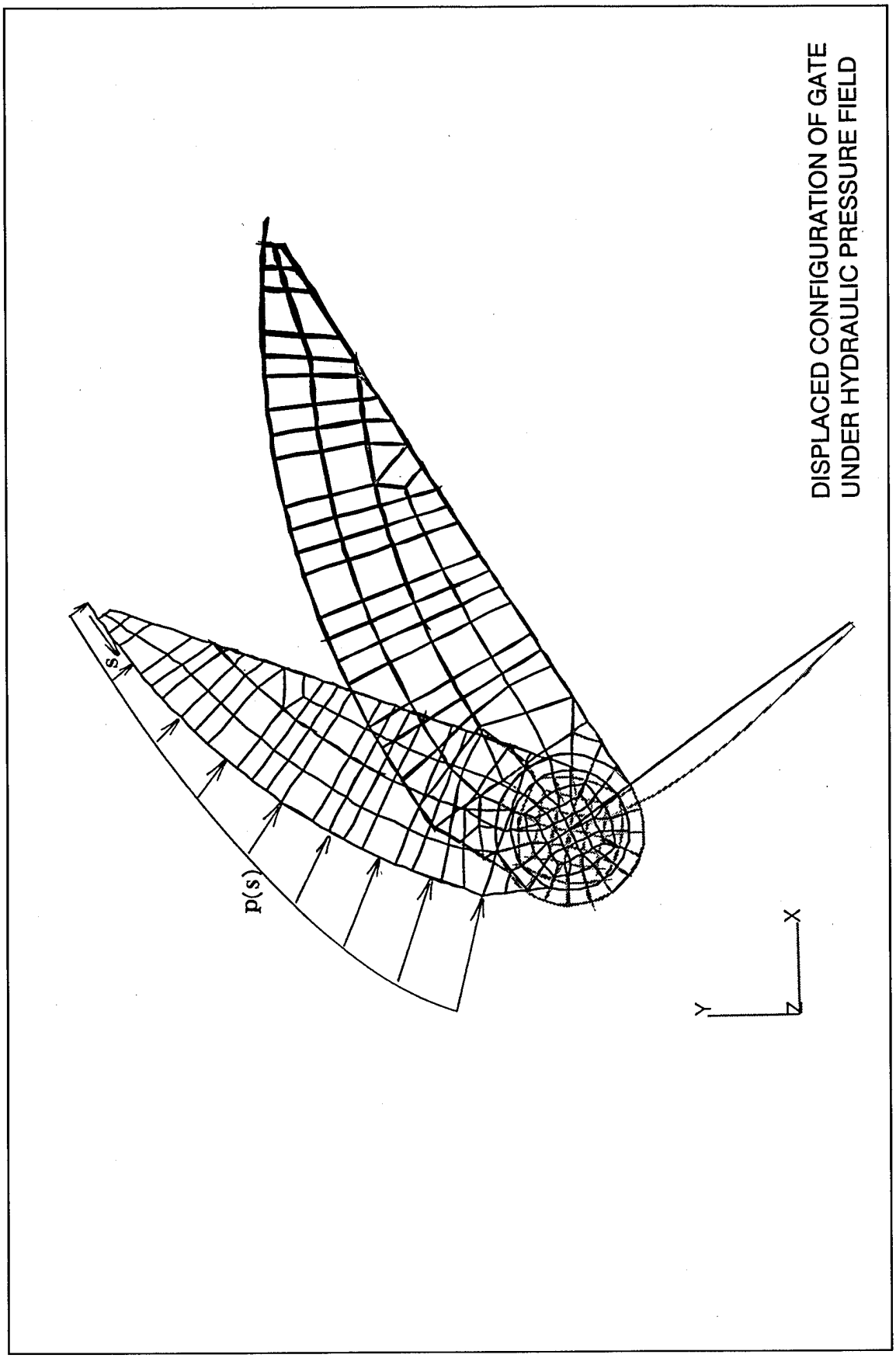
DISPLACED CONFIGURATION OF GATE
UNDER HYDRAULIC PRESSURE FIELD
s
p(s)
X
Y
Z

Plate 26

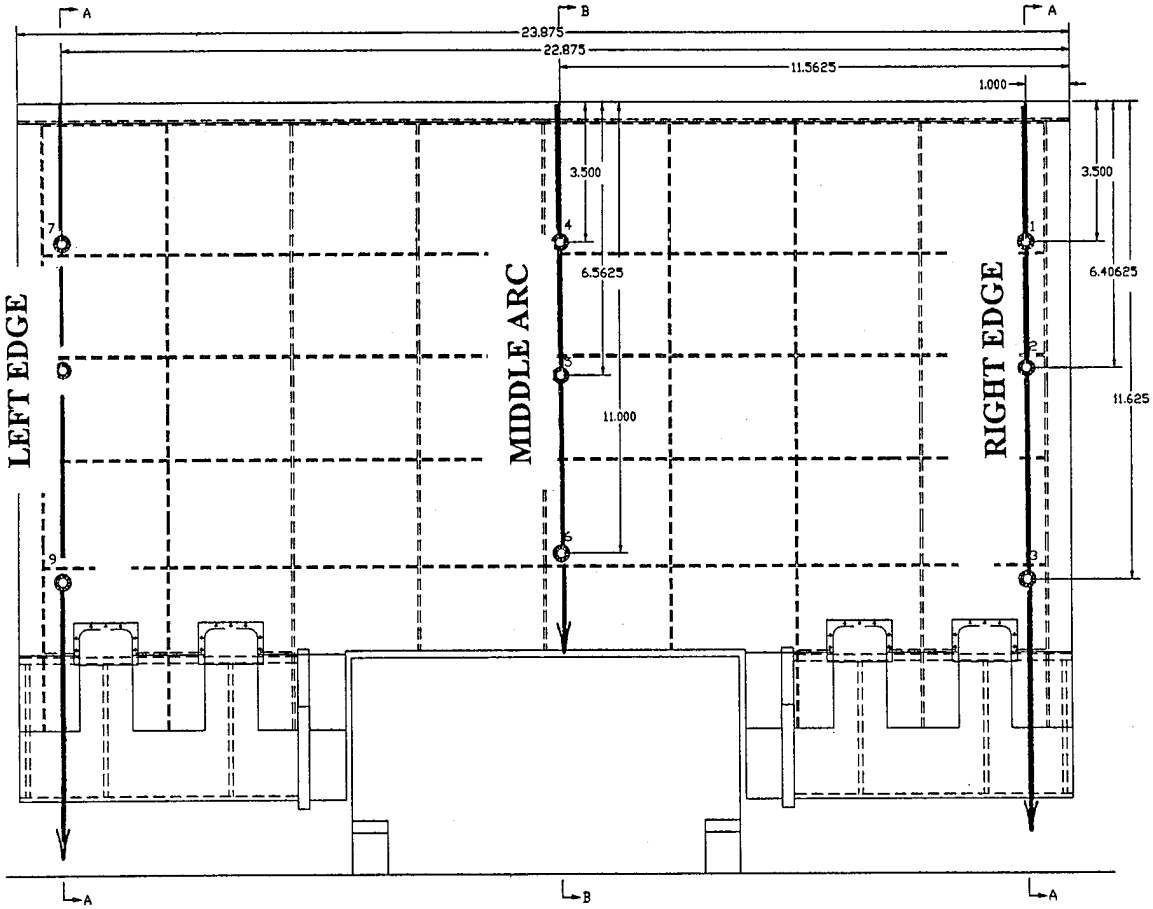

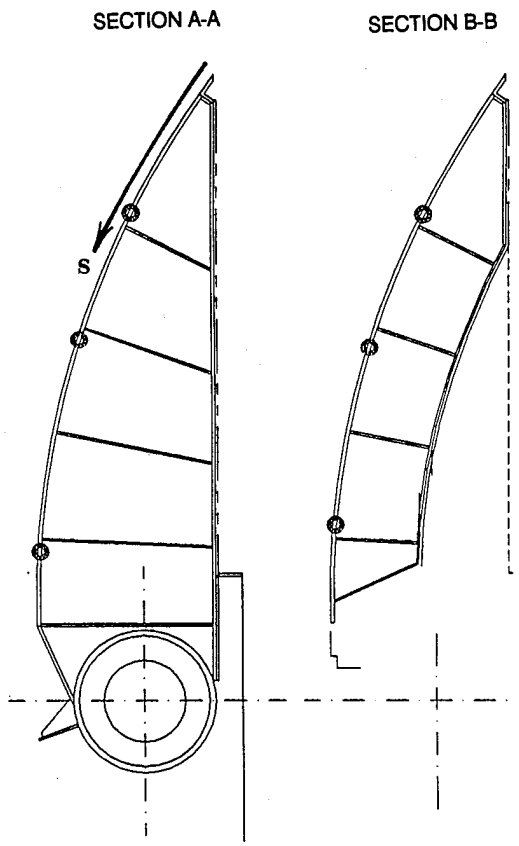

REFERENCE LONGITUDINAL ARCS ON
1:15-SCALE PHYSICAL MODEL OF GATE

NOTE: ALL DIMENSIONS ARE IN INCHES

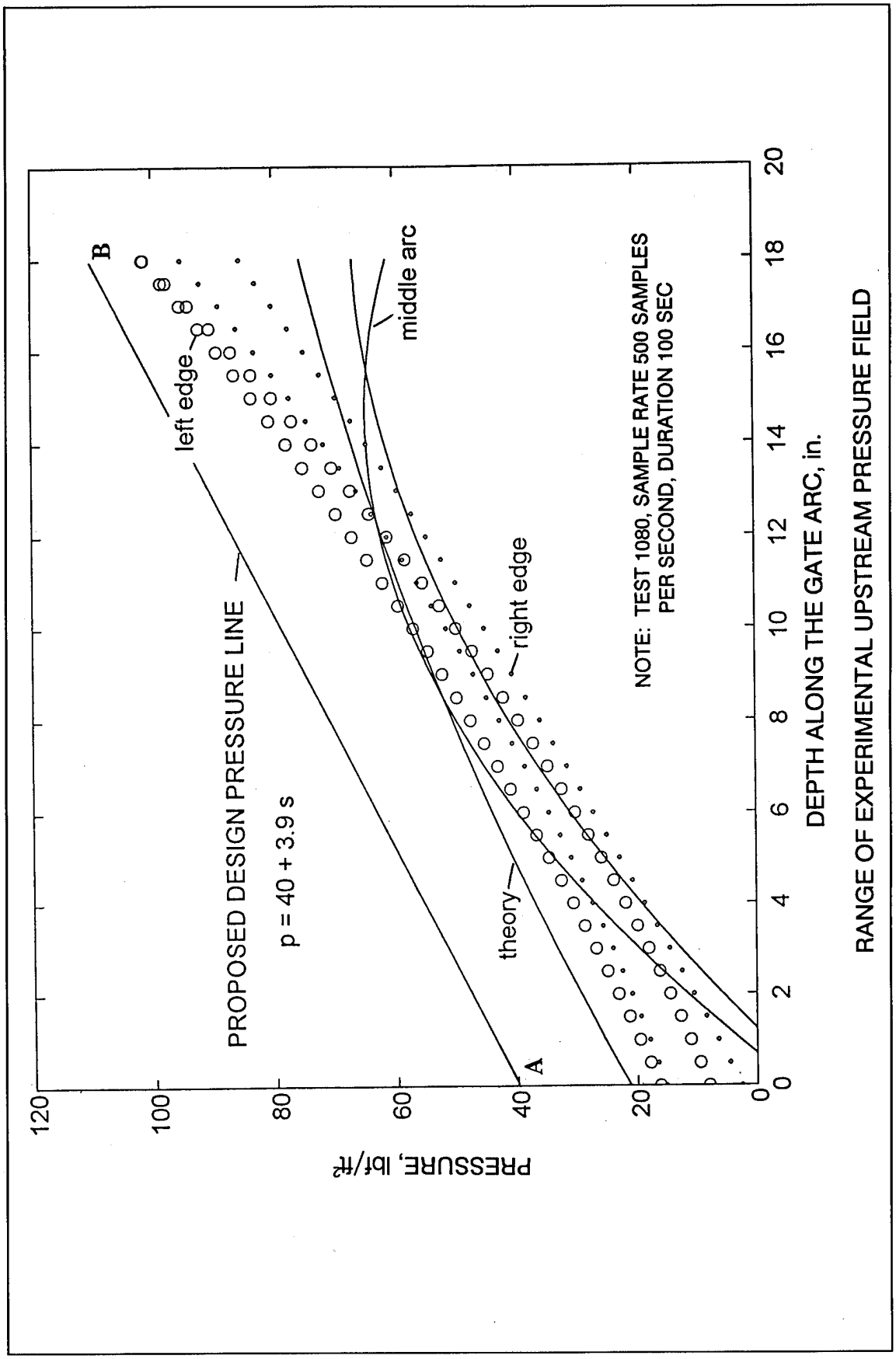

RANGE OF EXPERIMENTAL UPSTREAM PRESSURE FIELD

Plate 28

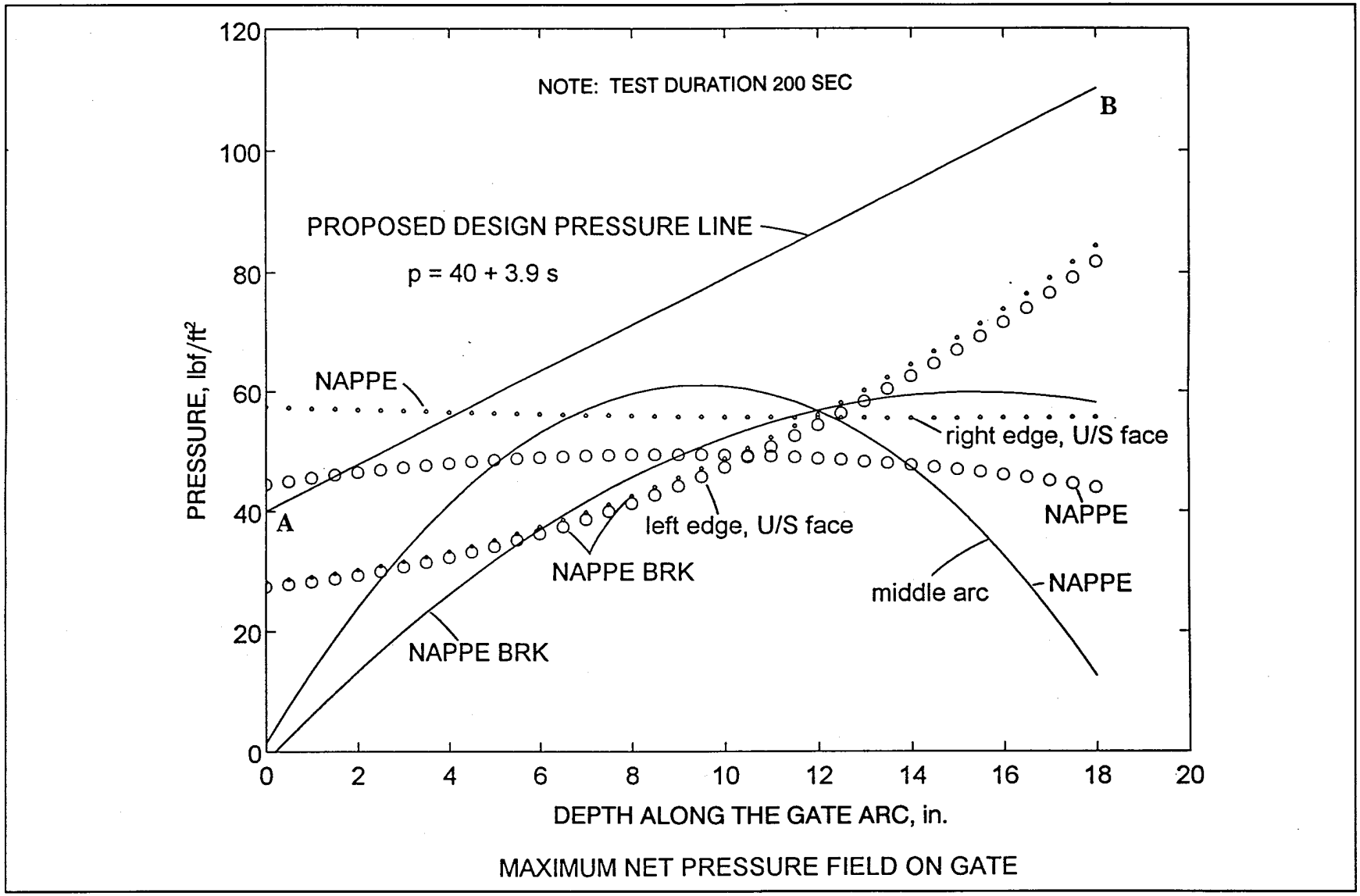

MAXIMUM NET PRESSURE FIELD ON GATE

Plate 29

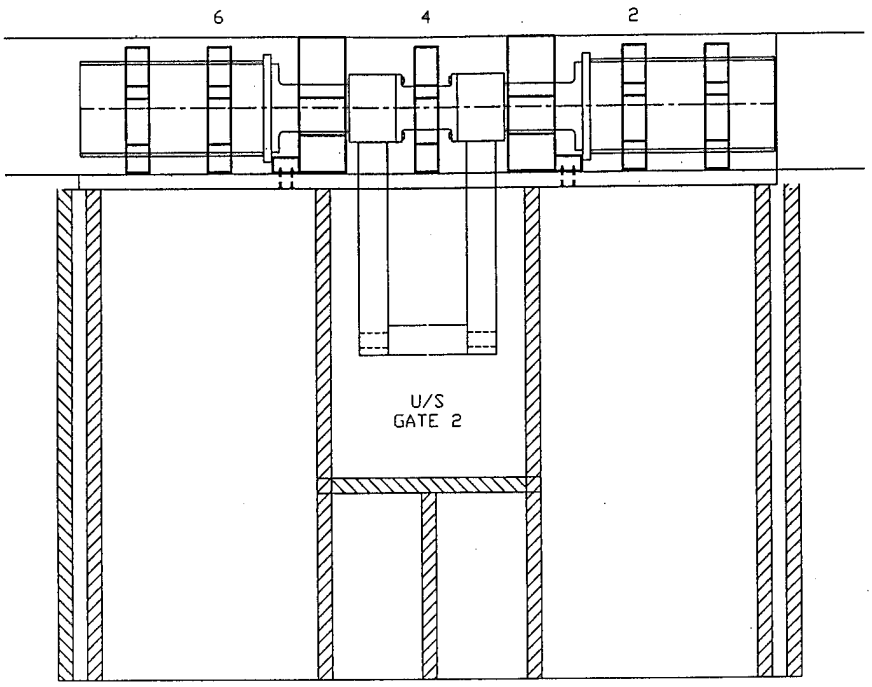

INSTRUMENTED BEARING BLOCKS 2,4, AND 6 -- MODEL

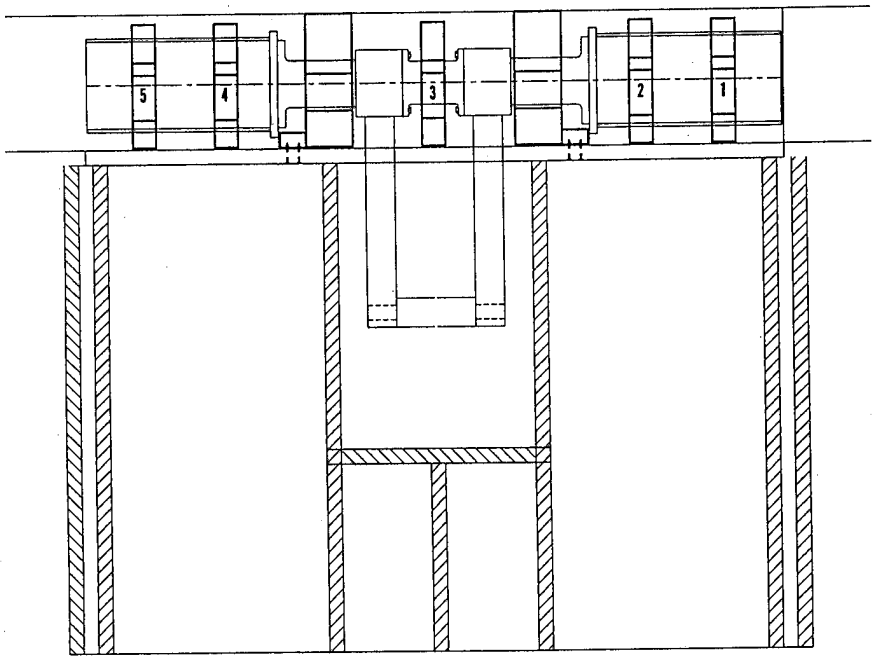

BEARING BLOCKS 1-5 -- PROTOTYPE

BEARING BLOCKS IN MODEL AND PROTOTYPE

Plate 30

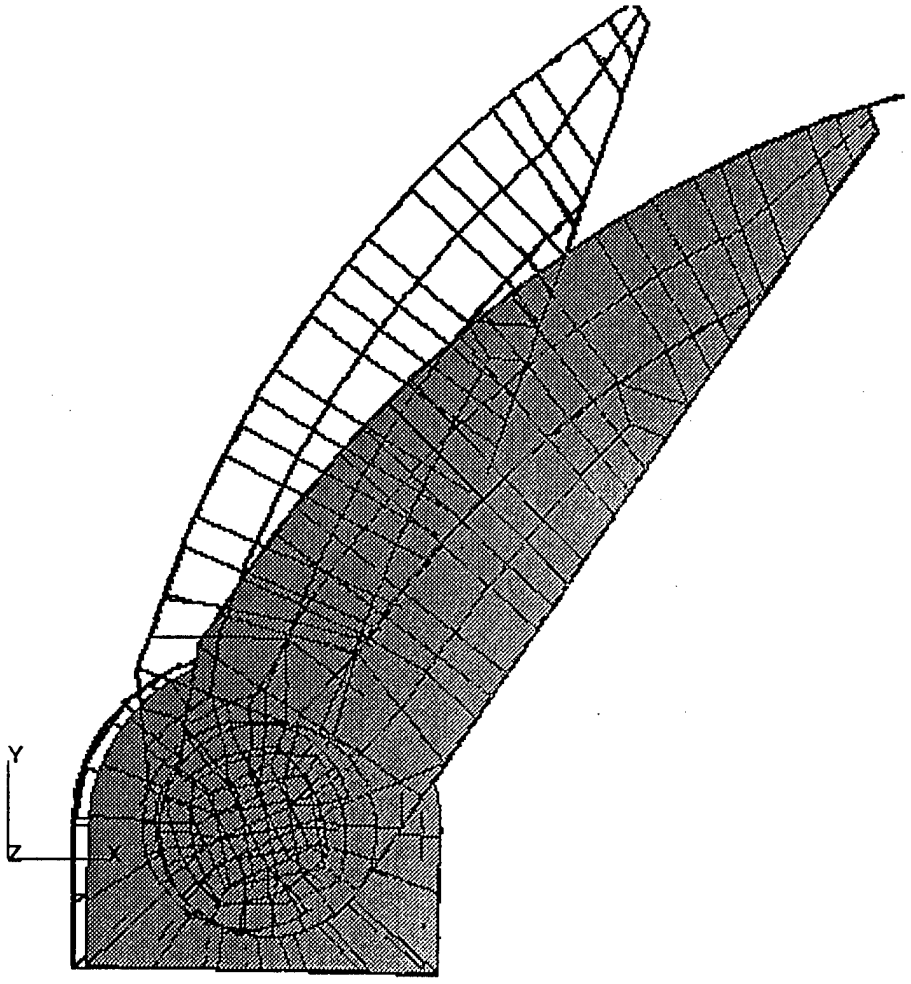

DISPLACED SHAPE
PRESSURE ENVELOPE AND DEAD LOAD
DISPLACEMENT FACTOR = 100

Plate 31

Plate 32

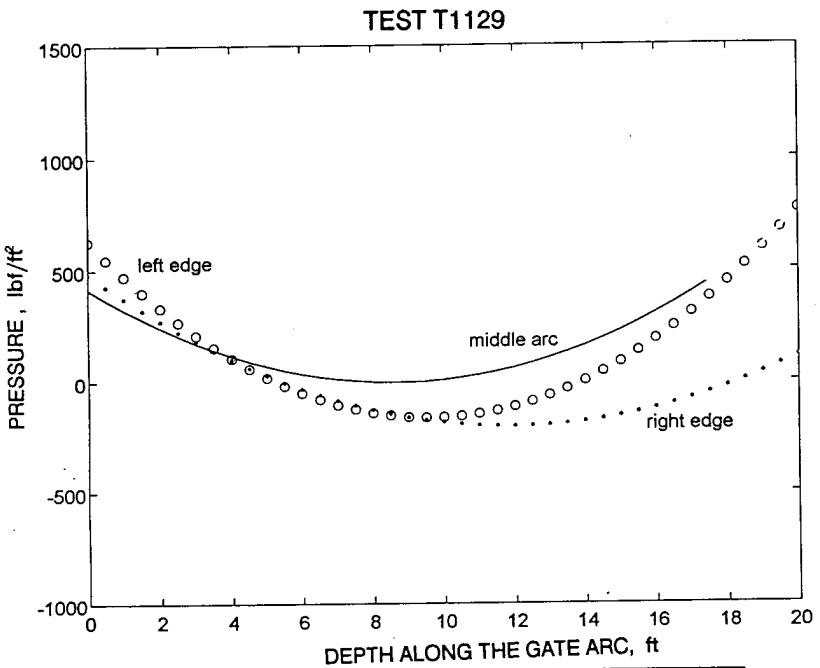

ANALYTICAL EXPRESSIONS FOR PRESSURE CURVES		
Longitudinal Arc on Gate Skin	Domain, s [ft]	Prototype Pressure Field [psf]
Right Edge	$s \in (0,20.0)$	$4.8324\ s^2 - 115.2660\ s + 483.0669$
Middle Arc	$s \in (0,17.5)$	$5.6794\ s^2 - 97.6724\ s + 415.5899$
Left Edge	$s \in (0,20.0)$	$8.6109\ s^2 - 165.2297\ s + 627.1341$

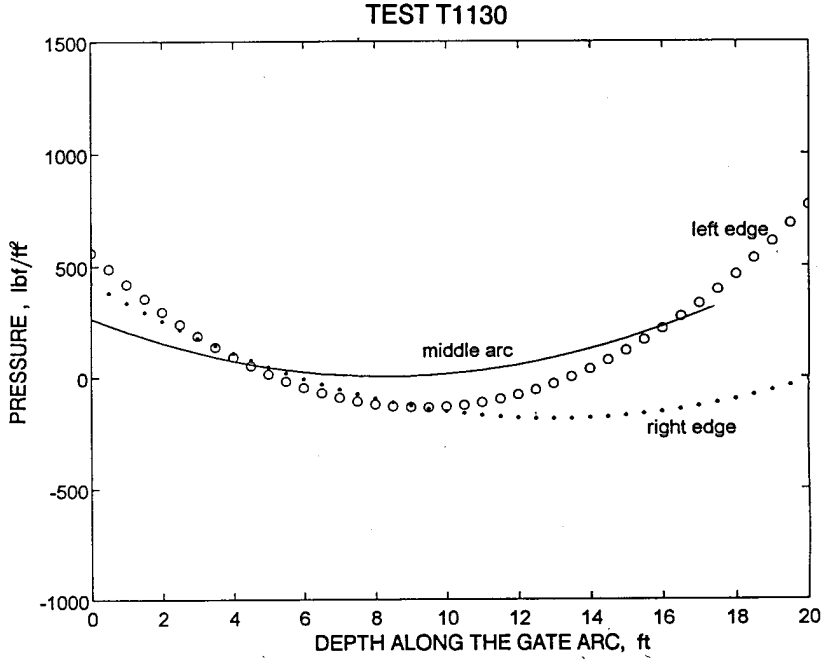

ANALYTICAL EXPRESSIONS FOR PRESSURE CURVES		
Longitudinal Arc on Gate Skin	Domain, s [ft]	Prototype Pressure Field [psf]
Right Edge	$s \in (0,20.0)$	$3.6066\ s^2 - 94.1083\ s + 426.4341$
Middle Arc	$s \in (0,17.5)$	$3.7953\ s^2 - 63.0753\ s + 265.5179$
Left Edge	$s \in (0,20.0)$	$7.9988\ s^2 - 149.5175\ s + 561.1763$

DESIGN PRESSURE LINE
TESTS T1129 AND T1130

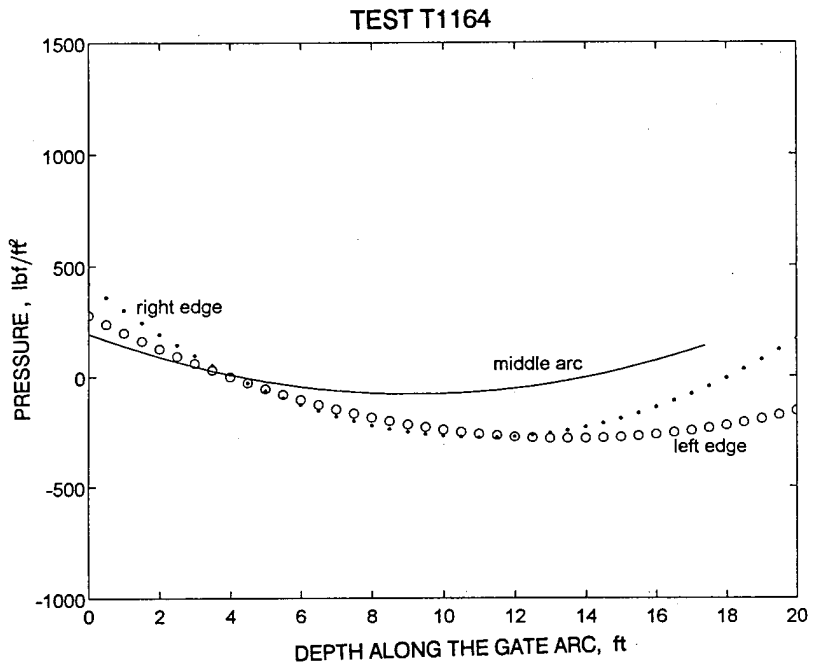

ANALYTICAL EXPRESSIONS FOR PRESSURE CURVES		
Longitudinal Arc on Gate Skin	Domain, s [ft]	Prototype Pressure Field [psf]
Right Edge	$s \in (0,20.0)$	$+5.6762\ s^2 - 126.1514\ s + 423.5218$
Middle Arc	$s \in (0,17.5)$	$+3.2779\ s^2 - 60.2666\ s + 196.9088$
Left Edge	$s \in (0,20.0)$	$+3.0400\ s^2 - 82.7087\ s + 280.4783$

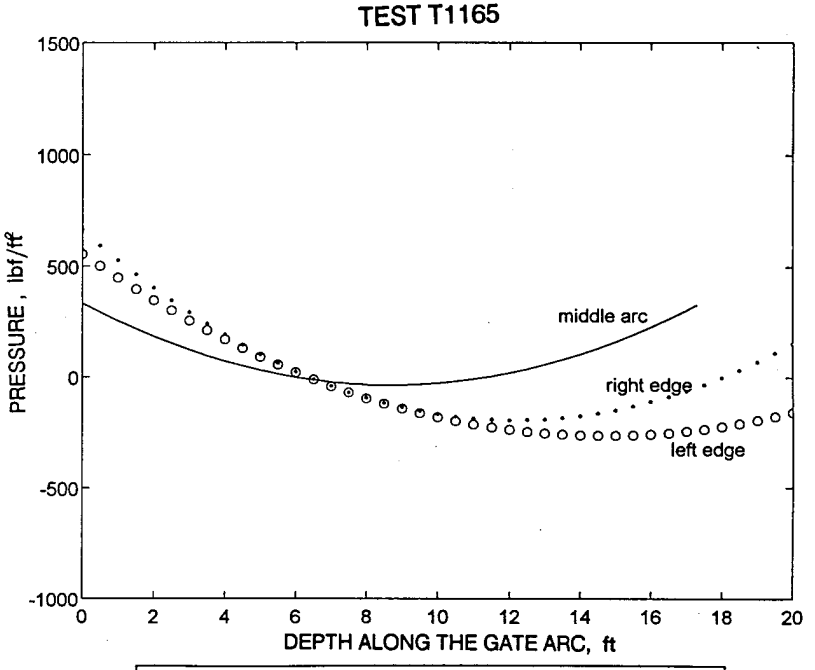

ANALYTICAL EXPRESSIONS FOR PRESSURE CURVES		
Longitudinal Arc on Gate Skin	Domain, s [ft]	Prototype Pressure Field [psf]
Right Edge	$s \in (0,20.0)$	$+5.7473\ s^2 - 140.2960\ s + 660.7862$
Middle Arc	$s \in (0,17.5)$	$+4.8929\ s^2 - 84.8570\ s + 333.4929$
Left Edge	$s \in (0,20.0)$	$+3.7860\ s^2 - 111.5296\ s + 554.3389$

DESIGN PRESSURE LINE
TESTS T1164 AND T1165

Plate 33

Plate 34

TEST T1133

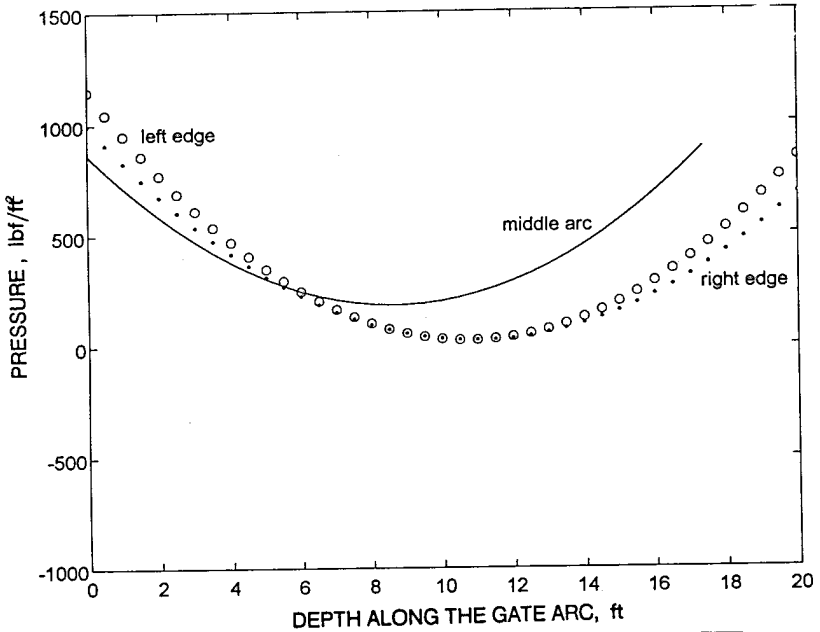

ANALYTICAL EXPRESSIONS FOR PRESSURE CURVES		
Longitudinal Arc on Gate Skin	Domain, s [ft]	Prototype Pressure Field [psf]
Right Edge	$s \in (0,20.0)$	$8.0422\ s^2 - 176.6383\ s + 994.6016$
Middle Arc	$s \in (0,17.5)$	$9.1649\ s^2 - 157.7013\ s + 863.3354$
Left Edge	$s \in (0,20.0)$	$9.6000\ s^2 - 207.8000\ s + 1146.100$

TEST T1134

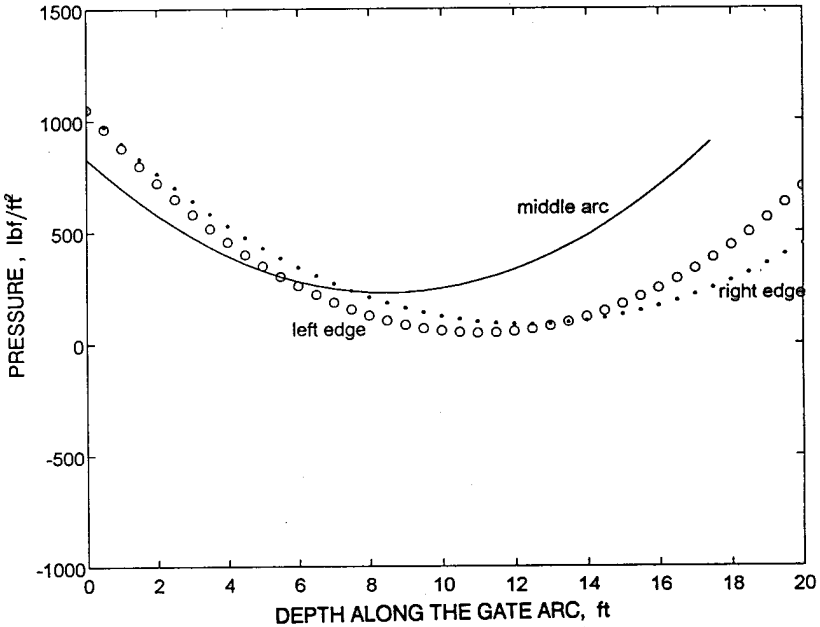

ANALYTICAL EXPRESSIONS FOR PRESSURE CURVES		
Longitudinal Arc on Gate Skin	Domain, s [ft]	Prototype Pressure Field [psf]
Right Edge	$s \in (0,20.0)$	$6.3000\ s^2 - 155.4000\ s + 1048.700$
Middle Arc	$s \in (0,17.5)$	$8.4194\ s^2 - 142.5470\ s + 829.4353$
Left Edge	$s \in (0,20.0)$	$8.2000\ s^2 - 181.3000\ s + 1049.800$

DESIGN PRESSURE LINE
TESTS T1133 AND T1134

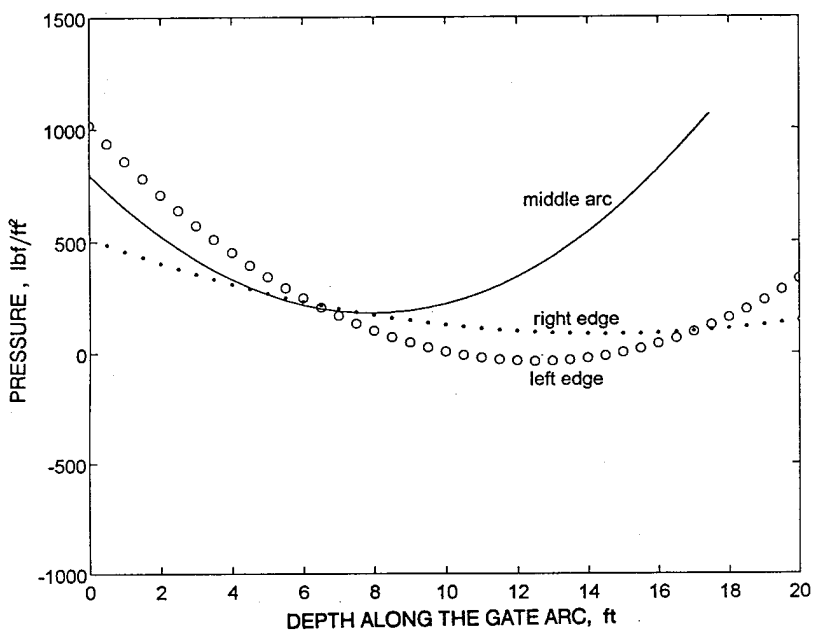

ANALYTICAL EXPRESSIONS FOR PRESSURE CURVES		
Longitudinal Arc on Gate Skin	Domain, s [ft]	Prototype Pressure Field [psf]
Right Edge	$s \in (0,20.0)$	$+2.0301\ s^2 - 59.0219\ s + 514.9835$
Middle Arc	$s \in (0,17.5)$	$+9.7798\ s^2 - 155.0666\ s + 797.2184$
Left Edge	$s \in (0,20.0)$	$+6.7000\ s^2 - 167.900\ s + 1016.500$

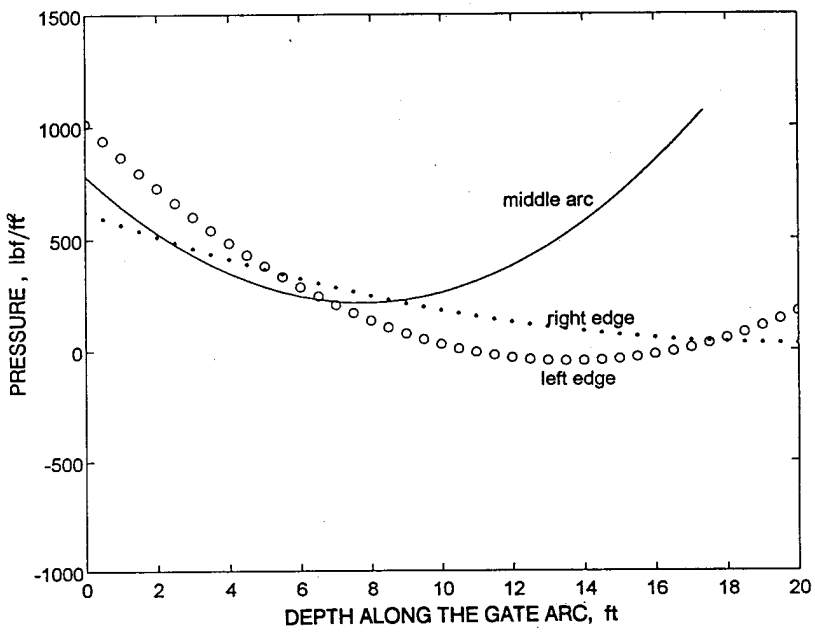

ANALYTICAL EXPRESSIONS FOR PRESSURE CURVES		
Longitudinal Arc on Gate Skin	Domain, s [ft]	Prototype Pressure Field [psf]
Right Edge	$s \in (0,20.0)$	$+1.4381\ s^2 - 58.4009\ s + 622.1805$
Middle Arc	$s \in (0,17.5)$	$+9.3179\ s^2 - 145.1614\ s + 780.9228$
Left Edge	$s \in (0,20.0)$	$+5.7000\ s^2 - 155.000\ s + 1013.300$

DESIGN PRESSURE LINE
TESTS T1166 AND T1167

Plate 35

Plate 36

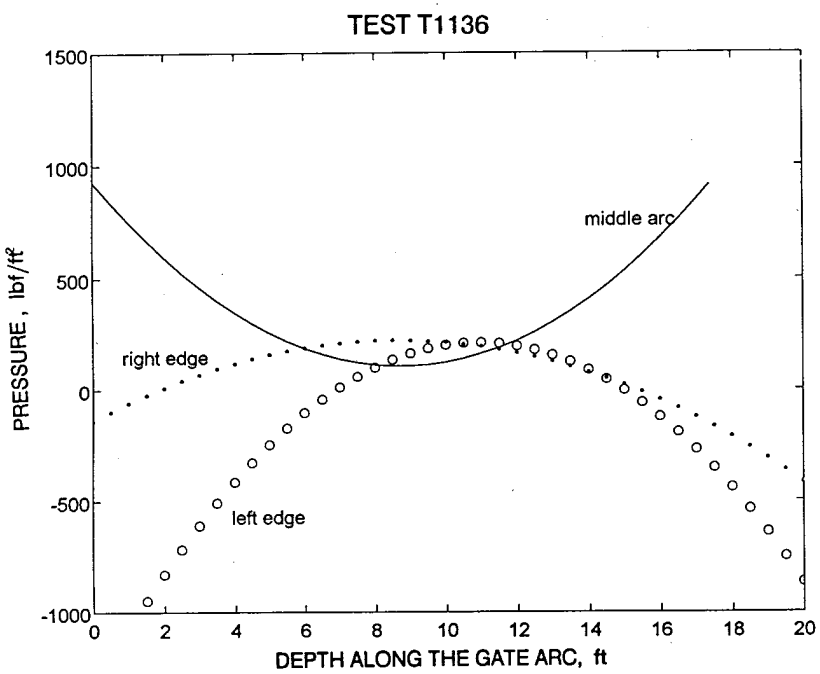

ANALYTICAL EXPRESSIONS FOR PRESSURE CURVES		
Longitudinal Arc on Gate Skin	Domain, s [ft]	Prototype Pressure Field [psf]
Right Edge	$s \in (0,20.0)$	$-4.9100\ s^2 + 84.2779\ s - 139.8572$
Middle Arc	$s \in (0,17.5)$	$10.7700\ s^2 - 188.1035\ s + 927.9033$
Left Edge	$s \in (0,20.0)$	$-13.1000\ s^2 + 285.2\ s - 1346.800$

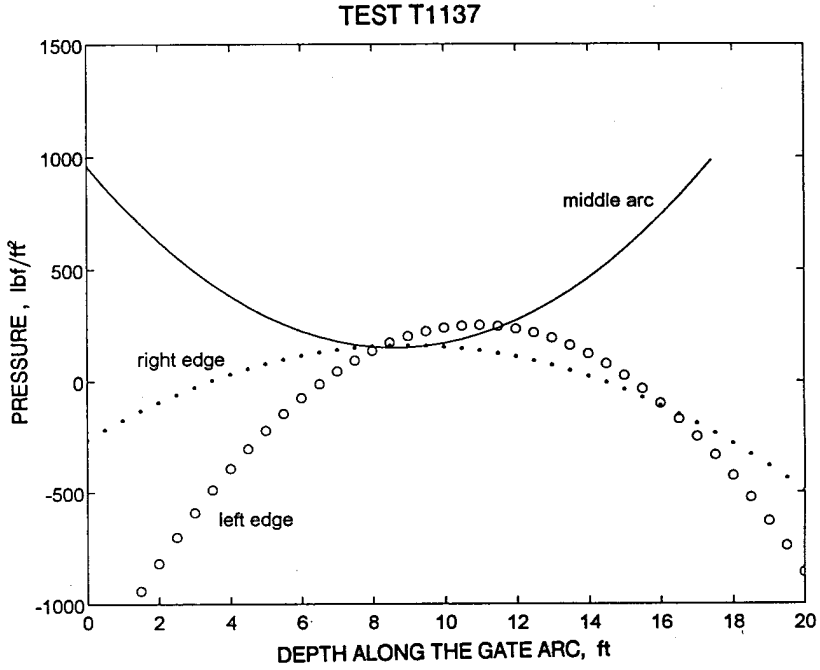

ANALYTICAL EXPRESSIONS FOR PRESSURE CURVES		
Longitudinal Arc on Gate Skin	Domain, s [ft]	Prototype Pressure Field [psf]
Right Edge	$s \in (0,20.0)$	$-5.2921\ s^2 + 94.3154\ s - 262.6130$
Middle Arc	$s \in (0,17.5)$	$10.8788\ s^2 - 187.9455\ s + 959.2971$
Left Edge	$s \in (0,20.0)$	$-13.4000\ s^2 + 292.8\ s - 1350.200$

DESIGN PRESSURE LINE
TESTS T1136 AND T1137

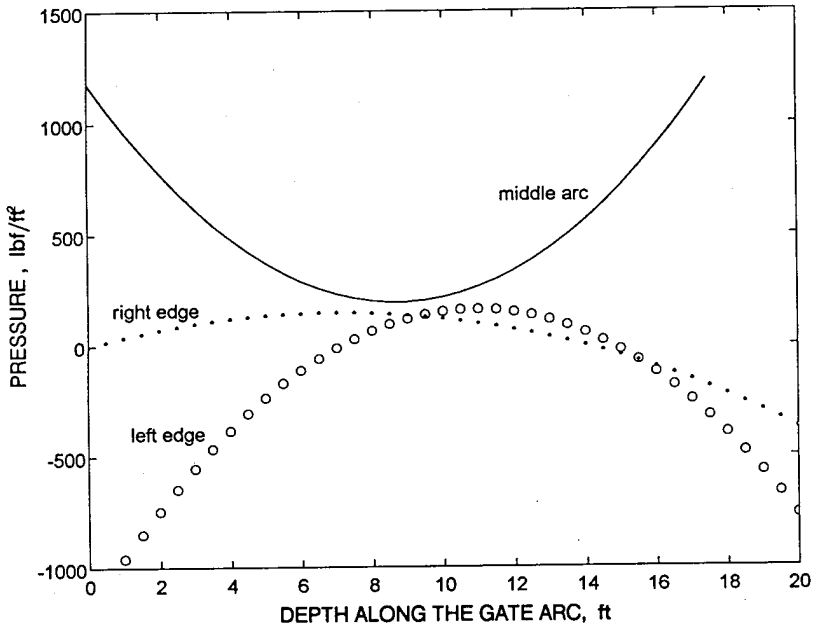

ANALYTICAL EXPRESSIONS FOR PRESSURE CURVES		
Longitudinal Arc on Gate Skin	Domain, s [ft]	Prototype Pressure Field [psf]
Right Edge	$s \in (0,20.0)$	$-3.1039\ s^2 + 43.5047\ s - 3.1585$
Middle Arc	$s \in (0,17.5)$	$13.1000\ s^2 - 227.0\ s + 1181.600$
Left Edge	$s \in (0,20.0)$	$-11.3000\ s^2 + 248.4\ s - 1197.600$

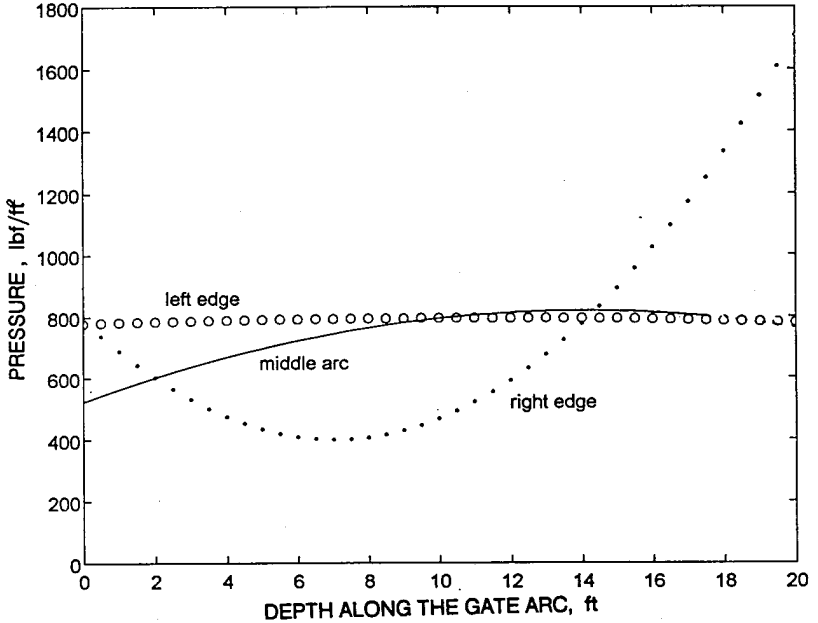

ANALYTICAL EXPRESSIONS FOR PRESSURE CURVES		
Longitudinal Arc on Gate Skin	Domain, s [ft]	Prototype Pressure Field [psf]
Right Edge	$s \in (0,20.0)$	$7.8201\ s^2 - 110.5347\ s + 790.4134$
Middle Arc	$s \in (0,17.5)$	$-1.5322\ s^2 + 42.6617\ s + 522.4232$
Left Edge	$s \in (0,20.0)$	$-0.1691\ s^2 + 3.4624\ s + 778.0848$

DESIGN PRESSURE LINE
TESTS T1138 AND T1179

Plate 37

Plate 38

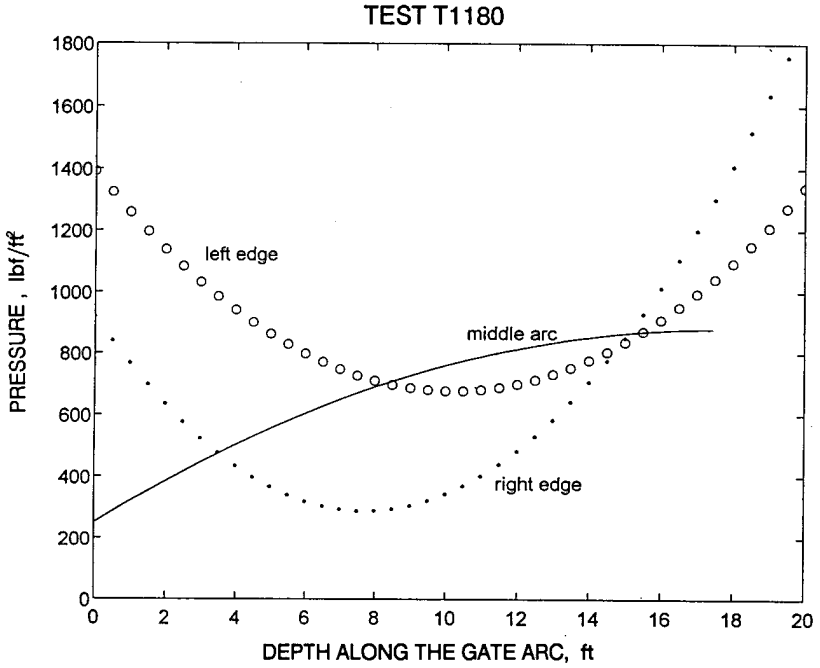

ANALYTICAL EXPRESSIONS FOR PRESSURE CURVES		
Longitudinal Arc on Gate Skin	Domain, s [ft]	Prototype Pressure Field [psf]
Right Edge	$s \in (0,20.0)$	$10.5945\ s^2 - 163.5804\ s + 919.1839$
Middle Arc	$s \in (0,17.5)$	$-1.9955\ s^2 + 70.9175\ s + 250.3818$
Left Edge	$s \in (0,20.0)$	$6.9\ s^2 - 140.3\ s + 1391.6$

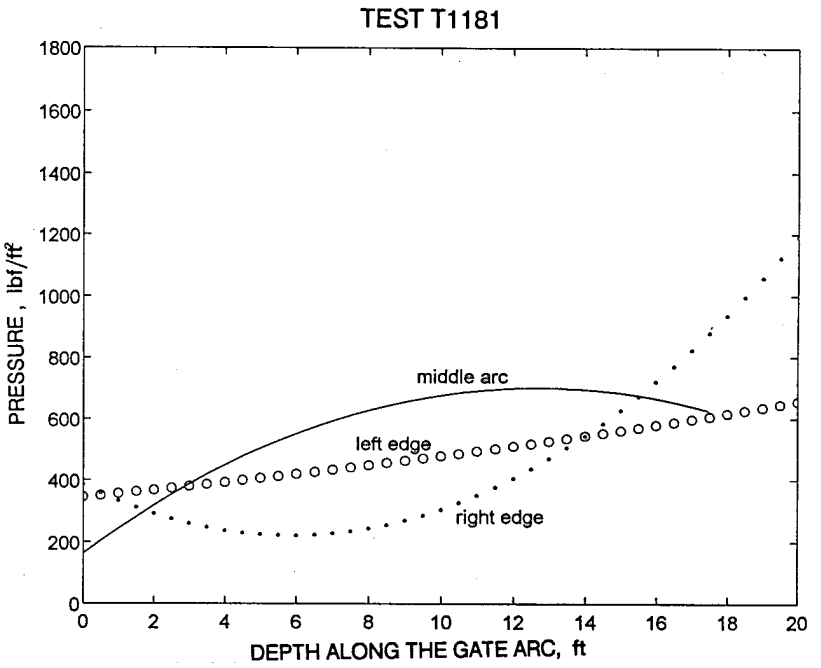

ANALYTICAL EXPRESSIONS FOR PRESSURE CURVES		
Longitudinal Arc on Gate Skin	Domain, s [ft]	Prototype Pressure Field [psf]
Right Edge	$s \in (0,20.0)$	$4.8231\ s^2 - 56.2069\ s + 385.1905$
Middle Arc	$s \in (0,17.5)$	$-3.3414\ s^2 + 84.9079\ s + 163.0884$
Left Edge	$s \in (0,20.0)$	$0.2265\ s^2 + 10.9476\ s + 345.6203$

DESIGN PRESSURE LINE
TESTS T1180 AND T1181

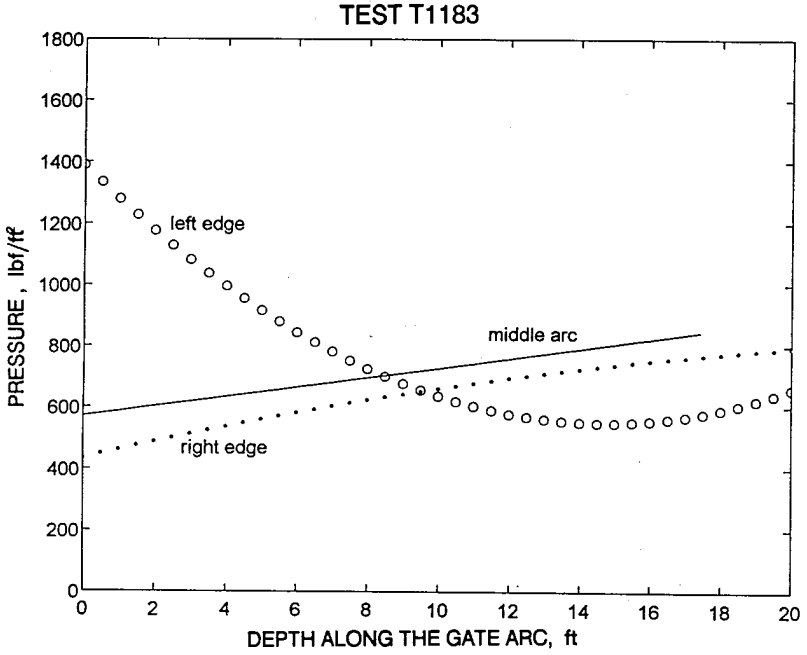

ANALYTICAL EXPRESSIONS FOR PRESSURE CURVES		
Longitudinal Arc on Gate Skin	Domain, s [ft]	Prototype Pressure Field [psf]
Right Edge	$s \in (0,20.0)$	$-0.4530\ s^2 + 26.9128\ s + 435.7306$
Middle Arc	$s \in (0,17.5)$	$0.0385\ s^2 + 15.0680\ s + 571.8688$
Left Edge	$s \in (0,20.0)$	$3.9\ s^2 - 114.2\ s + 1389.3$

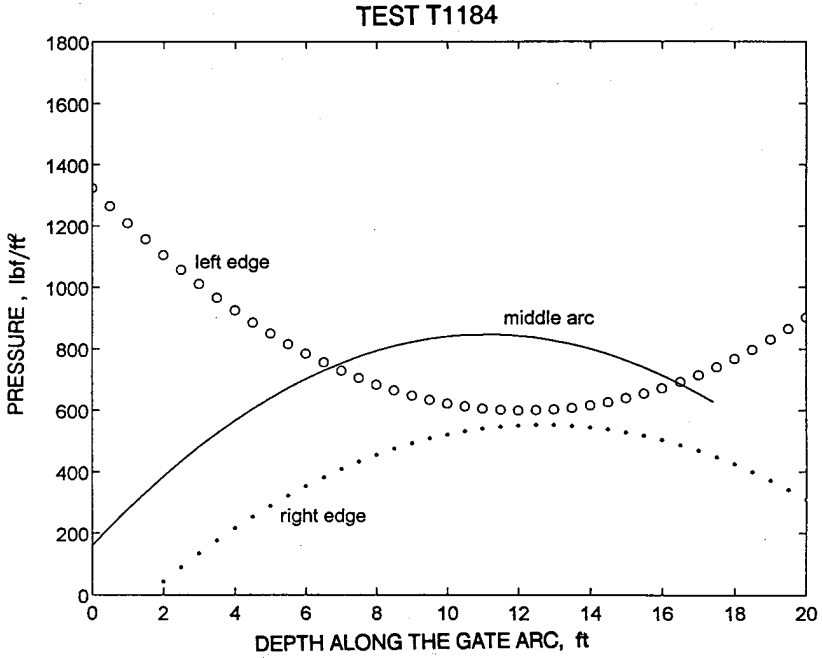

ANALYTICAL EXPRESSIONS FOR PRESSURE CURVES		
Longitudinal Arc on Gate Skin	Domain, s [ft]	Prototype Pressure Field [psf]
Right Edge	$s \in (0,20.0)$	$-4.4803\ s^2 + 113.4453\ s - 166.3154$
Middle Arc	$s \in (0,17.5)$	$-5.5631\ s^2 + 123.6245\ s + 160.7348$
Left Edge	$s \in (0,20.0)$	$4.9\ s^2 - 119.4\ s + 1323.1$

DESIGN PRESSURE LINE
TESTS T1183 AND T1184

Plate 39

Plate 40

TEST T1187

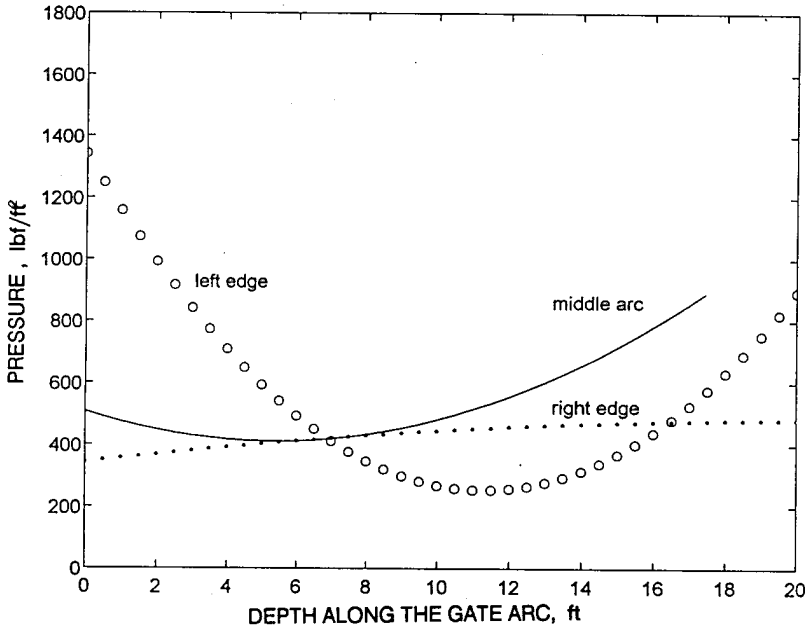

ANALYTICAL EXPRESSIONS FOR PRESSURE CURVES		
Longitudinal Arc on Gate Skin	Domain, s [ft]	Prototype Pressure Field [psf]
Right Edge	$s \in (0,20.0)$	$-0.3262\ s^2 + 13.4887\ s + 342.7067$
Middle Arc	$s \in (0,17.5)$	$3.3016\ s^2 - 35.5361\ s + 506.9004$
Left Edge	$s \in (0,20.0)$	$8.5\ s^2 - 192.6\ s + 1342.6$

TEST T1147

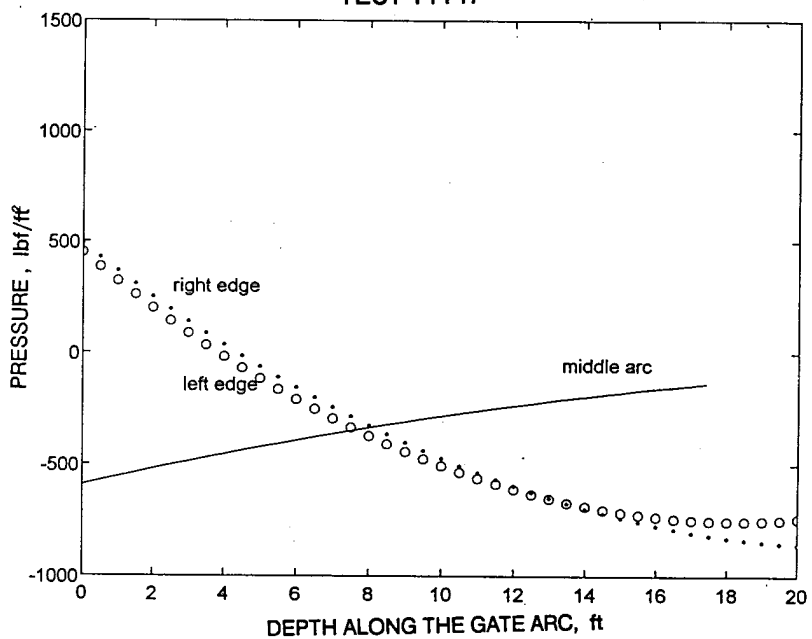

ANALYTICAL EXPRESSIONS FOR PRESSURE CURVES		
Longitudinal Arc on Gate Skin	Domain, s [ft]	Prototype Pressure Field [psf]
Right Edge	$s \in (0,20.0)$	$+2.9050\ s^2 - 125.5614\ s + 491.0501$
Middle Arc	$s \in (0,17.5)$	$-0.6236\ s^2 + 36.9377\ s - 591.9327$
Left Edge	$s \in (0,20.0)$	$+3.6212\ s^2 - 132.0175\ s + 450.2430$

DESIGN PRESSURE LINE
TESTS T1187 AND T1147

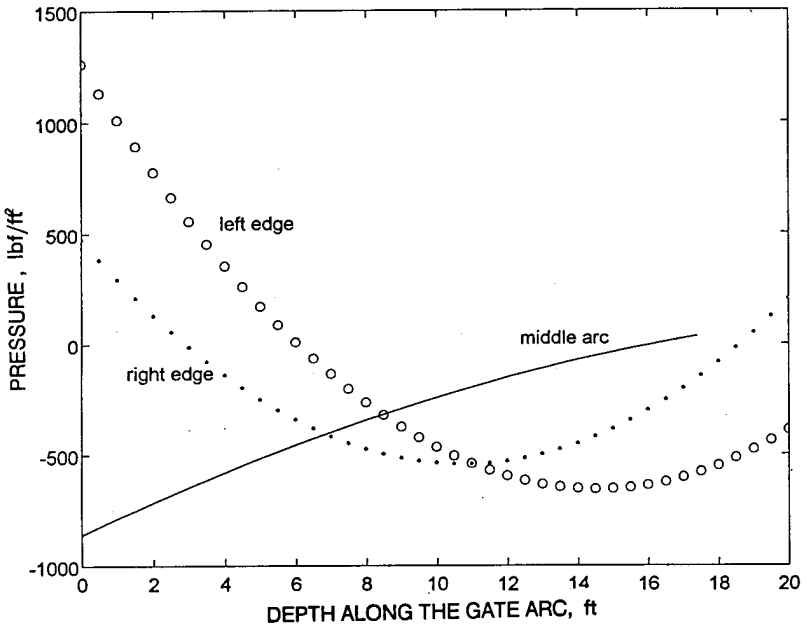

ANALYTICAL EXPRESSIONS FOR PRESSURE CURVES		
Longitudinal Arc on Gate Skin	Domain, s [ft]	Prototype Pressure Field [psf]
Right Edge	$s \in (0,20.0)$	$+8.7595\ s^2 - 188.6062\ s + 474.1452$
Middle Arc	$s \in (0,17.5)$	$-1.3679\ s^2 + 75.1482\ s - 856.8454$
Left Edge	$s \in (0,20.0)$	$+9\ s^2 - 263\ s + 1262.9$

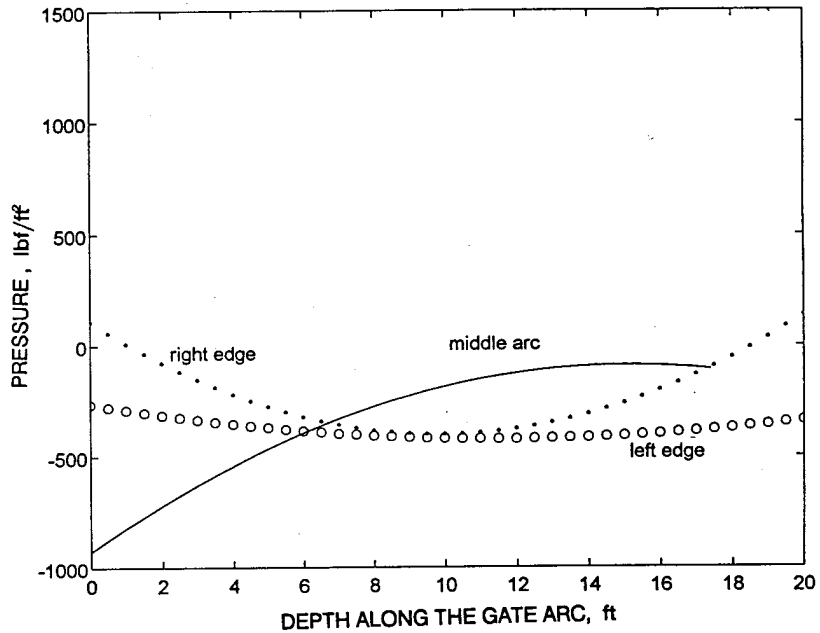

ANALYTICAL EXPRESSIONS FOR PRESSURE CURVES		
Longitudinal Arc on Gate Skin	Domain, s [ft]	Prototype Pressure Field [psf]
Right Edge	$s \in (0,20.0)$	$+5.2076\ s^2 - 102.6362\ s + 105.7978$
Middle Arc	$s \in (0,17.5)$	$-3.6746\ s^2 + 110.8452\ s - 925.9502$
Left Edge	$s \in (0,20.0)$	$+1.1583\ s^2 - 26.8233\ s - 266.3836$

DESIGN PRESSURE LINE
TESTS T1148 AND T1149

Plate 41

Plate 42

TEST T1150

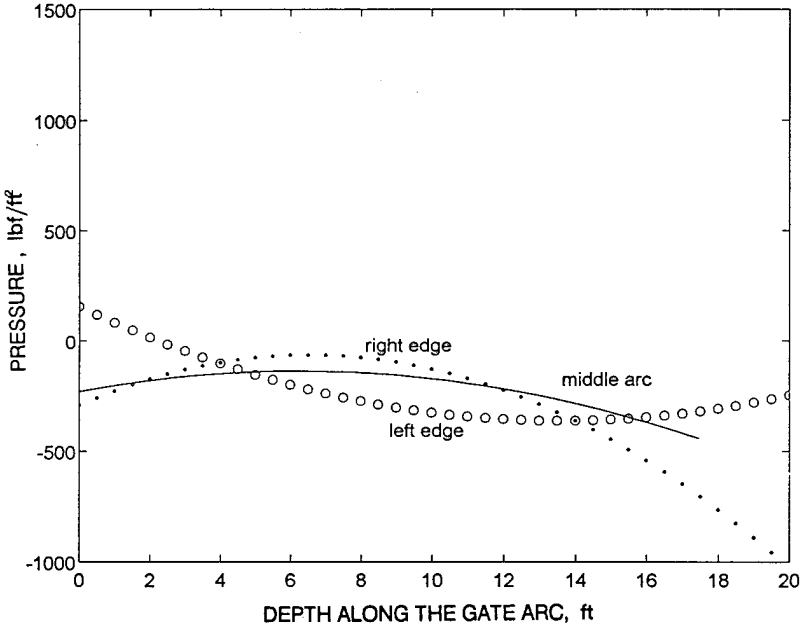

ANALYTICAL EXPRESSIONS FOR PRESSURE CURVES		
Longitudinal Arc on Gate Skin	Domain, s [ft]	Prototype Pressure Field [psf]
Right Edge	$s \in (0,20.0)$	$-5.3156\ s^2 + 69.5476\ s - 292.1451$
Middle Arc	$s \in (0,17.5)$	$-2.4117\ s^2 + 30.0621\ s - 230.7249$
Left Edge	$s \in (0,20.0)$	$+2.7863\ s^2 - 75.8778\ s + 155.4939$

TEST T1170

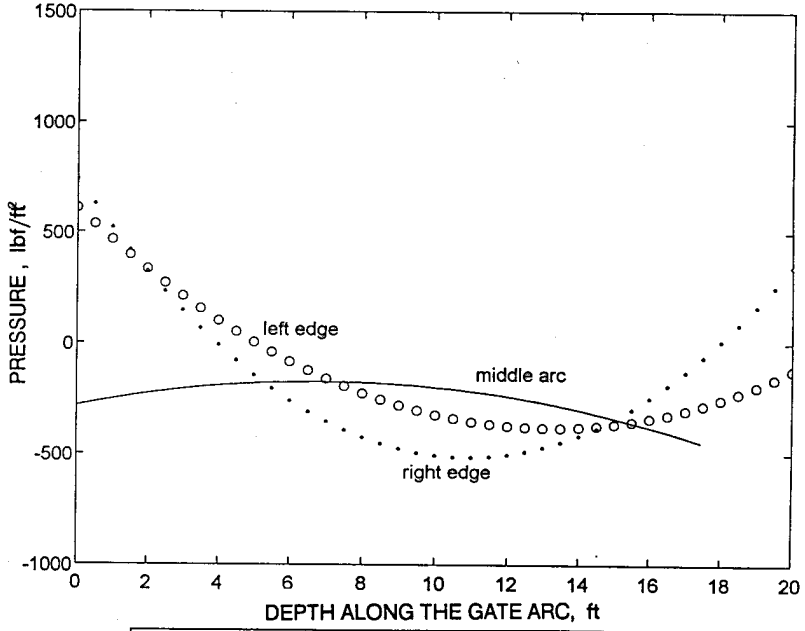

ANALYTICAL EXPRESSIONS FOR PRESSURE CURVES		
Longitudinal Arc on Gate Skin	Domain, s [ft]	Prototype Pressure Field [psf]
Right Edge	$s \in (0,20.0)$	$+10.4921\ s^2 - 229.5911\ s + 740.8055$
Middle Arc	$s \in (0,17.5)$	$-2.3889\ s^2 + 32.2058\ s - 281.6576$
Left Edge	$s \in (0,20.0)$	$+5.6463\ s^2 - 149.6412\ s + 609.8865$

DESIGN PRESSURE LINE
TESTS T1150 AND T1170

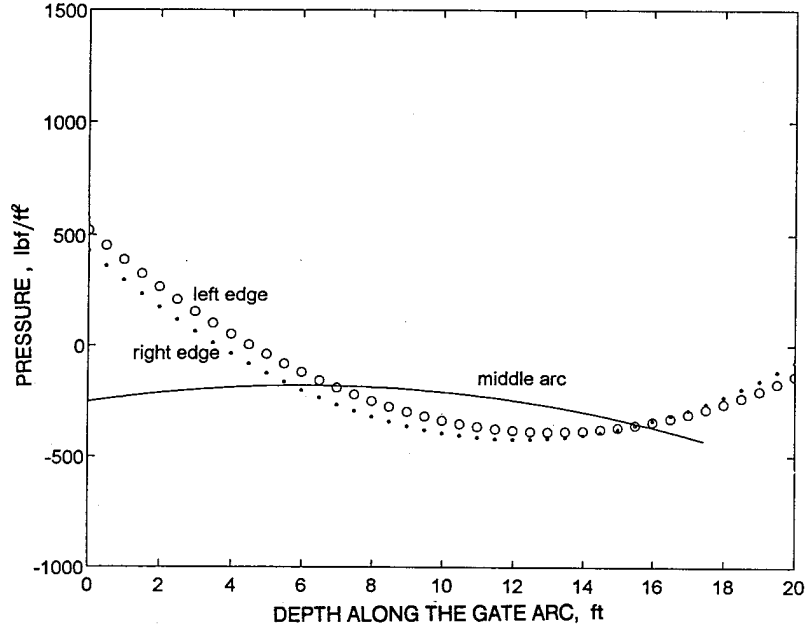

ANALYTICAL EXPRESSIONS FOR PRESSURE CURVES		
Longitudinal Arc on Gate Skin	Domain, s [ft]	Prototype Pressure Field [psf]
Right Edge	$s \in (0,20.0)$	$+5.7169\ s^2 - 139.6285\ s + 429.9926$
Middle Arc	$s \in (0,17.5)$	$-1.9498\ s^2 + 23.9009\ s - 253.0549$
Left Edge	$s \in (0,20.0)$	$+5.2900\ s^2 - 138.8463\ s + 521.6133$

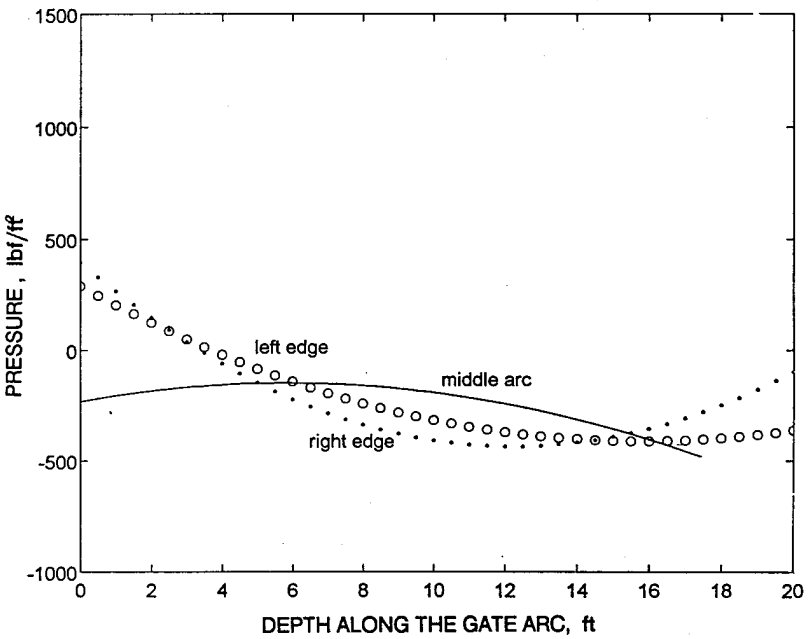

ANALYTICAL EXPRESSIONS FOR PRESSURE CURVES		
Longitudinal Arc on Gate Skin	Domain, s [ft]	Prototype Pressure Field [psf]
Right Edge	$s \in (0,20.0)$	$+5.5841\ s^2 - 136.2823\ s + 395.9376$
Middle Arc	$s \in (0,17.5)$	$-2.4740\ s^2 + 28.7663\ s - 229.6831$
Left Edge	$s \in (0,20.0)$	$+2.7930\ s^2 - 88.4251\ s + 288.4469$

DESIGN PRESSURE LINE
TESTS T1171 AND T1172

Plate 43

Plate 44

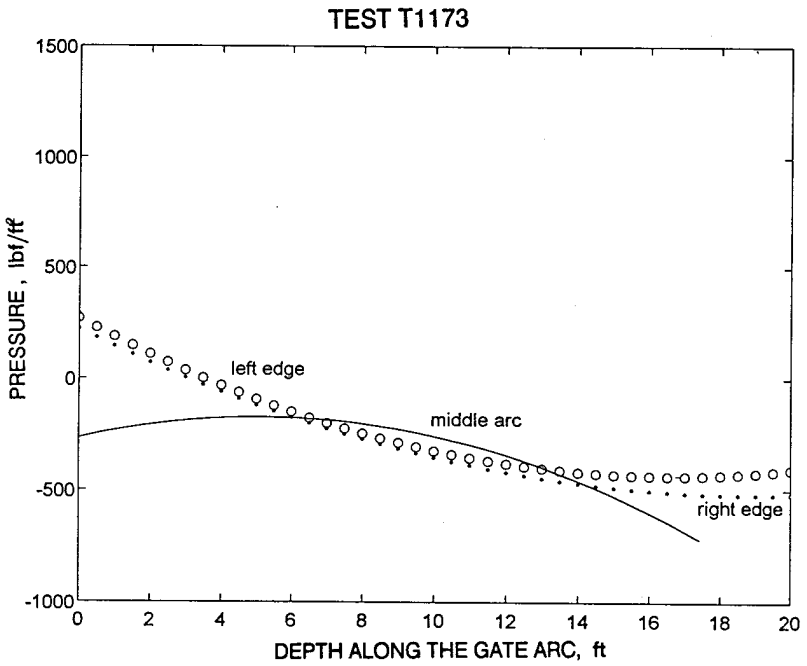

ANALYTICAL EXPRESSIONS FOR PRESSURE CURVES		
Longitudinal Arc on Gate Skin	Domain, s [ft]	Prototype Pressure Field [psf]
Right Edge	$s \in (0,20.0)$	$+2.0568\ s^2 - 77.9738\ s + 218.5264$
Middle Arc	$s \in (0,17.5)$	$-3.6108\ s^2 + 36.9385\ s - 267.0951$
Left Edge	$s \in (0,20.0)$	$+2.5436\ s^2 - 84.6497\ s + 266.6175$

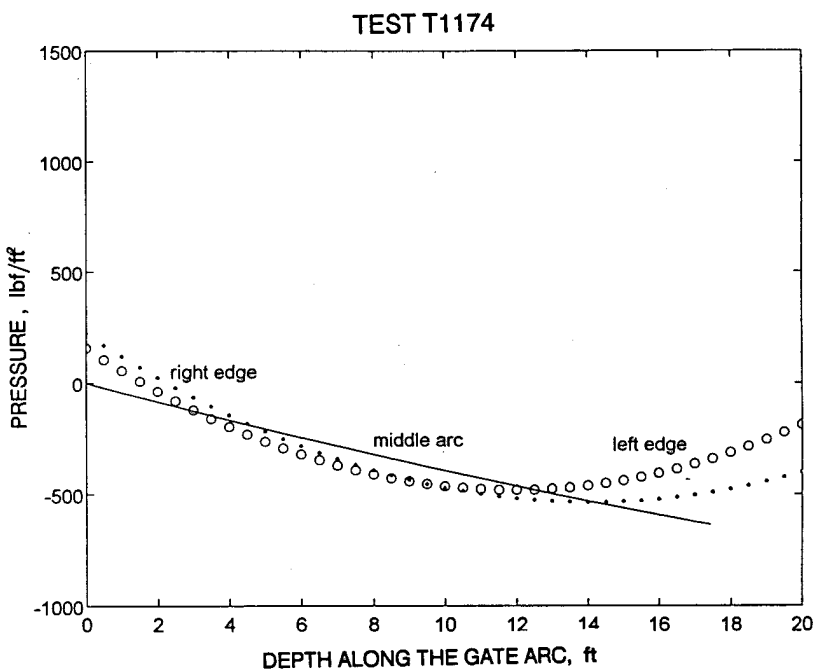

ANALYTICAL EXPRESSIONS FOR PRESSURE CURVES		
Longitudinal Arc on Gate Skin	Domain, s [ft]	Prototype Pressure Field [psf]
Right Edge	$s \in (0,20.0)$	$+3.8182\ s^2 - 107.6143\ s + 222.9910$
Middle Arc	$s \in (0,17.5)$	$+0.4061\ s^2 - 43.4444\ s - 1.0374$
Left Edge	$s \in (0,20.0)$	$+4.4745\ s^2 - 106.8299\ s + 156.6005$

DESIGN PRESSURE LINE
TESTS T1173 AND T1174

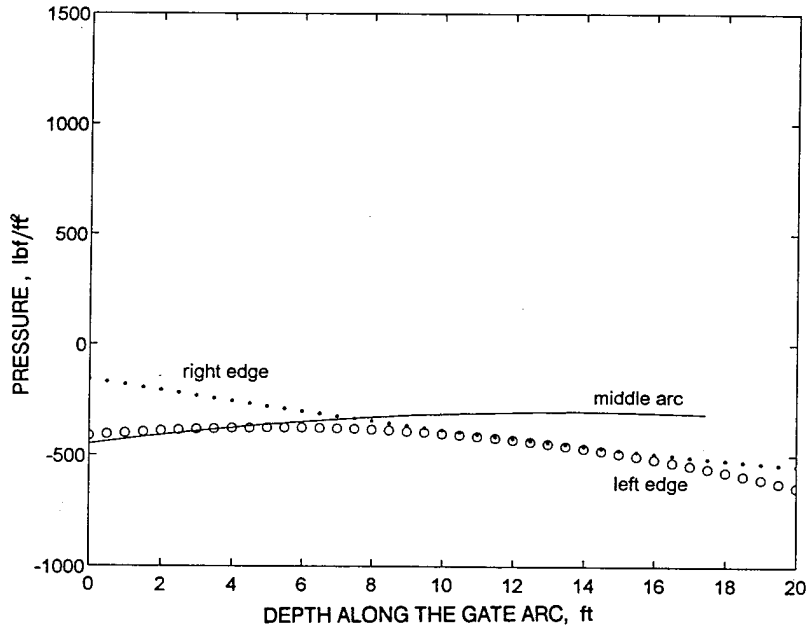

ANALYTICAL EXPRESSIONS FOR PRESSURE CURVES		
Longitudinal Arc on Gate Skin	Domain, s [ft]	Prototype Pressure Field [psf]
Right Edge	$s \in (0,20.0)$	$+0.3576\ s^2 - 26.7481\ s - 155.9909$
Middle Arc	$s \in (0,17.5)$	$-0.7682\ s^2 + 21.1040\ s - 449.2657$
Left Edge	$s \in (0,20.0)$	$-1.2399\ s^2 + 13.3228\ s - 413.5094$

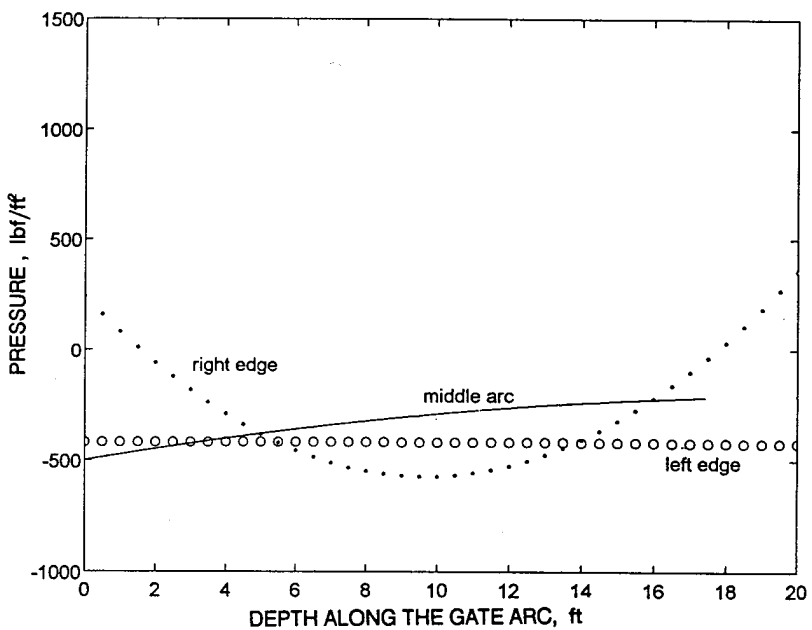

ANALYTICAL EXPRESSIONS FOR PRESSURE CURVES		
Longitudinal Arc on Gate Skin	Domain, s [ft]	Prototype Pressure Field [psf]
Right Edge	$s \in (0,20.0)$	$+8.7149\ s^2 - 168.5029\ s + 242.4715$
Middle Arc	$s \in (0,17.5)$	$-0.6307\ s^2 + 27.1943\ s - 499.6905$
Left Edge	$s \in (0,20.0)$	$-0.036\ s^2 + 0.4496\ s - 419.0499$

DESIGN PRESSURE LINE
TESTS T1175 AND T1176

Plate 45

Plate 46

TEST T1177

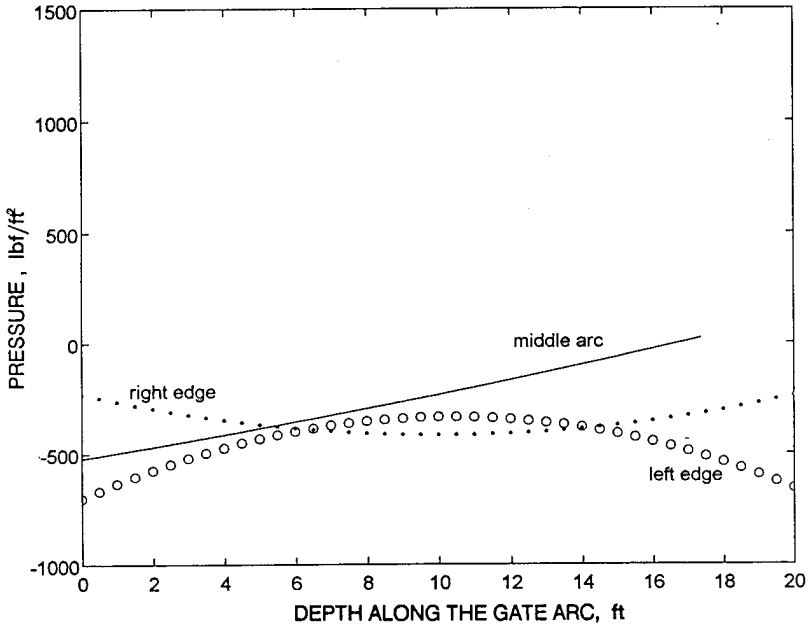

ANALYTICAL EXPRESSIONS FOR PRESSURE CURVES		
Longitudinal Arc on Gate Skin	Domain, s [ft]	Prototype Pressure Field [psf]
Right Edge	$s \in (0,20.0)$	$+1.8188\ s^2 - 36.8172\ s - 229.5827$
Middle Arc	$s \in (0,17.5)$	$+0.3417\ s^2 + 25.3103\ s - 519.9604$
Left Edge	$s \in (0,20.0)$	$-3.4578\ s^2 + 71.3865\ s - 703.3644$

TEST T1188

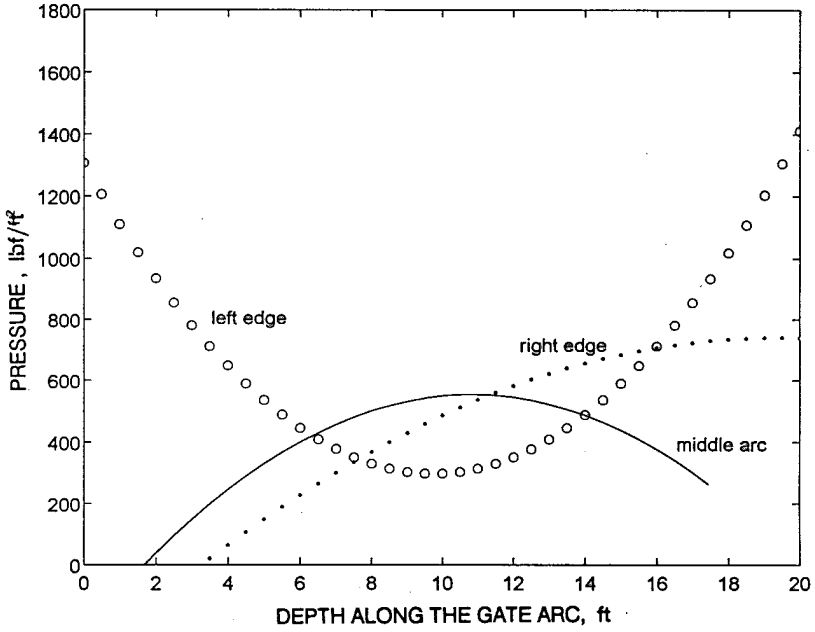

ANALYTICAL EXPRESSIONS FOR PRESSURE CURVES		
Longitudinal Arc on Gate Skin	Domain, s [ft]	Prototype Pressure Field [psf]
Right Edge	$s \in (0,20.0)$	$-2.8162\ s^2 + 109.8333\ s - 330.4590$
Middle Arc	$s \in (0,17.5)$	$-6.6221\ s^2 + 143.2369\ s - 220.1150$
Left Edge	$s \in (0,20.0)$	$10.6\ s^2 - 206.9\ s + 1305.8$

DESIGN PRESSURE LINE
TESTS T1177 AND T1188

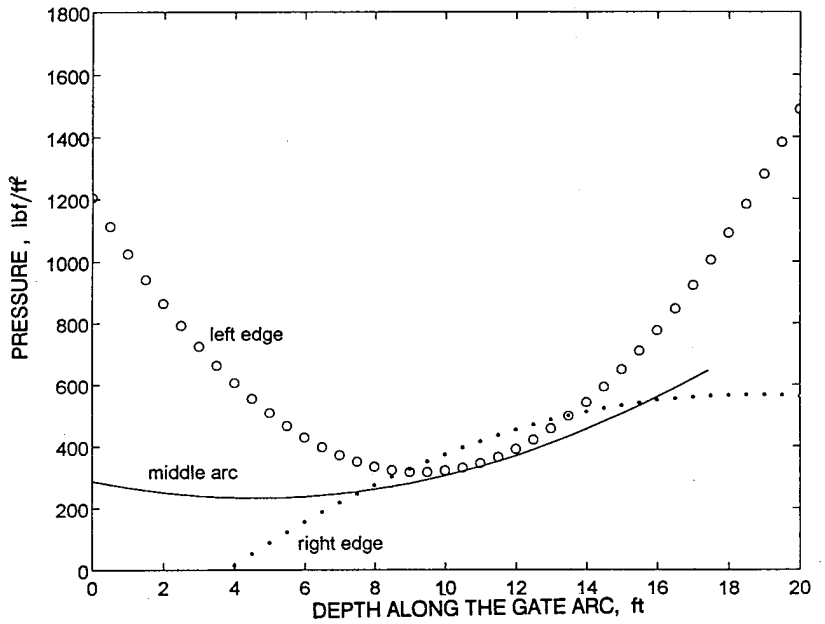

ANALYTICAL EXPRESSIONS FOR PRESSURE CURVES		
Longitudinal Arc on Gate Skin	Domain, s [ft]	Prototype Pressure Field [psf]
Right Edge	$s \in (0,20.0)$	$-2.5714\ s^2 + 95.8921\ s - 327.2144$
Middle Arc	$s \in (0,17.5)$	$2.5389\ s^2 - 23.6915\ s + 289.4643$
Left Edge	$s \in (0,20.0)$	$10.3\ s^2 - 190.9\ s + 1205.2$

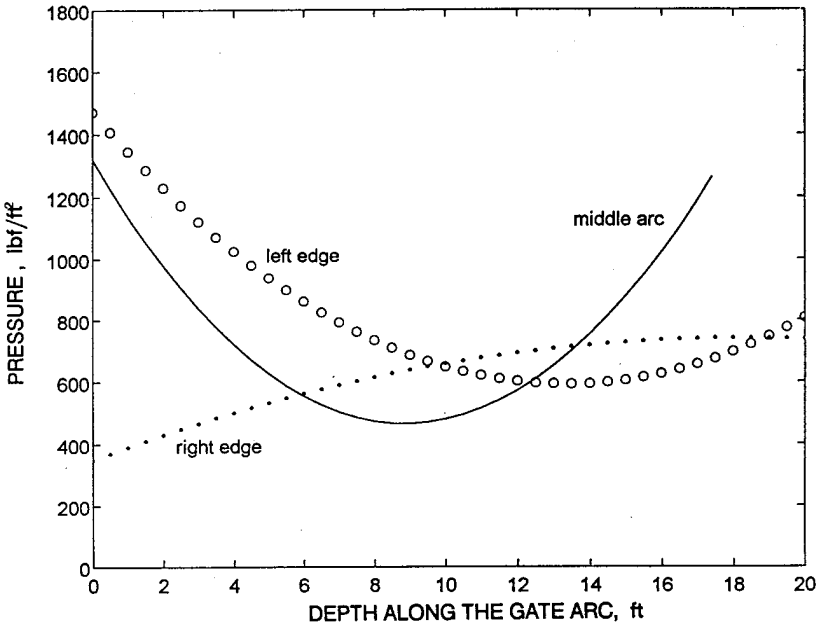

ANALYTICAL EXPRESSIONS FOR PRESSURE CURVES		
Longitudinal Arc on Gate Skin	Domain, s [ft]	Prototype Pressure Field [psf]
Right Edge	$s \in (0,20.0)$	$-1.1542\ s^2 + 42.5744\ s + 348.6314$
Middle Arc	$s \in (0,17.5)$	$10.9\ s^2 - 193\ s + 1319.6$
Left Edge	$s \in (0,20.0)$	$4.9\ s^2 - 131.2\ s + 1470.8$

DESIGN PRESSURE LINE
TESTS T1189 AND T1190

Plate 47

Plate 48

TEST T1191

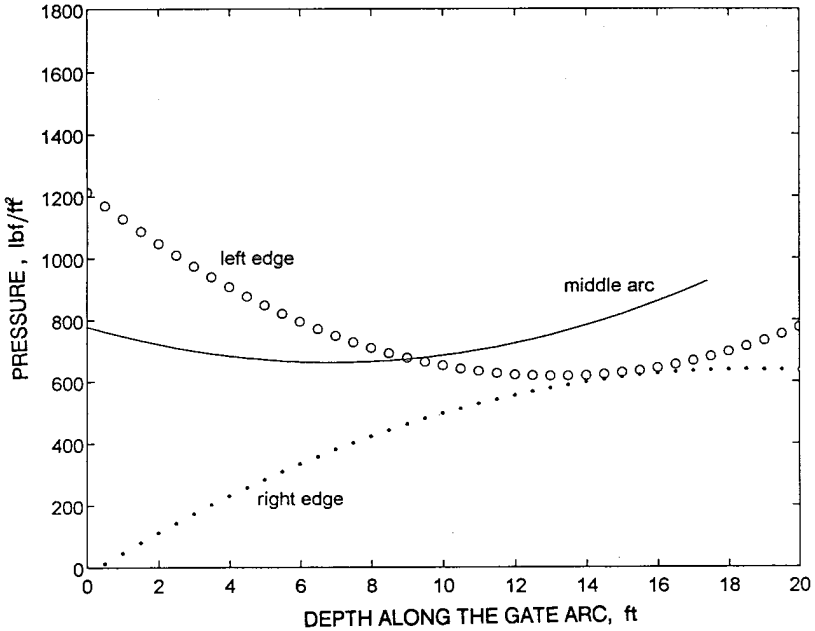

ANALYTICAL EXPRESSIONS FOR PRESSURE CURVES		
Longitudinal Arc on Gate Skin	Domain, s [ft]	Prototype Pressure Field [psf]
Right Edge	$s \in (0,20.0)$	$-1.9080\ s^2 + 71.1053\ s - 23.3292$
Middle Arc	$s \in (0,17.5)$	$2.4027\ s^2 - 33.2551\ s + 778.5306$
Left Edge	$s \in (0,20.0)$	$3.4\ s^2 - 90.5\ s + 1214.10$

TEST T1157

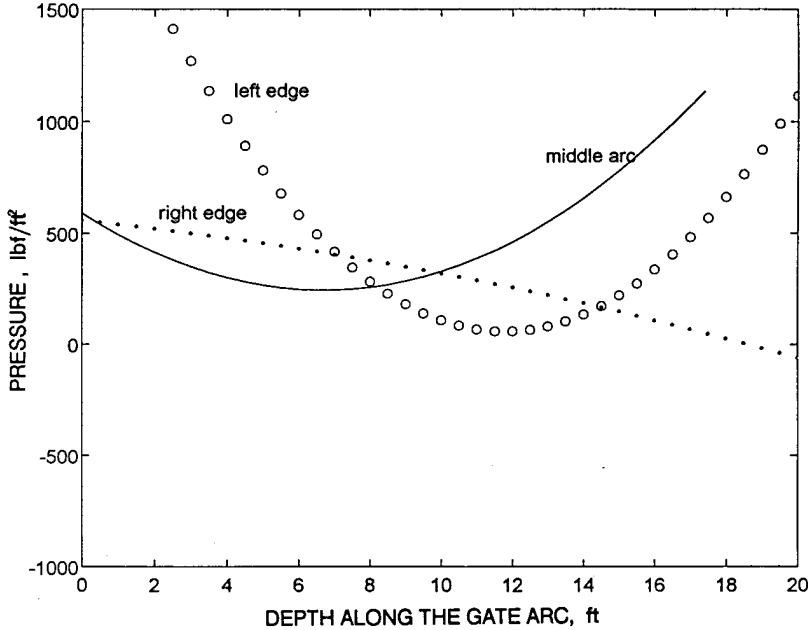

ANALYTICAL EXPRESSIONS FOR PRESSURE CURVES		
Longitudinal Arc on Gate Skin	Domain, s [ft]	Prototype Pressure Field [psf]
Right Edge	$s \in (0,20.0)$	$-0.6949\ s^2 - 17.1004\ s + 558.1922$
Middle Arc	$s \in (0,17.5)$	$+7.7724\ s^2 - 104.1197\ s + 591.2618$
Left Edge	$s \in (0,20.0)$	$+15.7\ s^2 - 371\ s + 2242.30$

DESIGN PRESSURE LINE
TESTS T1191 AND T1157

TEST T1158

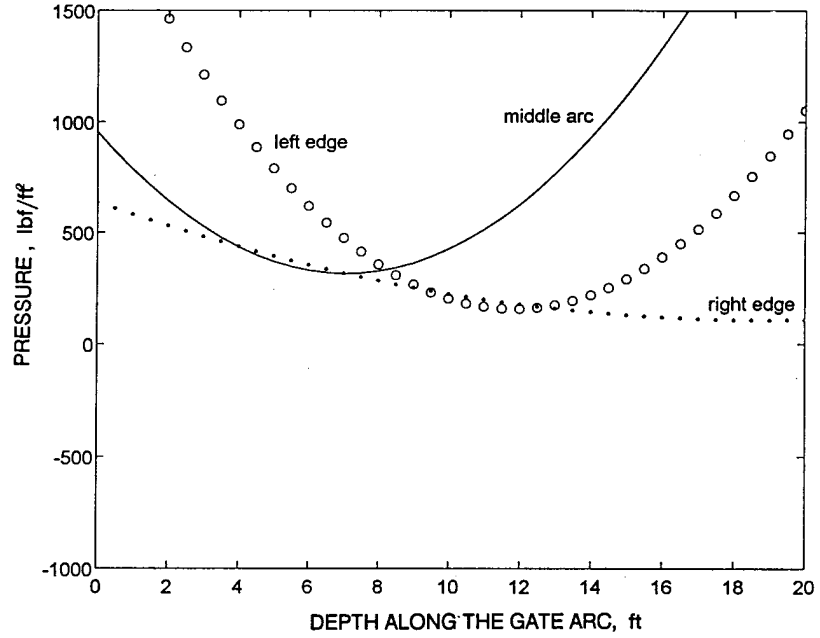

ANALYTICAL EXPRESSIONS FOR PRESSURE CURVES		
Longitudinal Arc on Gate Skin	Domain, s [ft]	Prototype Pressure Field [psf]
Right Edge	s ∈ (0,20.0)	+1.4701 s^2 - 55.7829 s + 635.8741
Middle Arc	s ∈ (0,17.5)	+12.8166 s^2 - 181.0689 s + 955.1730
Left Edge	s ∈ (0,20.0)	+13.5 s^2 - 318.8 s + 2046.80

TEST T1192

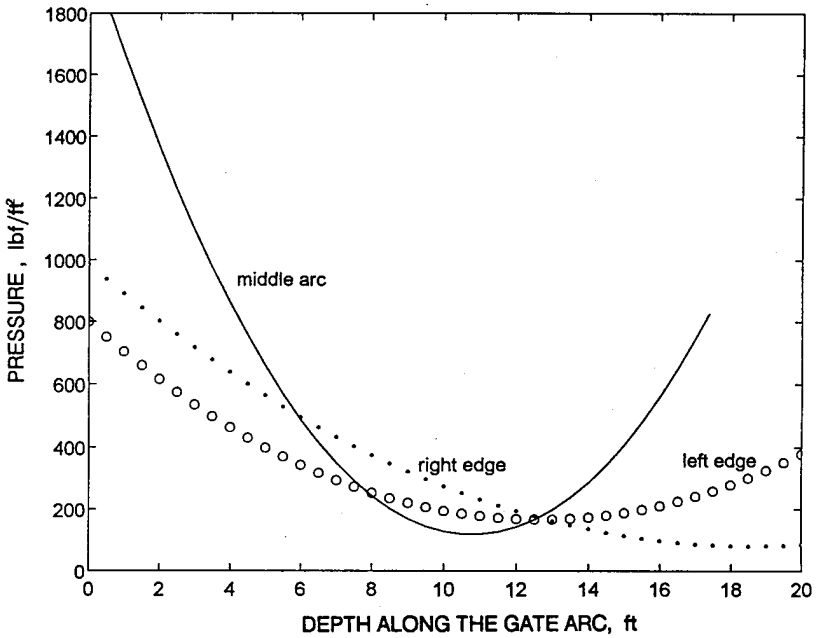

ANALYTICAL EXPRESSIONS FOR PRESSURE CURVES		
Longitudinal Arc on Gate Skin	Domain, s [ft]	Prototype Pressure Field [psf]
Right Edge	s ∈ (0,20.0)	2.6229 s^2 - 97.4294 s + 985.2492
Middle Arc	s ∈ (0,17.5)	16.2 s^2 - 348.5 s + 1996.2
Left Edge	s ∈ (0,20.0)	3.9403 s^2 - 99.8309 s + 798.6494

DESIGN PRESSURE LINE
TESTS T1158 AND T1192

Plate 49

Plate 50

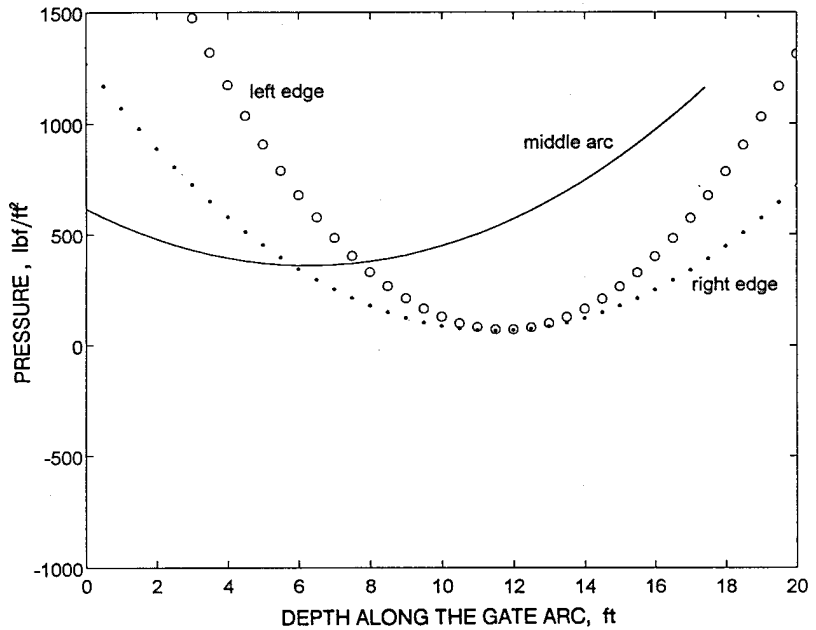

ANALYTICAL EXPRESSIONS FOR PRESSURE CURVES		
Longitudinal Arc on Gate Skin	Domain, s [ft]	Prototype Pressure Field [psf]
Right Edge	$s \in (0,20.0)$	$+9.1\ s^2 - 208.8\ s + 1269.2$
Middle Arc	$s \in (0,17.5)$	$+6.4928\ s^2 - 81.8183\ s + 617.0607$
Left Edge	$s \in (0,20.0)$	$+18.3\ s^2 - 430.0\ s + 2599.30$

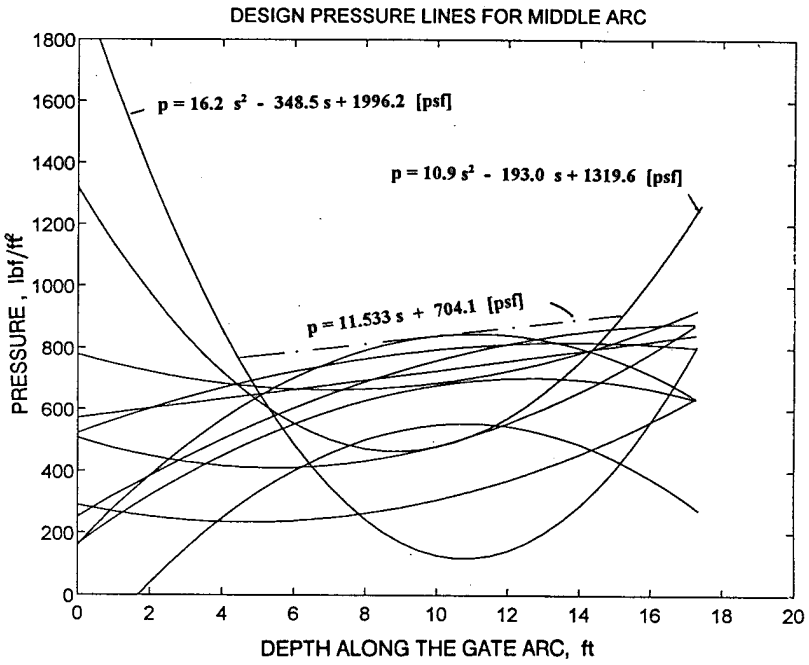

DESIGN PRESSURE LINE
TEST T1161

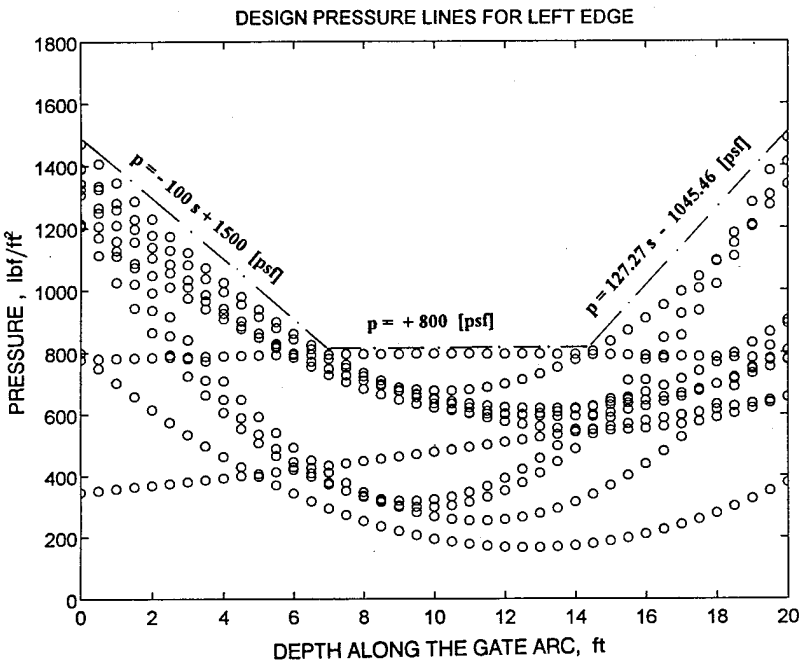

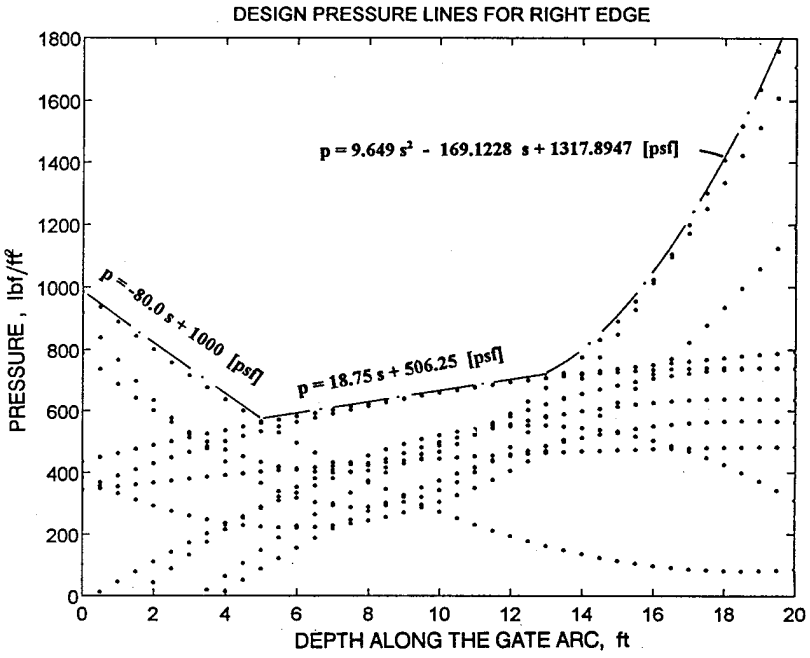

DESIGN PRESSURE LINES
LEFT AND RIGHT EDGES

Plate 51

REPORT DOCUMENTATION PAGE

Form Approved
OMB No. 0704-0188

1. AGENCY USE ONLY *(Leave blank)*	2. REPORT DATE	3. REPORT TYPE AND DATES COVERED
	November 1995	Report 1 of a Series

4. TITLE AND SUBTITLE

Montgomery Point Lock and Dam Gate Study; Report 1, Hydraulic Forces and Characteristics Acting on Spillway Gates

5. FUNDING NUMBERS

6. AUTHOR(S)

Bobby P. Fletcher
Luis A. de Bejar

7. PERFORMING ORGANIZATION NAME(S) AND ADDRESS(ES)

U.S. Army Engineer Waterways Experiment Station
3909 Halls Ferry Road, Vicksburg, MS 39180-6199

8. PERFORMING ORGANIZATION REPORT NUMBER

Technical Report
HL-95-14

9. SPONSORING/MONITORING AGENCY NAME(S) AND ADDRESS(ES)

U.S. Army Engineer District, Little Rock
P.O. Box 867
Little Rock, AR 72203-0867

10. SPONSORING/MONITORING AGENCY REPORT NUMBER

11. SUPPLEMENTARY NOTES

Available from National Technical Information Service, 5285 Port Royal Road, Springfield, VA 22161.

12a. DISTRIBUTION/AVAILABILITY STATEMENT

Approved for public release; distribution is unlimited.

12b. DISTRIBUTION CODE

13. ABSTRACT *(Maximum 200 words)*

Model tests of the navigation pass spillway proposed for the Montgomery Point Lock and Dam project were conducted with various anticipated pool and tailwater elevations and spillway gate positions to determine the hydraulic forces acting on the spillway gate, hydraulic characteristics of the spillway, stilling basin energy dissipation, and stability of riprap in the approach and exit channels from the spillway.

The 1:15-scale section model simulated a 90-ft approach and exit channel width, spillway, three spillway gates, and stilling basin. Data were collected with a data acquisition system capable of collecting data for prescribed lengths of time and sampling at desired rates.

Tests conducted to determine the vibration characteristics of the instrumented model spillway gate and bearings supporting the gate indicated that their natural frequencies were too high to influence the magnitude of the measured hydraulic dynamic forces.

(Continued)

14. SUBJECT TERMS

Debris passage
Hydraulic forces
Nappe venting
Spillway
Torque-tube gates
Tow boat turbulence

15. NUMBER OF PAGES

105

16. PRICE CODE

17. SECURITY CLASSIFICATION OF REPORT	18. SECURITY CLASSIFICATION OF THIS PAGE	19. SECURITY CLASSIFICATION OF ABSTRACT	20. LIMITATION OF ABSTRACT
UNCLASSIFIED	UNCLASSIFIED		

13. (Concluded).

Test results are presented in pressure contour plots, time-history plots, tables, and graphs. The test results provided information for design guidance to ensure the integrity of the spillway, spillway gates, stilling basin, and riprap.